Université du Québec

Institut National de la Recherche Scientifique
Centre Eau Terre Environnement

CHARACTERIZATION AND NUMERICAL MODELING OF THE BEDROCK AQUIFER IN THE FOX CREEK AREA, ALBERTA

Par

Laura Isabel Guarin Martinez

Mémoire présenté pour l'obtention du grade de
Maître ès Sciences (M.Sc.)
en sciences de la Terre

Jury d'évaluation

Président du jury et examinateur interne	Daniel Paradis CGC, Québec
Examinateur externe	Brian Smerdon Faculty of Science - Earth & Atmospheric Sciences University of Alberta
Directeur de recherche	Claudio Paniconi INRS-ETE, Université du Québec
Codirecteur de recherche	Christine Rivard CGC, Québec

REMERCIEMENTS

Derrière chaque page de ce mémoire de maitrise se cachent des personnes, qui, de par leurs encouragements, leur aide, leur patience, et leur gentillesse, m'ont donnée la force d'avancer.

Je voudrais tout d'abord remercier mes superviseurs, Claudio Paniconi et Christine Rivard. Merci Claudio pour le temps et la patience que tu as employés à m'initier à la modélisation hydrogéologique. Merci Christine pour tes encouragements, tes efforts dans les corrections de mes travaux, et pour m'avoir inculqué ton perfectionnisme scientifique.

Je remercie aussi les évaluateurs de ce mémoire, Daniel Paradis et Brian Smerdon, pour le temps investi dans leurs révisions et leurs commentaires constructifs. Un merci tout particulier à John Molson pour son aide et sa disponibilité lors du développement du modèle FLONET.

Je souhaite également exprimer mon immense gratitude envers mes parents, Lina et Julian, mon frère, Daniel, et toute ma famille, qui, malgré la distance, étaient toujours là pour moi avec un mot d'encouragement.

Un merci tout spécial à Matthieu Cedou pour son soutien, son écoute, et ses encouragements constants, ainsi qu'à tous mes amis de Québec, Margherita, Majo, Dan, Maria Isabel, Felipe, Farah, Charis et tant d'autres.

RÉSUMÉ

Des préoccupations environnementales liées à l'exploitation des hydrocarbures non conventionnels sont apparues au cours de la dernière décennie. La région de Fox Creek, située dans le centre-ouest de l'Alberta, a été l'une des régions les plus actives pour la production d'hydrocarbures au Canada au cours des 50 dernières années, et a donc été choisie comme sujet d'étude.

La CGC a débuté un projet dans cette région en 2019, dont l'objectif principal est d'étudier les impacts potentiels des activités pétrolières et gazières sur les aquifères peu profonds. Ce projet multidisciplinaire et multi-institutionnel comprend différents volets. Cette maîtrise de recherche visait spécifiquement à caractériser l'aquifère rocheux fracturé d'un bassin versant d'une superficie de 425 km2 de la région de Fox Creek et à améliorer la compréhension des connexions hydrauliques potentielles entre les unités géologiques profondes et les aquifères superficiels. Dans ce contexte, des modèles numériques avec les logiciels FLONET et CATHY ont été développés pour simuler les écoulements locaux et semi-régionaux sur une section transversale. Pour ce faire, nous avons utilisé des données hydrogéologiques issues des bases de données provinciales, des rapports et des articles, et des données météorologiques. Les modèles 2D ont été calés en utilisant la piézométrie régionale, en essayant de trouver la bonne combinaison de paramètres de conductivité hydraulique et de taux de recharge. Des scénarios ont été développés pour déterminer quelles seraient les conditions nécessaires pour avoir une remontée des fluides à partir de la formation la plus profonde vers la surface. Les résultats de cette maîtrise, en plus des deux modèles numériques, comprennent une revue de littérature exhaustive sur les propriétés des formations rocheuses présentes dans la région et un bilan hydrique pour la région d'étude, qui inclut la définition d'un intervalle pour la recharge de l'aquifère.

Les travaux réalisés dans le cadre de cette maîtrise ont montré que la région d'étude est caractérisée par : 1) un système d'écoulement des eaux souterraines contrôlé par la topographie, 2) des propriétés hydrogéologiques très hétérogènes, 3) une recharge à l'aquifère rocheux faible, allant de 0 à 70 mm/an et 4) un écoulement actif concentré dans la partie supérieure de la Formation de Paskapoo, qui est plus fracturée (~100 m). La modélisation des quatre premières formations rocheuses à partir de la surface (Paskapoo, Scollard, Battle et Wapiti) avec FLONET a également démontré qu'un lien hydraulique entre les formations géologiques profondes et celles peu profondes est très improbable.

Mots-clés : Modélisation de l'écoulement souterrain ; caractérisation hydrogéologique ; Formation de Paskapoo ; bilan hydrique ; Fox Creek ; Alberta

ABSTRACT

Environmental concerns related to unconventional hydrocarbon exploitation have arisen in the last decade. The Fox Creek area, located in west-central Alberta, has been one of the most active regions for hydrocarbon production in Canada over the last 50 years and was therefore chosen as the subject of this study.

The Geological Survey of Canada (GSC) began a project in this region in 2019, with the primary objective of studying the potential impacts of oil and gas activities on shallow aquifers. This multidisciplinary and multi-institutional project includes different components. This MSc research specifically aimed to characterize the fractured bedrock aquifer of a 425 km2 watershed in the Fox Creek area and improve the understanding of potential hydraulic connections between deep geological units and shallow aquifers. In this context, two numerical models with FLONET and CATHY were developed to simulate the local and semi-regional flow over a cross-section. To do so, hydrogeological data from the provincial databases, reports, and papers, as well as meteorological data, were used. The two-dimensional (2D) models were calibrated using the regional piezometry to find the right combination of hydraulic conductivity and recharge rate parameters. Scenarios were developed to determine what conditions would be necessary to have upward flow from the deepest formation towards the surface. The results of this Master's thesis, in addition to the two numerical models, consist of a comprehensive literature review on the properties of the rock formations present in the region and a water budget for the study area, which includes the assessment of a recharge interval.

The work carried out as part of this MSc research showed that the study area is characterized by 1) a topography-driven groundwater flow system, 2) highly heterogeneous hydrogeological properties, 3) a low recharge rate to the bedrock aquifer, ranging from 0 to 70 mm/year, and 4) an active flow concentrated in the upper part of the Paskapoo Formation, where more fractures are present. Modeling the four upper bedrock formations (Paskapoo, Scollard, Battle and Wapiti) with FLONET also demonstrated that a hydraulic connection between the deep geological formations and shallow aquifers is very unlikely.

Keywords: Groundwater flow modeling; hydrogeological characterization; Paskapoo Formation; water budget; Fox Creek; Alberta

SOMMAIRE RÉCAPITULATIF

INTRODUCTION

Au Canada, près du tiers (30 %) de la population dépend des eaux souterraines pour son approvisionnement en eau (Figure 1.1, Government of Canada, 2013). En Alberta, ce pourcentage est un peu plus faible que la moyenne canadienne (23 %), mais la ressource en eau souterraine est toujours considérée comme étant d'une importance cruciale à des fins municipales, agricoles et industrielles. Par exemple, plus de 600 000 Albertains en région rurale dépendent des eaux souterraines pour l'eau potable (Government of Canada, 2013). Selon Babakhani *et al.* (2019), les eaux souterraines constituent une source d'eau alternative de plus en plus importante pour l'industrie pétrolière et gazière dans la région de Fox Creek, en Alberta, par rapport aux eaux de surface.

Des activités liées à l'exploration et l'exploitation des hydrocarbures non conventionnels, qui comprennent des opérations de fracturation hydraulique, ont lieu en Alberta depuis 2008. Ce genre d'activités, particulièrement en Amérique du Nord, mais aussi dans plusieurs autres pays, ont soulevé certaines préoccupations, principalement liées à l'épuisement et à la contamination des eaux souterraines peu profondes, aux émissions atmosphériques et aux événements sismiques. La région de Fox Creek (Alberta), située à 260 km au nord-ouest d'Edmonton, a été sélectionnée pour un projet de la CGC, dans lequel ce mémoire de maîtrise s'insère, principalement parce que d'importantes activités pétrolières et gazières y ont eu lieu au cours des cinq dernières décennies. Celles-ci pourraient potentiellement avoir affecté la quantité et la qualité des eaux souterraines (Alberta Energy Regulator, 2015). Smerdon *et al.* (2016) avaient souligné qu'une caractérisation de l'aquifère plus poussée serait nécessaire pour pleinement évaluer les impacts potentiels de l'industrie et garantir un approvisionnement en eau durable.

ZONE D'ÉTUDE

La zone d'étude sélectionnée pour le projet de la CGC correspond à un bassin versant situé à 20 km au sud-ouest de la ville de Fox Creek, qui s'étend sur 700 km^2 (Figure 2.1). Le ruisseau Tony Creek, orienté dans une direction générale ouest-est, est le cours d'eau principal de ce bassin versant. Le sous-bassin versant de ce ruisseau couvre environ 425 km^2. Celui-ci correspond à la zone principalement étudiée dans ce projet de recherche.

i. Climat et hydrogéologie

La région de Fox Creek dans le centre-ouest de l'Alberta est classée, selon la classification de Köppen et Geiger basée sur les températures et les précipitations (Hufty, 2001), comme un climat continental humide avec des étés chauds (Dfb). Les températures moyennes mensuelles les plus chaudes et les plus froides sont respectivement de 15,6°C (en juillet) et -10°C (en janvier) (Government of Canada, 2020). La région de Fox Creek présente des taux de précipitations parmi les plus élevés de l'Alberta. Cependant, à cause de la relation complexe entre l'humidité de l'océan Pacifique qui traverse les montagnes Rocheuses et la topographie locale, le climat est très variable en termes de température et de précipitation. Les moyennes annuelles de température et de précipitation sont respectivement de 2,6°C et 520 mm pour la station de Fox Creek Junction, qui possède les séries de données les plus longues et les plus complètes. Les précipitations sont plus élevées pendant les mois d'été, particulièrement en juillet (101.1 mm), et les plus faibles en février (16.1 mm). Smerdon *et al*. (2019) ont présenté une valeur de « surplus d'eau » (*water surplus*) d'environ 70 mm/an pour la ville de Fox Creek en soustrayant une estimation de l'évapotranspiration (525 mm/an) aux précipitations (595 mm/an).

ii. Géologie

La région de Fox Creek est située dans le vaste bassin sédimentaire de l'ouest canadien. Les quatre formations au sommet de la succession rocheuse sont, de la plus ancienne à la plus jeune : Wapiti, Battle, Scollard et Paskapoo (Figure 2.5 et Figure 2.6) (Smerdon *et al*., 2019). Ces formations non marines, allant du Crétacé supérieur au Paléocène, sont composées de grès, de mudstone et de siltstone, à l'exception de la formation Battle qui est dominée par les mudstones.

La Formation de Wapiti est un assemblage de dépôts fluviaux et de plaines d'inondation du Crétacé, avec localement des sédiments lacustres. Elle est composée d'une alternance de sillstones et de sandstones. La formation de Wapiti est recouverte par la formation de Battle, datant également du Crétacé, qui est discontinue et relativement mince (moins de 18 m). Comme cette dernière est formée majoritairement de mudstone, elle est considérée comme pratiquement imperméable. À certains endroits, la formation de Battle a été complètement érodée. La Formation de Scollard sus-jacente est composée de dépôts crétacés et paléogènes de grès et de siltstone, interstratifiés avec du mudstone.

Enfin, la formation de Paskapoo est constituée d'une succession complexe de mudstone et de siltstone interstratifiés avec des chenaux de grès (Atkinson & Hartman, 2017 ; Babakhani *et al*., 2019), ce qui la rend très hétérogène. Ces chenaux de grès peuvent avoir jusqu'à 15 m

d'épaisseur, mais ont généralement une épaisseur de 5 à 10 m (Chen *et al.*, 2007a). L'ensemble de la formation de Paskapoo s'étend sur plus de 65 000 km^2 et cette dernière représente la plus importante réserve d'eau souterraine de la province et le plus important système aquifère des Prairies canadiennes. Cette formation est connue pour avoir une composition très variable spatialement, autant à l'échelle locale que régionale, étant généralement plus sableuse dans sa partie sud (Grasby *et al.*, 2008). Cette formation a été divisée en trois unités hydrostratigraphiques, en fonction du pourcentage de grès généralement présent : les aquifères de Haynes et de Sunchild et l'aquitard de Lacombe (Lyster & Andriashek, 2012). Les sédiments non consolidés sont généralement minces dans cette région et plutôt perméables, principalement composés de sédiments assez grossiers.

OBJECTIFS DE RECHERCHE

En appui au projet de la CGC visant l'évaluation des impacts potentiels de l'exploitation des hydrocarbures sur les ressources en eau, l'objectif général de ce mémoire de maîtrise est de caractériser l'aquifère rocheux dans le bassin versant de 700 km^2 constituant la région d'étude, et en particulier dans le sous-bassin versant du ruisseau Tony Creek de 425 km^2, dans la région de Fox Creek (Alberta). Pour ce faire, les données existantes et acquises ont été compilées et ont permis de définir les propriétés hydrogéologiques des différentes formations étudiées. Celles-ci ont par la suite été utilisées pour développer deux modèles hydrogéologiques pour étudier l'écoulement dans l'aquifère d'abord en conditions saturées en régime permanent, puis à nappe libre dans la zone vadose en régime transitoire. Ces modélisations numériques visaient également à évaluer les impacts potentiels des activités industrielles réalisées en profondeur sur les aquifères peu profonds.

Les objectifs spécifiques de ce projet de recherche étaient les suivants :

i. Collecter, valider et analyser les données existantes sur les caractéristiques des puits, la profondeur de la nappe et les propriétés hydrogéologiques ;
ii. Compléter les informations existantes dans la zone d'étude en acquérant des données de terrain supplémentaires ;
iii. Estimer la recharge en utilisant plusieurs méthodes ;
iv. Développer un modèle conceptuel 2D basé sur les modèles géologiques provinciaux (Atkinson & Hartman, 2017; Corlett *et al.*, 2019), incluant les quatre formations rocheuses supérieures et les sédiments de surface (épaisseur ~1 km), et sur les valeurs trouvées à l'objectif (i) pour les propriétés et les conditions frontières ;

v. Développer un modèle hydrogéologique d'écoulement 2D d'une profondeur d'environ 1 km avec le logiciel FLONET (Molson & Frind, 2017), en utilisant des conditions saturées de nappe libre en régime permanent et en n'intégrant que les formations rocheuses afin d'étudier différentes hypothèses, dont celles liées à la paramétrisation et aux conditions nécessaires pour une remontée des fluides profonds vers la surface ;
vi. En se basant sur les résultats du modèle FLONET, développer un modèle hydrogéologique d'écoulement 2D intégrant la formation de Paskapoo et les sédiments de surface avec le logiciel CATHY (CATchment Hydrologic), en utilisant des conditions transitoires et non saturées ;
vii. Faire une analyse de sensibilité pour différents paramètres, notamment la conductivité hydraulique, la recharge et l'anisotropie.

MÉTHODOLOGIE

i. Compilation et analyse des données disponibles

À partir de la base de données provinciale (AWWID) (Alberta Environment and Parks, 2018), les données de 441 puits situés dans la zone d'étude ont été analysées. Une vérification préliminaire a été effectuée sur les données disponibles. Par exemple, nous avons vérifié que les niveaux d'eau étaient supérieurs à la profondeur totale du puits et que chaque puits avait des coordonnées géographiques valides. Si deux ou plusieurs puits avaient les mêmes coordonnées, la moyenne des valeurs était retenue et assignée comme valeur unique à ces coordonnées. La plupart de ceux-ci semblaient être des doublons (ou être très proches), car leurs valeurs étaient très semblables; dans ce cas, les doublons ont été supprimés. Une autre vérification a été réalisée sur les puits contenant des informations sur le pompage, afin de retenir seulement ceux contenant les informations appropriées (i.e. niveaux d'eau dynamiques et taux de pompage) pour estimer des valeurs de capacité spécifique.

Suite à cette validation, l'ajout de nos données de terrain et un rapport de la compagnie Chevron (qui a plusieurs puits dans la région, (Chevron Canada Limited, 2017), 329 valeurs étaient disponibles pour la profondeur des puits et 249 données de profondeur des eaux souterraines ont pu être utilisées. Afin de produire une carte piézométrique, les élévations de l'eau souterraine ont été déterminées en soustrayant ces données de profondeur à l'élévation de la surface du sol estimée avec le modèle numérique d'élévation du Canada (MNÉC). Étant donné que les données étaient rares à différents endroits dans la région d'étude, cette carte a été réalisée avec la méthode de krigeage avec dérive externe, en utilisant la topographie comme variable secondaire. En effet, une forte corrélation (R^2=0.92) relie la topographie et les données d'élévation des eaux

souterraines dans cette région. Cette information indique également que l'écoulement est fortement contrôlé par la topographie.

La collecte de données a également permis de définir des intervalles de valeurs pour les propriétés hydrauliques des différentes formations. La formation de Paskapoo est évidemment de loin celle pour laquelle le plus de données sont disponibles et, en conséquence pour cette formation très hétérogène, celle pour laquelle cet intervalle est le plus grand. De plus, les valeurs de débits et de rabattements dynamiques ont permis d'estimer des valeurs de conductivité hydraulique déduites de la capacité spécifique (*Cs*). Les valeurs de capacité spécifique sont considérées comme une bonne approximation de la transmissivité, notamment dans les zones où aucune donnée de transmissivité ou de conductivité hydraulique n'est disponible. Les valeurs de conductivité hydraulique ont ensuite été calculées à partir des valeurs de *Cs* en utilisant les longueurs des crépines disponibles dans la base de données.

ii. Travaux de terrain

Neuf puits d'observation ont été forés dans la formation de Paskapoo à l'automne 2020, avec des profondeurs allant de 35 à 90 m. À cause de la pandémie, des essais de perméabilité dans les puits et dans les sédiments de surface n'ont pu être effectués qu'à l'automne 2021 et ceux-ci n'ont donc pas pu être intégrés dans ce mémoire. Des capteurs de pression et des baromètres ont été installés dans ces puits d'observation afin d'obtenir des données continues pour la pression (charge hydraulique) et la température. La première collecte de ces données a été effectuée à l'automne 2021 (un an de données). Ces données sont donc aussi arrivées trop tard pour être intégrées dans ce mémoire. Dû aux dommages causés par un animal à la station de jaugeage installée sur le ruisseau Tony Creek à l'automne 2020, aucune donnée de débit n'a pu être récoltée encore. Les débits n'ont donc pas pu être utilisés pour le calage des modèles. Une seconde installation, plus robuste, a été faite à l'automne 2021.

iii. Évaluation de la recharge

Étant donné qu'il est difficile d'obtenir des estimations fiables de la recharge, l'utilisation de plusieurs méthodes est recommandée (Rivard *et al.*, 2014; Scanlon *et al.*, 2002). En raison de l'absence de données provenant de la station de jaugeage et des puits de surveillance dans la zone d'étude au moment de la réalisation de ce travail, les méthodes d'évaluation à partir de la séparation des hydrogrammes et des débits d'étiage de 7 jours de cours d'eau, ainsi que des hydrogrammes de puits n'ont pas pu être utilisés. Néanmoins, une estimation approximative a été obtenue à partir de données météorologiques, en évaluant l'excédent d'eau estimé en utilisant

les précipitations et l'évapotranspiration de référence (ou potentielle) pour la période 2016-2019. Un bilan hydrique a également été estimé à l'aide d'outils GIS sur une grille de 100 m x 100 m sur la zone d'étude. Les données sur les précipitations (*P*) ont été obtenues à partir des données météorologiques disponibles, provenant de stations météorologiques proches, et les données manquantes ont été complétées en utilisant les stations à la fois les plus proches et avec les caractéristiques les plus semblables à l'aide du logiciel GWHAT. L'évapotranspiration (*ET*) a été estimée en utilisant la méthode de Thornthwaite basée sur la température, et le ruissellement (*Ro*) a été estimé avec la méthode SCS (USDA, 1985) en utilisant le sol dominant et l'utilisation des terres sur chaque cellule de la grille à partir des cartes provinciales.

iv. Modélisation numérique bidimensionnelle

Pour ce projet, un modèle conceptuel 2D a d'abord été développé en utilisant pour la délimitation des unités les modèles géologiques de la province (Atkinson & Hartman, 2017; Corlett *et al.*, 2019), ainsi que les données disponibles pour les différentes formations géologiques et les connaissances générales acquises sur ce système hydrogéologique (voir les sections 4.5 et 4.6). Pour ce faire, une coupe transversale de 13 km suivant l'écoulement définie à partir de la carte piézométrique a été utilisée, permettant de considérer l'écoulement perpendiculaire à cette coupe comme négligeable. Les quatre formations supérieures de la succession sédimentaire ont été incluses dans ce modèle, permettant une représentation du système sur une épaisseur d'environ 1000 m.

Pour ce projet, les logiciels FLONET et CATHY (CATchment HYdrologic), décrits dans la section 4.3, ont été utilisés pour simuler les flux locaux et semi-régionaux de la coupe transversale. Le modèle FLONET, plus simple, a d'abord été développé pour simuler les conditions d'écoulement en régime permanent, pour tester les différentes valeurs de conductivité hydraulique et de recharge estimées préalablement, pour étudier l'hétérogénéité des différentes unités et leur contribution à l'écoulement global, et pour déterminer les conditions requises pouvant mener à une remontée des fluides. De plus, une analyse de sensibilité utilisant les paramètres qui ont le plus d'impact sur la réponse du modèle a été effectuée. Comme les sédiments de surface sont généralement minces et rarement saturés, ils n'ont pas été intégrés dans ce premier modèle d'environ 1 km d'épaisseur.

Les résultats et les connaissances acquises lors de cette première modélisation hydrogéologique ont été utilisés pour le développement du modèle hydrogéologique avec CATHY. En effet, il a été décidé pour ce modèle de ne considérer que la formation de Paskapoo puisque le modèle FLONET avait montré que la grande majorité de l'écoulement se concentre dans cette formation.

Dans un premier temps, des conditions similaires à celles du modèle FLONET ont été reproduites afin de comparer les résultats des deux modèles (hauteur de la nappe phréatique et recharge). Pour ce faire, un scénario ne considérant pas les sédiments de surface a d'abord été simulé sur une période de 100 ans afin d'obtenir un état à l'équilibre (i.e. proche du régime permanent). Par la suite, les différentes unités de sédiments superficiels, incluant des fonctions de van Genuchten pour définir leurs propriétés en condition non saturée, ont été incluses, de même que l'emmagasinement spécifique pour modéliser l'écoulement en condition non saturée. Enfin, des distributions quotidiennes de pluie et de neige ont été définies, basées sur la différence entre les données de précipitations et l'évaporation potentielle pour la période 2007-2010, et ajoutées au modèle CATHY. Cette période de quatre ans a été choisie, car c'est une des plus complètes. Pour prendre en compte la dynamique de la neige, la méthode degré-jour a également été appliquée. Ceci permet d'accumuler la neige en hiver, et de la rendre disponible pour l'infiltration lorsque la température de l'air est supérieure à 0°C, puisque CATHY considère toutes les précipitations comme de la pluie.

RÉSUMÉ DES PRINCIPAUX RÉSULTATS DE RECHERCHE

i. Propriétés hydrogéologiques, carte piézométrique et recharge

La profondeur médiane des puits de la région d'étude est de 60 m, avec un niveau médian d'eau à une profondeur 24 m (par rapport à la surface). Ces puits traversent les sédiments de surface (dont l'épaisseur est généralement < 20 m et en moyenne de 12 m) et sont tous complétés dans la formation de Paskapoo. Basé sur les longueurs d'intervalles disponibles dans les données lithologiques, ces puits semblent être principalement composés de roches à grains fins (mudstone, siltstone et shale, 52%) suivies de près par le grès (46%); le reste est essentiellement du charbon (2%).

Des valeurs de propriétés hydrogéologiques ont été obtenues à partir d'essais de pompage réalisés dans la partie nord de la formation Paskapoo (Hughes *et al*., 2017b) et de carottes de roche en laboratoire, principalement dans la partie sud (Grasby *et al.*, 2007; Hughes *et al.*, 2017a; Riddell *et al.*, 2009). Les résultats de ces études confirment que la formation de Paskapoo est très hétérogène, avec des valeurs de conductivité hydraulique variant sur plusieurs ordres de grandeur. Les valeurs de conductivité hydraulique estimées à l'aide d'essais de pompage sont beaucoup plus élevées que celles estimées avec les essais sur les carottes de roche, parce que ces essais *in situ* tiennent compte des fractures. Ces valeurs sont interprétées comme étant représentatives de la partie supérieure de la Formation Paskapoo (≈100m). Le tableau 4.1 résume les valeurs de conductivité hydraulique fournies par la littérature pour la Formation

Paskapoo. Les valeurs des propriétés hydrauliques des formations de Scollard, Battle et Wapiti obtenues dans la littérature sont présentées dans le tableau 4.2 (Riddell *et al.*, 2009; Smerdon *et al.*, 2019).

Les valeurs de *Cs* calculées pour la zone d'étude ont été considérées représentatives de valeurs de transmissivité (Figure 6.7). Par conséquent, les conductivités hydrauliques ont été estimées à partir de ces valeurs et des longueurs des crépines (Figure 6.9). La valeur médiane trouvée pour ces valeurs est d'un ordre de grandeur inférieur aux valeurs de *K* trouvées par (Hughes *et al.*, 2017b) à partir des essais de pompage. Ces dernières sont sans doute plus élevées parce que seuls les puits prometteurs (c'est-à-dire avec de bons débits) sont généralement testés. Les valeurs calculées à partir de *Cs* sont donc potentiellement plus représentatives de la zone d'étude parce qu'elles ont été estimées à partir de l'ensemble des puits forés spécifiquement dans cette zone.

- **Carte piézométrique**

Une carte piézométrique de l'aquifère de Paskapoo a été obtenue dans le cadre du projet de la CGC à partir de 249 niveaux d'eau et de la topographie utilisée comme variable secondaire. Cette carte (Figure 6.11) montre que l'eau souterraine s'écoule vers les principaux cours d'eau et donc majoritairement du sud vers le nord dans le bassin versant de Tony Creek, car ce ruisseau est situé très au nord dans le bassin. En raison de la méthode d'interpolation utilisée, les élévations des eaux souterraines sont probablement surestimées dans certaines zones, particulièrement dans les hauts topographiques. Néanmoins, cette carte fournit une distribution des élévations des charges hydrauliques qui paraît plus représentative des conditions réelles que la carte préliminaire qui avait été obtenue en utilisant uniquement les élévations des eaux souterraines.

- **Bilan hydrique**

La méthode du bilan hydrique a fourni les valeurs suivantes pour la région à l'étude : pour des précipitations totales de 552 mm/an, l'évapotranspiration potentielle serait de 495 mm/an et le ruissellement annuel de 151,3 mm. Étant donné ces valeurs très élevées d'évapotranspiration et de ruissellement, les valeurs mensuelles et annuelles de recharge étaient souvent négatives. Par conséquent, un intervalle pour la recharge annuelle moyenne de 0 à 70 mm a été considéré en se basant sur les études précédentes et la méthode du bilan hydrique.

ii. Résultats de la modélisation

Les résultats obtenus avec FLONET ont mis en évidence : (i) deux systèmes hydrogéologiques distincts, séparés par une unité quasi imperméable (la Formation Battle) ; (ii) un écoulement

concentré dans la Formation de Paskapoo, et majoritairement dans la partie supérieure plus fracturée ; (iii) l'influence prépondérante de la conductivité hydraulique de la partie supérieure de la Formation Paskapoo sur la réponse du modèle ; (iv) l'absence probable de connexion entre les formations profondes et superficielles.

Pour reproduire les valeurs de charges hydrauliques interpolées à partir de la carte piézométrique le long de la coupe modélisée, les valeurs de conductivité hydraulique (*K*) des premiers 100 mètres de la formation Paskapoo utilisées dans le modèle hydrogéologique FLONET sont généralement plus faibles que celles répertoriées dans la base de données provinciale pour les essais de pompage longue durée réalisés dans la partie nord de la formation de Paskapoo et ce, même avec une recharge de 70 mm/an. Les valeurs de *K* intégrées dans le modèle (après calage) sont situées entre le 20^{e} et 50^{e} percentile des valeurs de capacité spécifique (*Cs*) estimées avec l'ensemble des puits de la région d'étude. L'ensemble de la formation de Paskapoo a été divisée en quatre zones distinctes : trois zones latérales dans ses 100 premiers mètres (appelées Paskapoo 1.1, 1.2 et 1.3) et une seule zone sous-jacente représentant le reste de la formation (Paskapoo 2) (see Figure 7.12). Une valeur de conductivité hydraulique (*K*) a été assignée à chacune de façon à minimiser l'écart entre les charges hydrauliques simulées et interpolées.

Les résultats du premier scénario dans CATHY ont assez bien reproduit les conditions obtenues avec le scénario optimisé (final) de FLONET. Ces résultats ont montré que l'état d'équilibre (donc près du régime permanent) est obtenu pour la recharge et la résurgence, mais certaines variables, comme le niveau de la nappe, l'écoulement de surface (overland flow), et l'apport souterrain (return flow) continuent de changer légèrement, même après 100 ans. Une valeur de recharge de 86 mm/an a été obtenue avec ce scénario, ce qui reste dans le même ordre de grandeur que la valeur utilisée dans FLONET. La hauteur de la nappe simulée est très similaire à la nappe interpolée, excepté à chaque extrémité de la coupe où elle est un peu plus basse, probablement dû au fait que le modèle ne contient que la formation de Paskapoo et la nappe interpolée dans les extrémités de la coupe est située dans les sédiments de surface plus perméables. L'ajout des unités de sédiments non consolidés a également résulté, localement, en des changements de gradients topographiques importants, ce qui influence fortement l'infiltration, générant des valeurs plus élevées d'écoulement de surface et d'apport souterrain. La recharge a ainsi été réduite (66 mm/an) par rapport au scénario précédent et une meilleure adéquation avec la nappe phréatique interpolée a été obtenue.

CATHY a permis de simuler le comportement saisonnier des précipitations et de l'évapotranspiration, ainsi que l'effet de l'accumulation et de la fonte de neige qui a été intégré en

se servant de la méthode de degré-jour. La recharge annuelle diminue légèrement (2%) lorsque la neige s'accumule pendant les mois d'hiver, même si elle augmente au printemps lorsque la neige fond. Cette faible augmentation est due au fait que la neige fondue est majoritairement évacuée par le ruissellement de surface au printemps.

Le modèle CATHY a également permis la quantification de différents paramètres dans l'espace et le temps, dont la profondeur de la nappe, la saturation de surface, le ruissellement de surface, et le flux de retour, qui permettent de mieux comprendre la dynamique de l'écoulement.

TABLE OF CONTENTS

LISTE OF FIGURES

LISTE OF TABLES

1 INTRODUCTION

Groundwater plays an important role in the hydrologic cycle, notably because it generally feeds surface streams and ecosystems such as wetlands in Canada. Characterizing groundwater is critical for effective water resource management, especially in light of the continuing increase in water demand and climate change. In particular, estimating groundwater recharge is an essential step towards the quantitative assessment and sustainable use of groundwater resources, and it has been an active and challenging area of research in the past decades (Croteau *et al.*, 2010).

Both groundwater and surface water are influenced by a variety of physiographic and climatic factors and by complex processes. Therefore, numerical models have often been used to study surface and groundwater systems. Some of these studies have also considered the impacts of climate change (Ferguson & Maxwell, 2010; Sulis *et al.*, 2011), solute transport (Gatel *et al.*, 2019), different levels of complexity (Gauthier *et al.*, 2009), groundwater recharge (Guay *et al.*, 2013; Rivard *et al.*, 2014; Smerdon *et al.*, 2008), and runoff generation (Camporese *et al.*, 2009).

In Canada, groundwater has historically been poorly studied compared to surface water. Almost one-third (30%) of the Canadian population relies on groundwater for its water supply (Figure 1.1) (Government of Canada, 2013). In Alberta, this percentage is a little lower than the Canadian average (23%), but groundwater is still considered crucially important for a variety of municipal, agricultural, and industrial purposes. For instance, more than 600,000 rural Albertans depend on groundwater for drinking water (Government of Alberta, 2019). Unconventional hydrocarbon development activities, that include hydraulic fracturing operations, have taken place in Alberta since 2008, and have raised some concerns, mainly related to shallow groundwater depletion and contamination, atmospheric emissions, and seismic events. The Fox Creek area (Alberta), located 260 km northwest of Edmonton, was selected for this MSc study, mainly because there have been extensive oil and gas activities for the last 50 years, both conventional and unconventional, that could potentially affect groundwater quantity and quality (Alberta Energy Regulator, 2015). According to Babakhani *et al.* (2019), groundwater is an increasingly important alternative source of water for the industry in the Fox Creek area compared to surface water. Smerdon *et al.* (2016) had underlined that further characterization to supplement current hydrogeological knowledge would be required to assess potential impacts, ensuring a sustainable water supply.

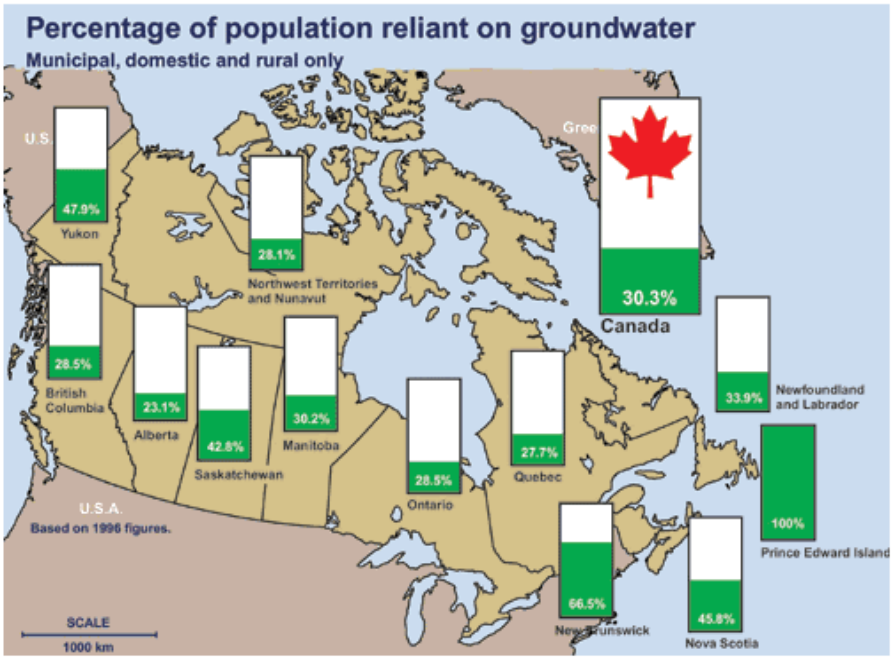

Figure 1.1. Percentage of the population of Canada reliant on groundwater. Source: Statistics Canada, Environment Accounts and Statistics Division, special compilation using data from Environment Canada, Municipal Water Use Database.

As part of a larger project led by the Geological Survey of Canada (GSC) that aims at studying potential impacts of hydrocarbon development on non-saline aquifers, this Master's thesis consists of characterizing shallow aquifers using existing and acquired data and in developing numerical models to study groundwater flow, groundwater recharge, and aquifer properties.

This report first describes the study area and the objectives of this study (Chapters 2 and 3), followed by a literature review (Chapter 4). Chapter 5 presents the research methodology, then Chapters 6 and 7 present the results related to the numerical simulations performed with two hydrogeological models. The last chapter presents the discussion and conclusion.

2 DESCRIPTION OF THE STUDY AREA

2.1 General context

The Town of Fox Creek is situated 260 km northwest of Edmonton in west-central Alberta (Figure 2.1 (a)). The selected study area is a watershed situated 20 km southwest of this municipality and extends over 700 km^2 (Figure 2.1 (b)). The vast majority of this region is covered by forest and contains infrastructure related to the forestry and oil and gas industries. It is therefore largely unpopulated (Smerdon *et al.*, 2019). Over 775 oil and gas wells are present in the 700 km^2 study area. These wells are completed in the Duvernay Formation, a source rock located at about 3.5 km depth in this region.

Tony Creek, oriented in a general west-east direction, is the largest stream in this watershed. It is a tributary of the Little Smoky River that is generally oriented in this area in a south-north direction. Tony Creek's sub-watershed covers approximately 425 km^2 and represents the main study area for this report.

Elevations in the Fox Creek study area, shown in Figure 2.1 (b), range from 786 m above sea level (asl) in the north-east to 1180 m asl in the south-west, including a flat area in the east (Smoke Lake). Flow within the regional bedrock aquifer is topography-driven to a large degree. Shallow water wells in the area are almost all related to work done by the oil and gas industry. No residential or farm wells are present in the watershed.

The land cover in the study area is largely dominated by forest: needleleaf, broadleaf, and mixed forests cover 80% of the watershed, corresponding to 545 km^2, while the industrial facilities (e.g., well pads, pipelines) cover less than 2% (Government of Canada, 2015). The dominant soil types are brunisolic, gleysolic, and luvisolic (Soil Landscapes of Canada Working Group, 2010). More permeable soils characterize the western part of the study area (i.e., in the Tony Creek watershed).

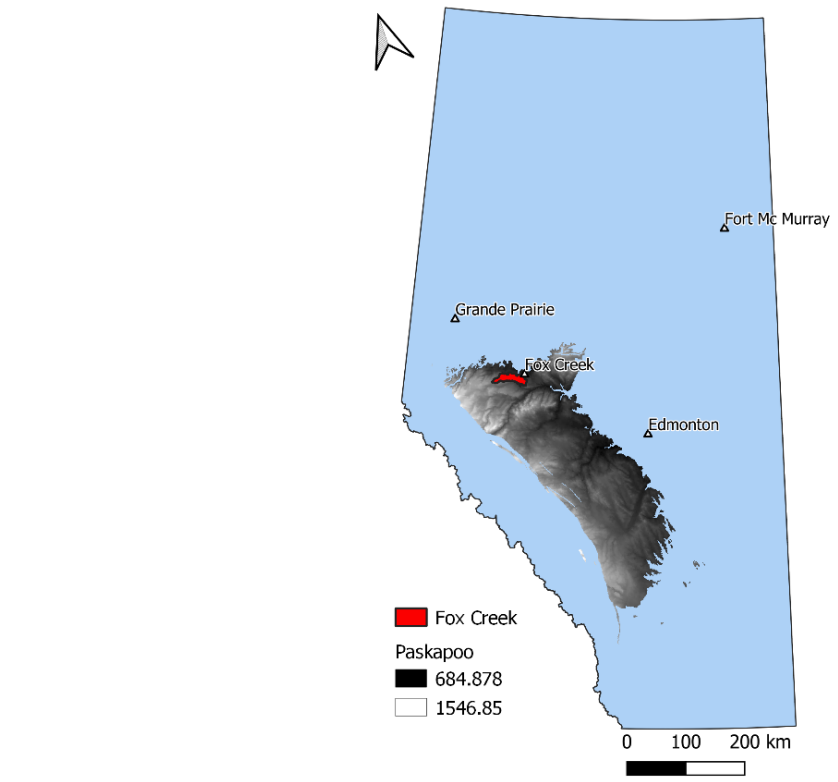

(a)

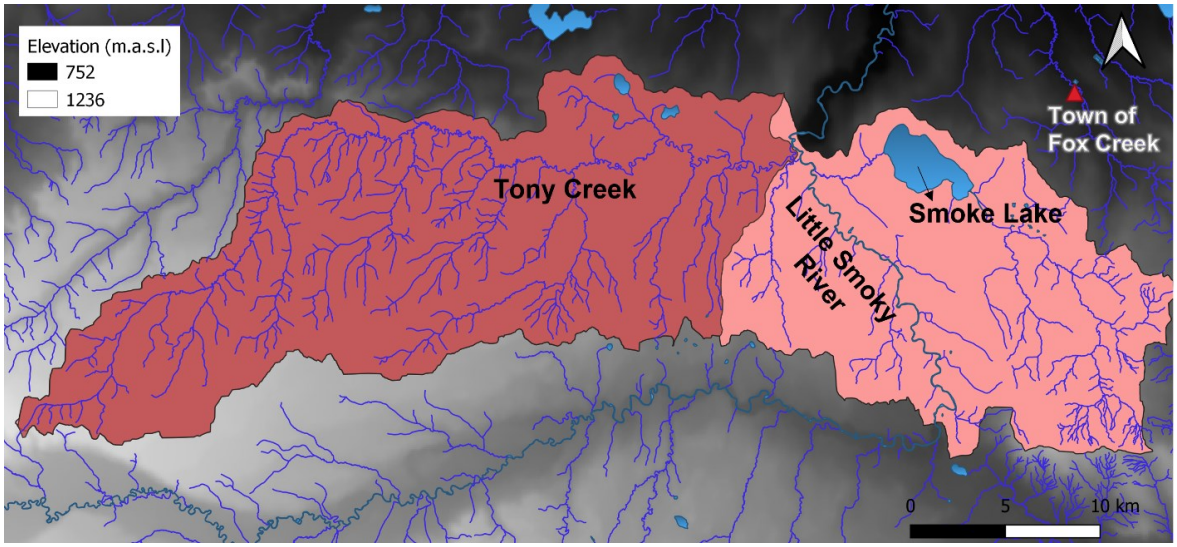

(b)

Figure 2.1. (a) Location of the study area in Alberta. The topography of the Paskapoo Formation is also shown. (b) Delineation of the Fox Creek study area (700 km^2) that includes the Tony Creek subwatershed in red (425 km^2). The Little Smoky River, which drains the Tony Creek subwatershed and the eastern region, is also shown.

2.2 Climate and hydrology

The Fox Creek area is classified according to the Köppen and Geiger classification based on temperature and precipitation as a warm-summer humid continental climate (Dfb) (Hufty, 2001). The climate in this region is cold and temperate. The mean summer (Jun-Jul-Aug-Sep) and winter (Dec-Jan-Feb-Mar) temperatures are respectively, 12.8 and -7.7°C. The Fox Creek area has some of the highest precipitation rates in Alberta. However, because of the complex relationship between moisture from the Pacific Ocean crossing the Rocky Mountains and local topography, the climate is highly variable in terms of temperature and precipitation, even on a monthly basis. Smerdon *et al.* (2019) reported from ClimateNA gridded data long-term climate-normal values for the 1981-2010 period for the town of Fox Creek: 595 mm/y for precipitation and 525 mm/y for reference evaporation, thus corresponding to an average water surplus of 70 mm/y.

Located within the plains region of the Western Boreal Forest, this region presents annual precipitation that is commonly less than potential evapotranspiration. While the largest rainfall events occur in July, this corresponds to the month with the highest temperature and thus evapotranspiration, and the resulting soil water storage capacity generally buffers runoff from rainfall (Devito *et al.*, 2005). The hydrology of the Fox Creek area is strongly influenced by the seasons. Since the Rocky Mountains feed the Little Smoky River, higher discharge occurs in the spring and summer months due to the yearly spring snowmelt and increased precipitation (Chunn *et al.*, 2019). This is also the case for Tony Creek, which experiences relatively high flows in the late spring and early summer, and low flows during the winter months.

Six weather stations are located within or close to the study area (less than 25 km from the Town of Fox Creek). Table 2.1 presents three stations (Fox Creek Auto, Pass Creek Auto, and Tony Auto) belonging to Alberta Agriculture and Forestry (AAF) (Government of Alberta, 2020), while Table 2.2 presents three stations (Fox Creek Junction, Pass Creek Lo, and Tony Lo) from Environment and Climate Change Canada (ECCC) (Government of Canada, 2020). Three additional stations, located between 26 and 35 km from the Town of Fox Creek, are also presented in Table 2.2 (Meekwap, Kaybob 3, and Eagle Lo).

The Fox Creek Auto, Pass Creek Auto, and Tony Auto weather stations are tipping bucket-type rain gauges, measuring only liquid forms of precipitation (rain). Snow falling into the gauge will usually result in a delayed reading when melting occurs, and a significant portion of this snow can be lost through sublimation and wind action. Therefore, these measurements are not considered reliable for total precipitation and their use is not recommended outside of the June-July-August period.

Table 2.1. Available weather stations (Government of Alberta, 2020).

Station	Data	Distance to the study area (km)	Elevation (m)
Fox Creek Auto	2011-2020	5	850
Pass Creek Auto	2016-2020	Adjacent	1080.7
Tony Auto	2016-2020	4	1007

Table 2.2. Available weather stations (Government of Canada, 2020)

Station	ID	Data	Distance to the study area (km)	Elevation (m)
Fox Creek Junction	307K73D	1991-2012	4	829
Pass Creek Lo	3065000	1954-2011	Adjacent	1135.4
Tony Lo	3066500	1957-2011	Inside the study area	1026.3
Meekwap	3074494	1989-2011	26.3	836
Kaybob 3	3063620	1973-2011	34.5	1002.8
Eagle Lo	3062150	1958-2011	27	1042.4

The three weather stations from ECCC located within or near the study area include data from 1991. The percentage of missing data for the Pass Creek and Tony Lo stations averages 70%. Total precipitation is higher during the summer months (June/July), with rain levels peaking in June and July. The Fox Creek Junction station has one of the longest continuous records providing total annual precipitation of 520 mm/y and a mean annual temperature of 2.6°C (Figure 2.2).

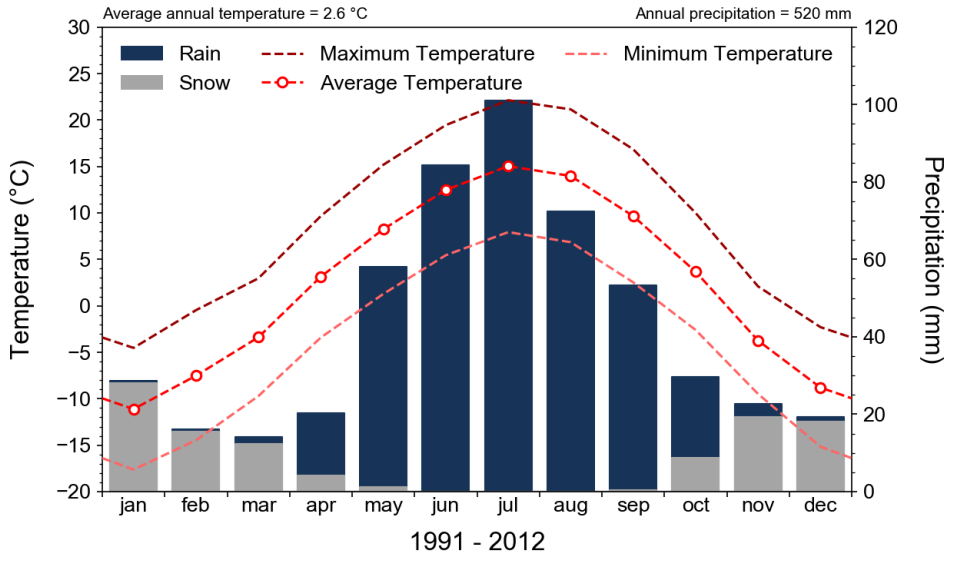

Figure 2.2. Raw data of the Fox Creek Junction station between 1991 and 2012. Data from Government of Canada (2020), visualized with GWHAT (Gosselin *et al.*, 2017).

Mean annual and extremes monthly temperature and precipitation for the ECCC and AAF stations are provided in Table 2.3. The mean annual values for Tony Lo and Pass Creek stations are not representative due to the high number of missing data.

Table 2.3. Annual and extreme monthly means for total precipitation and temperature for the stations close or within the study area (Government of Alberta, 2020; Government of Canada, 2020).

Parameter	Fox Creek Junction (1991-2011)	Tony Lo (1991-2011)	Pass Creek Lo (1991-2011)	Fox Creek Auto (2011-2019)	Tony Auto (2016-2019)	Pass Creek Auto (2016-2019)
Mean total annual precipitation (mm)	520	337.5	364.9	427.2	584.2	559.6
Mean annual rain (mm)	412.2	332.8	360.9	427.2	584.2	559.6
Mean annual snow (mm)	107.6	-	-	-	-	-
Mean annual temperature (°C)	2.6	10.4	9.7	3.96	3.3	2.96
Minimum mean monthly total precipitation (February, mm)	16.1	-	-	-	-	-
Maximum mean monthly total precipitation (July, mm)	101.1	110.8	110.5	115.5	148.1	136.9
Minimum mean monthly temperature (January, °C)	-11.1	9.0	8.0	-7.2	-5.8	-7.5
Maximum mean monthly temperature (July, °C)	15	14.5	14.6	14.5	12.9	14.4

Figure 2.3 illustrates the spatial distribution of annual rain for the 2016-2020 period, including Fox Creek Auto (493.6 mm/y), Pass Creek Auto (559.6 mm/y), and Tony Auto (584.2 mm/y). Only these three stations were used for this figure because the three stations from the Government of Canada do not have data after 2012. This spatial distribution was obtained through the inverse distance weighted (IDW) interpolation method. The Thiessen method produced similar results, but the IDW method was selected because it provides smoother changes across the study area.

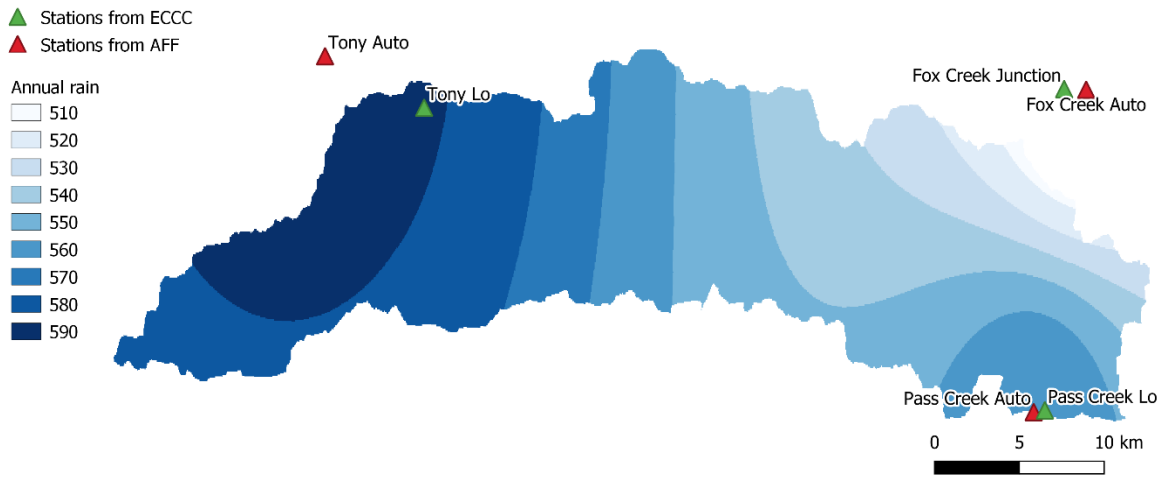

Figure 2.3. Location of the six weather stations closest to the study area and spatial distribution of rain for 2016-2019 obtained using the Fox Creek Auto, Pass Creek Auto and Tony Auto weather stations from AAF (consulted 11-2020). Note: Snow data are not available for these stations.

Historical weather data provided by Environment and Climate Change Canada (EC), Alberta Environment and Parks (AEP), and Alberta Agriculture and Forestry (AF) have been interpolated by AF (https://acis.alberta.ca). These data include precipitation, temperature, humidity, solar radiation, and snow pack water equivalent across the province over 9.6 km x 9.6 km cells (corresponding to townships). Data for each township were estimated using the hybrid IDW interpolation employing a pre-defined search radius (60 km for precipitation and 200 km for temperature) or a maximum of eight of the closest stations. If these conditions were not satisfied, the nearest neighbor was used regardless of its distance.

The 700 km^2 study area includes 15 townships with daily data from 1961 to 2020 (Figure 2.4). The area of the watershed covering each cell and its percentage of the total watershed area was estimated using geographic information system (GIS) tools. The mean total precipitation obtained for this 1961-2020 period is 623.5 mm/y, therefore a significantly higher value than those obtained from local weather stations (for instance, 540 mm/y for the Fox Creek Junction station). This might be due to the different time period and selection criteria when no data are available.

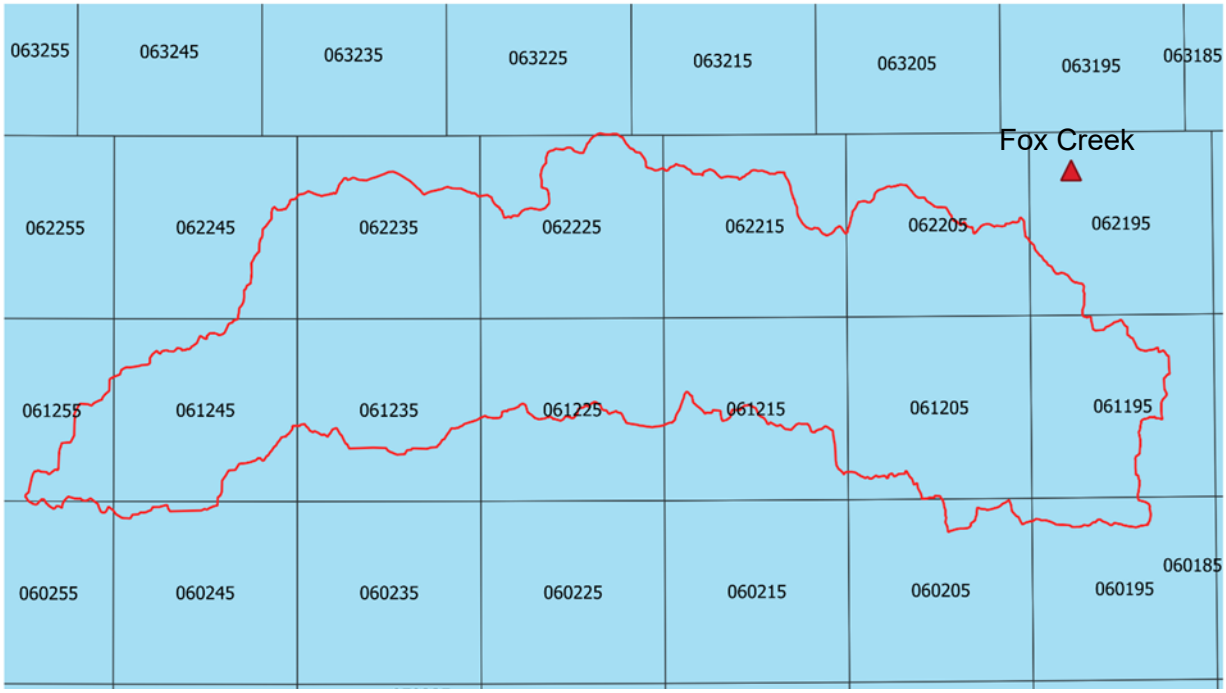

Figure 2.4. Township distribution within the Fox Creek study area used to estimate interpolated weather data since 1961. (Date from Alberta Agriculture and Forestry, Alberta Climate Information Service (ACIS), https://acis.alberta.ca, consulted 11-2020)

2.3 Geological and hydrogeological contexts

The four upper bedrock formations in the sedimentary succession in this area consist of the Upper Cretaceous−Paleogene Wapiti, Battle, Scollard, and Paskapoo formations, listed from oldest to youngest (Figure 2.5 and Figure 2.6) (Smerdon *et al.*, 2019). These non-marine formations are mainly composed of sandstone, mudstone, and siltstone, except for the Battle Formation, which is mudstone-dominated. Unconsolidated deposits are usually thin (< 20 m) in this region and are generally permeable. They are mostly composed of coarse-grained sediments, but may contain clay, making roads slippery during heavy rainfall. The Wapiti Formation is an assemblage of Cretaceous fluvial and floodplain deposits, with localized lacustrine sediments. Overlying the Wapiti Formation is the discontinuous and relatively thin (less than 18 m) Battle Formation, considered nearly impermeable based on its fine-grained composition. In certain places, the Battle Formation has been locally removed by erosion. The Scollard Formation above is composed of Cretaceous to Paleogene deposits of sandstone and siltstone, interbedded with mudstone.

Finally, the Paskapoo Formation is the uppermost bedrock unit that extends across the study area and corresponds to the regional bedrock aquifer. It is dominated by siltstone and mudstone and

is interbedded with highly permeable coarse-grained channel sandstone (Atkinson & Hartman, 2017; Babakhani *et al.*, 2019). The characteristic channel sandstone beds can reach 15 m, but are typically 5 to 10 m thick (Chen *et al.*, 2007a). The Paskapoo Formation extends over more than 65 000 km^2 and is known to have a highly variable composition, being generally sandier in its southern portion (Grasby *et al.*, 2008). This formation has been divided into three hydrostratigraphic units, based on the occurrence of sandstones: the Haynes and Sunchild aquifers and the Lacombe aquitard (Lyster & Andriashek, 2012). A few measurements on paleocurrents suggest a general northeastward trend that may suggest that aquifer units within the Paskapoo have greater continuity, on average, along that orientation (Chen *et al.*, 2007a).

Demchuk and Hills (1991) had first proposed a stratigraphic subdivision of the Paskapoo Formation based on its composition, notably on the occurrence of sandstone. The Haynes Member is the lowermost unit, which corresponds to a conglomeratic sandstone-dominated thick and massive unit. The overlying Lacombe Member consists of interbedded siltstone, mudstone, shale, and coal with minor fine to medium-grained sandstone and is thought to directly overlie the Scollard Formation in the north where the Haynes Member is absent. The uppermost Dalehurst Member is sandstone-dominated, being composed of interbedded sandstone, siltstone, mudstone, and shale, with some coal bed seams ranging from 1.3 m to 6.1 m in thickness. This member is present only in the foothills of Alberta (Demchuk & Hills, 1991). Given its geographic and stratigraphic position, the Sunchild aquifer is suggested to be correlative to the Dalehurst Member, characterized by permeable sandstone bodies that display variable interconnectivity (Lyster & Andriashek, 2012).

Hydraulic conductivity values for the Paskapoo Formation reported in the literature vary over several orders of magnitude and show a bimodal distribution, representing the contrast between the higher permeability of coarse-grained sandstone and fractures, and the lower permeability of the siltstone and mudstone matrix. The hydraulic conductivity values range from 10^{-10} m/s to 10^{-3} m/s (Atkinson & Hartman, 2017; Grasby *et al.*, 2008; Riddell *et al.*, 2009). The considerable range confirms that the Paskapoo Formation is an extremely heterogeneous system.

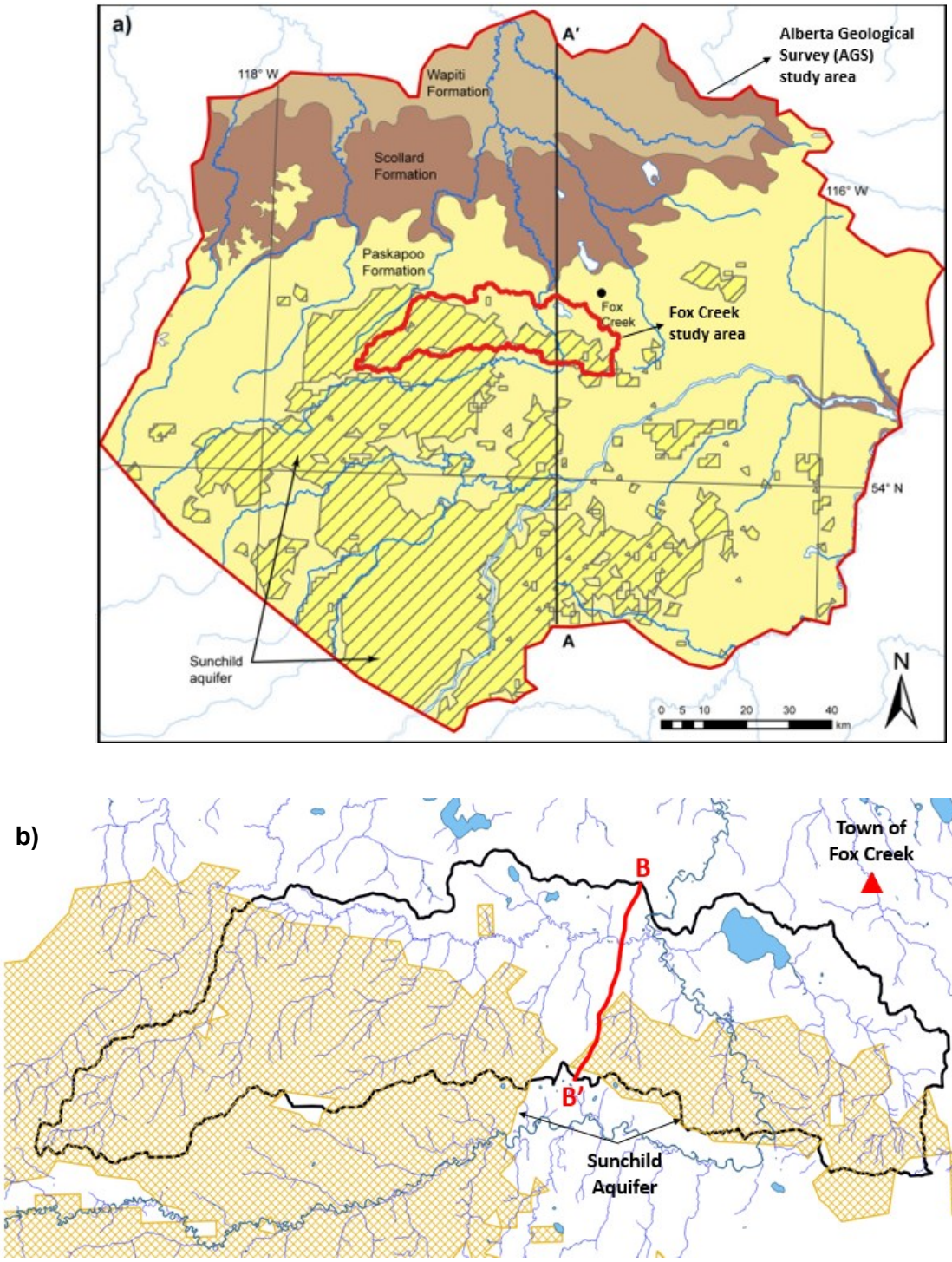

Figure 2.5. (a) Bedrock geology map of the 22 000 km^2 region studied by the province of Alberta (from Atkinson & Hartman, 2017). Our study area (700 km^2) is shown in red. Cross-section A-A′ is shown in Figure 2.6. (b) Zoom on the 700 km^2 study area to better visualize the Sunchild aquifer (in yellow). Cross-section B-B' will be introduced later (section 6).

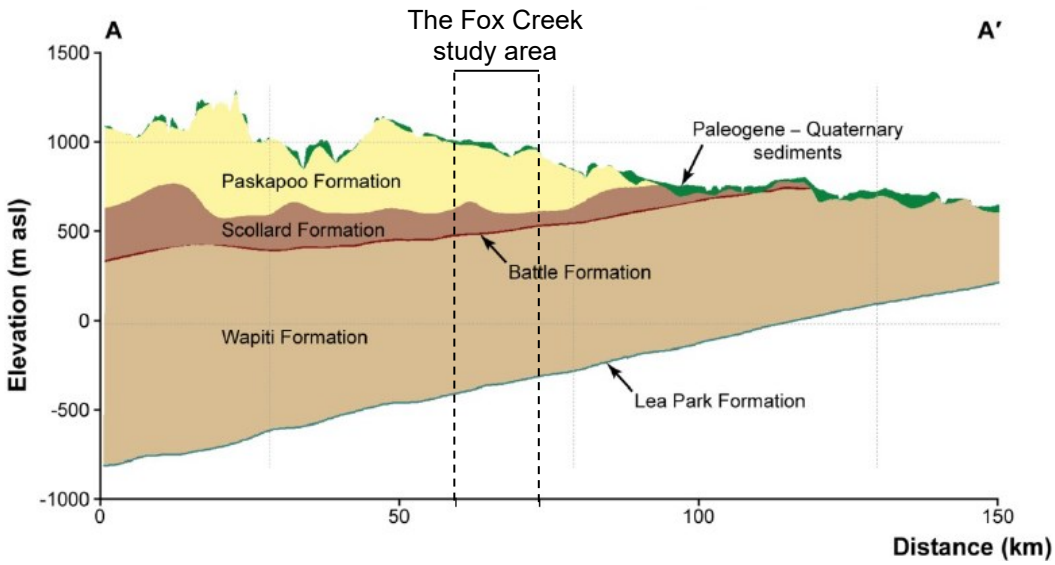

Figure 2.6. Cross-section A-A' from Figure 2.5 (a) shows the wedge-shaped geometry of bedrock units (from Atkinson & Hartman, 2017). The location of the Fox Creek study area is also shown.

3 OBJECTIVES

In support of the GSC's project to assess the potential impacts of hydrocarbon development on water resources, the general objective of this MSc thesis was to characterize the bedrock aquifer in a 700 km^2 watershed, particularly in the 425 km^2 Tony Creek subwatershed, within the Fox Creek area (Alberta). For this purpose, existing and collected data were compiled and used to define the hydrogeological properties of the bedrock formations. These data were then used to develop two hydrogeological models to study the flow in the aquifer, first under saturated conditions in a steady state, then under variably saturated conditions in a transient state. The numerical modeling also aimed to assess the potential impacts of industrial activities carried out at depth on shallow aquifers by investigating potential hydraulic connections between the Wapiti and Paskapoo formations.

The specific objectives for this research project were to:

i. Collect, validate and analyze existing data on well characteristics, water table depth and hydrogeological properties;

ii. Complement the existing information in the study area by acquiring additional field data;

iii. Estimate recharge using several methods;

iv. Develop a 2D conceptual model (~1 km thick) based on the provincial geological models (Atkinson & Hartman, 2017; Corlett *et al.*, 2019), including the upper four bedrock formations and surficial sediment units, and on the values found in objective (i) for properties and boundary conditions;

v. Based on the conceptual model, develop a 2D hydrogeological model with FLONET (Molson & Frind, 2017) under saturated and steady state conditions, including only the bedrock formations to investigate different hypotheses such as those related to the parametrization and the required conditions to have upward flow towards the surface;

vi. Building on the FLONET model, develop a 2D hydrogeological model including the Paskapoo Formation and the surficial sediments using CATHY (Bixio *et al*., 2000; Camporese *et al*., 2010) under unsaturated and transient conditions;

vii. Conduct a sensitivity analysis for different parameters, including hydraulic conductivity, recharge, and anisotropy.

4 LITERATURE REVIEW

This chapter first reviews basic concepts of hydrogeology, then describes general groundwater models, some of which incorporate unsaturated zone and surface flow processes.

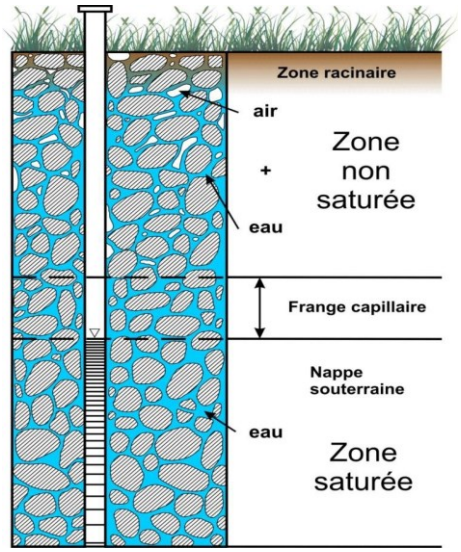

Figure 4.1. Subsurface zones.

4.1 Basic concepts of hydrogeology

Water is present in the soil, filling interstices formed by pores and fractures. In the unsaturated zone, these interstices contain both air and water. Below, in the saturated zone, they are completely filled with water. A transition zone, called the capillary fringe, represents the zone where all pores are filled with water, held by capillary forces (Figure 4.1). The water table is located at the interface between the capillary fringe and saturated zone (Freeze & Cherry, 1979).

4.1.1 Water budget and groundwater recharge

The continual movement of water over, above, and below the surface of the Earth describes the water cycle. The water cycle is a closed-loop system including evaporation processes, condensation, precipitation, infiltration, and runoff. When the precipitation reaches the ground, a part of it returns to the atmosphere by evaporation or transpiration, a part flows as surface runoff (also called overland flow) or subsurface runoff, and the remaining part infiltrates into the ground. Subsurface runoff may return to the surface in topographic depressions (called return flow). Surface and subsurface runoff flows into rivers, becoming a part of the stream flow. These water budget components are illustrated in Figure 4.2.

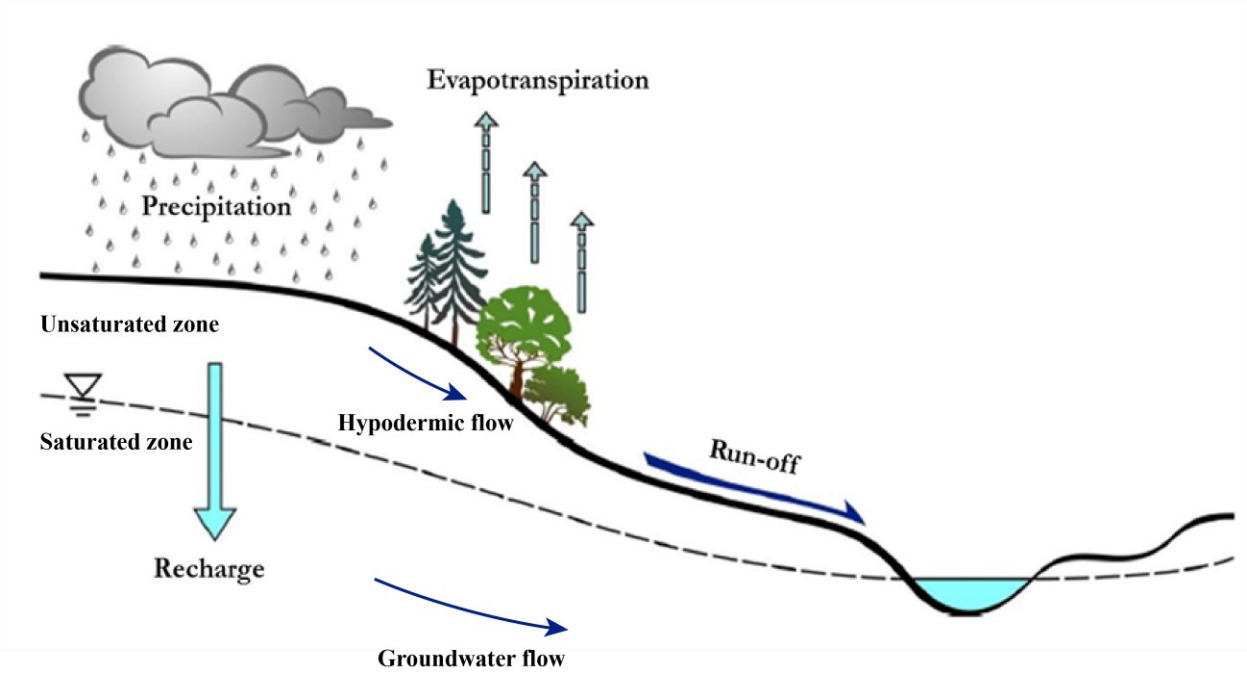

Figure 4.2. Components of the water budget (modified from Ferlatte et al., 2014).

A water budget is an accounting of water movement into and out of, and a storage change within, some control volume (Scanlon *et al.*, 2002). At a watershed scale, this can be stated as shown in equation (1).

$$\boldsymbol{P + Q_{in} = ET + Q_{out} + \Delta S} \quad (1)$$

where P is precipitation; Q_{in} and Q_{out} are water flow into and out of the site, respectively; ET is evapotranspiration; and ΔS is change in water storage.

Groundwater recharge is a key component of the hydrological cycle, defined as the downward flow of water reaching the water table, adding to groundwater storage (Healy, 2010). Hence, recharge theoretically corresponds to the residual of surface and subsurface runoff, evapotranspiration, and changes in storage from precipitation.

Several methods or approaches to estimate recharge are available, including river hydrograph separation, river 7-day low-flows, regional soil moisture balance, and numerical models. Choosing an appropriate and reliable technique based on data availability, scale and other factors is not straightforward (Scanlon *et al.*, 2002). To obtain first estimates of aquifer recharge, simple and fast methods, such as river hydrograph separation and river 7-day low-flows, may be used. Subsequently, a water budget can be calculated, then a groundwater flow numerical model can

be developed to include geological conditions, and/or a coupled surface/subsurface model to include consideration of additional water partitioning mechanisms in the water cycle (Rivard *et al.*, 2014).

4.1.2 Groundwater flow modeling

4.1.3 Hydrogeological models

Groundwater models are a powerful tool for water resources management, assessment, and protection (Baalousha, 2016). The development of the most appropriate groundwater flow model depends on the particular hydrogeological conditions, needs, and limitations of a particular study area, such as data availability. The appropriate approach to modeling a domain is selected based on the spatial and temporal dimensionality, level of heterogeneity, water table dynamics, and variably saturated flow representation (Beckers *et al.*, 2009). The development of a conceptual model is a critical early step. It integrates all the knowledge acquired on the given region and thus allows us to simplify its representation while keeping the essential features of the physical hydrogeological system (Wels *et al.*, 2012).

The degree of complexity to be represented depends on the modeling scope. According to the principle of parsimony, a numerical model should be simplified as much as possible, which implies that the evaluation of the processes to be simulated and their level of accuracy must be done very carefully (Hill, 2006).

An example of a simple model of groundwater flow is Laplace's equation for a 3D confined, homogeneous, and isotropic aquifer under steady-state conditions:

$$\frac{\partial^2 h}{\partial x^2} + \frac{\partial^2 h}{\partial y^2} + \frac{\partial^2 h}{\partial z^2} = 0 \qquad (2)$$

where h is the hydraulic head and x, y, and z are the rectangular coordinates with z generally taken to be positive upward. However, these characteristics do not fit all study areas, and models must often incorporate some complexity to varying degrees. Because the equations representing unconfined, unsaturated, and transient flow are more complex and require more parameters (e.g., moisture content, porosity, specific storage, hydraulic conductivity as a function of moisture content), the development of such models is more demanding and simulations can lead to numerical instability. Therefore, further simplifications are often made. For instance, some groundwater models for unconfined aquifers simulate the water table dynamics by considering only the saturated zone, ignoring the unsaturated zone above it. These models apply either a

known recharge or a known initial water table level at the top of the aquifer (Scanlon *et al.*, 2002), thus neglecting physical processes in the vadose (or unsaturated) zone. More complex variably saturated models consider the movement of water in the vadose zone, as described by Richards' equation, simulating flow from the vadose zone into the saturated aquifer. However, since Richards' equation is nonlinear and a finer vertical discretization is required, a more significant computing effort is required (Wels *et al.*, 2012), not to mention the need for much more data.

Steady-state simulations are used to model equilibrium conditions representing "average" hydrological balance or conditions under which changes in aquifer storage can be considered negligible (e.g., over a period of several years), while transient simulations are used to model time-dependent problems. For example, steady-state simulations are often used to estimate the ratio of recharge to hydraulic conductivity, primarily to represent the regional flow. In contrast, transient simulations are useful for providing information about the system hydrodynamics (including recharge) over time and for simulating local flow. As a good modeling practice, Wels *et al.* (2012) recommend first developing and calibrating a steady-state model using average flow conditions for model calibration. Then, if necessary, transient or dynamic aspects of the groundwater flow system can be modeled using the calibrated steady-state model as initial conditions.

Numerous groundwater modeling codes are available to solve the groundwater flow equations (e.g., MODFLOW, FEFLOW, FLONET). Their differences reside mainly in the type of numerical resolution (finite differences or finite elements), mesh discretization, dimensionality (2D or 3D), and the ability to represent certain aspects of groundwater flow (e.g., variably saturated flow, time dependency).

4.1.4 Coupled surface water / groundwater (SW/GW) models

Integrated surface water / groundwater (SW/GW) physically based models are able to incorporate fully-distributed atmospheric inputs, topographic features, and soil properties to simulate the hydrological cycle. In these models, surface flow is typically described using one or two-dimensional approximations of the Saint-Venant equations for overland and/or channel flow, while the groundwater component is expressed in three dimensions using Richards' equation describing variably saturated subsurface flow.

A standard formulation of Richards' equation is (Maxwell *et al.*, 2014):

$$S_s S_w(h) \frac{\partial h}{\partial t} + \phi \frac{\partial S_w(h)}{\partial t} = \nabla \cdot \mathbf{q} + q_s + q_e \quad (3)$$

where the specific volumetric (Darcy) flux is denoted by $\mathbf{q}$ [LT^{-1}]:

$$\mathbf{q} = -\boldsymbol{K_s} k_r(h) \nabla(\mathrm{h} + \mathrm{z}) \quad (4)$$

and where $\boldsymbol{K_s}$ is the saturated hydraulic conductivity tensor [LT^{-1}], k_r is the relative permeability [-], S_s is the specific storage coefficient [L^{-1}], ϕ is the porosity [-], S_w is the relative saturation [-] (often written as the soil moisture or volumetric water content θ divided by the saturated moisture content, the latter usually assumed to be equal to the porosity), q_s is a general source/sink term that might represent pumping or injection [T^{-1}], and q_e is a general source/sink term that represents exchange fluxes [LT^{-1}].

Coupled models that solve the surface and subsurface flow equations are being increasingly used (Maxwell *et al.*, 2014) to represent different physical processes that influence the hydrologic response at different spatial scales (i.e., small catchments to large river watersheds) (Chemingui *et al.*, 2015; Goderniaux *et al.*, 2009; Loague *et al.*, 2005; Smerdon *et al.*, 2007; Stisen *et al.*, 2011; Sulis *et al.*, 2011; Zerihun *et al.*, 2005). A large number of coupled models are currently available, including: InHm (VanderKwaak & Loague, 2001), Parallel Flow (ParFlow) (Kollet & Maxwell, 2006), CATchment Hydrology (CATHY) (Camporese *et al.*, 2010), HydroGeoSphere (HGS) (Therrien *et al.*, 2012), OpenGeoSys (OGS) (Kolditz *et al.*, 2012), Mike-SHE (Abbott *et al.*, 1986) and MODHMS (Panday & Huyakorn, 2004).

Processes in a physically based spatial model are described by an equation representing a mass, energy, or momentum balance (Paniconi & Putti, 2015). The input data of a physically based spatial model includes: the topography of the site (digital terrain model), the geometry of the domain (including the number and thickness of layers), the physical properties of the soil (hydraulic conductivity, porosity, etc.), and the initial and boundary conditions. The outputs for each node are typically flow velocity, flow magnitude, pressure, and water content (Paniconi & Putti, 2015).

The differences between the various models mainly concern: 1) the formulation of the governing equations (including dimensionality); 2) interface boundary conditions that enforce at least pressure and mass flux continuity at the surface/subsurface interface; and 3) numerical approaches for spatial and temporal discretization and coupling (Maxwell *et al.*, 2014). In terms of coupling strategy, there are three distinct formulations for integrating hydrostatic surface and

subsurface flow: first-order exchange (Panday & Huyakorn, 2004; Therrien *et al.*, 2012), continuity of pressure (Kollet & Maxwell, 2006; Therrien *et al.*, 2012), and boundary condition switching (Camporese *et al.*, 2015).

Two intercomparison studies of coupled surface-subsurface models based on a series of benchmarks have been conducted (Kollet *et al.*, 2017; Maxwell *et al.*, 2014), presenting the results of seven coupled surface-subsurface models in each case. The simulation results found a good agreement for the simple test cases, while the more complicated test cases showed some of the differences in physical process representations and numerical solution approaches between the models.

An assessment of interactions between groundwater and surface water using both HELP and CATHY models on a small-scale catchment was carried out by Guay *et al.* (2013). Both approaches were found to be useful in understanding the interactions between groundwater and surface water, but quite different results in terms of the detailed responses were obtained. The CATHY model could better reproduce the water levels and their fluctuations for equal precipitation and ET rates. It also allowed a better spatial and temporal representation of the different components of the hydrological cycle and of the interactions between surface water and groundwater.

4.2 Selected models

Molson and Frind (2017) developed the FLONET model; a two-dimensional groundwater model restricted to saturated steady-state hydrogeological systems. Based on its versatility and the reduced computing cost, FLONET has thus been selected for one part of this study. A FLONET model was developed to simulate average flow conditions, determine the required heterogeneity level, and test different hypotheses. The characteristics of FLONET are presented in section 4.4.

The coupled SW/GW CATHY model (Camporese *et al.*, 2010) was selected for the second part of the modeling study as it allows for the inclusion of the unsaturated zone and transient simulations. Thus CATHY allowed the incorporation of additional information on the flow system, such as surficial sediments, unsaturated hydraulic conductivity functions, and time-variable atmospheric inputs (rain and snow). The characteristics of CATHY are presented in section 4.4. CATHY has been successfully applied to represent various geological, hydrogeological, and hydrological conditions (Camporese *et al.*, 2009; Chemingui *et al.*, 2015; Gatel *et al.*, 2019; Gauthier *et al.*, 2009; Sulis *et al.*, 2011). The model has also shown robust results over a large range of spatial scales (0.0027–356 km^2) (Camporese *et al.*, 2010).

4.3 The FLONET model

The FLONET model (Molson and Frind (2017) is a two-dimensional groundwater model that solves the flow equation using the dual formulation, i.e., expressing the flow equation in terms of hydraulic potential ϕ [L] (equation (5)) and streamfunction ψ [L^2/T] (equation (6)). It is therefore restricted to saturated steady-state hydrogeological systems.

$$\frac{\partial}{\partial x}\left(K_{xx}\frac{\partial \phi}{\partial x}\right)+\frac{\partial}{\partial y}\left(K_{yy}\frac{\partial \phi}{\partial y}\right)=0 \quad \textbf{(5)}$$

$$\frac{\partial}{\partial x}\left(K_{xx}\frac{\partial \psi}{\partial x}\right)+\frac{\partial}{\partial y}\left(K_{yy}\frac{\partial \psi}{\partial y}\right)=0 \quad \textbf{(6)}$$

where, x and y are the horizontal and vertical coordinate directions [L]; K_{xx} and K_{yy} are the principal components of the hydraulic conductivity tensor [L/T]; ϕ is the hydraulic potential [L]; and ψ is the streamfunction [L^2/T].

A structured, deformed-rectangular mesh generator (GRID) is available within FLONET. It creates triangular elements (by further dividing rectangular elements) based on topography, top and bottom of the geological units, and discretization parameters, such as the number of rows and columns and minimum layer thickness selected by the user. The GRID extension provides a 2D mesh composed of deformable elements, well adapted to complex geometries.

The main inputs for this model are hydraulic conductivity and recharge, while porosity is used for calculating groundwater velocity. Two types of boundary conditions can be defined for the flow simulation: a fixed potential (Dirichlet condition) and a flux boundary (Neumann condition). Both types may be specified at boundary nodes, along boundary segments, or at internal nodes.

The Galerkin finite element approach is used to solve equations (5) and (6). The finite element approach allows grid elements to deform, thereby accurately representing the water table geometry and internal hydrostratigraphic layers. Triangular elements are used along with a preconditioned conjugate-gradient matrix solver. An iterative approach is used in unconfined aquifers when a free water table is assigned, allowing the domain to deform vertically to conform to the equilibrium water table position. The hydraulic head solution algorithm iterates until a user-defined convergence criterion is satisfied. Once the hydraulic head solution has converged, the streamfunction solution will proceed.

Outputs include steady-state hydraulic heads, streamfunctions, and flow velocities when only groundwater flow is simulated. If simulations for advective-dispersive contaminant transport or

groundwater age are required, a subsequent simulation is necessary (using the transport module TR2). FLONET also simulates particle tracking using the head-derived flow velocities. Particle tracking is helpful in a variety of situations, in particular for tracking the plume of miscible contaminants and for identifying capture zones (i.e., the total area supplying groundwater to a pumped well). For a specific stream segment (e.g., environmentally sensitive), particle tracking can also identify the area corresponding to the portion of the watershed that contributes to baseflow.

4.4 The CATchment HYdrology (CATHY) model

CATHY is a coupled physically based, spatially distributed model for surface-subsurface simulations (Bixio *et al.*, 2000; Camporese *et al.*, 2010). The model is based on the resolution of a one-dimensional diffusion wave approximation of the Saint-Venant equation for overland and channel routing nested within a solver for the three-dimensional equation for subsurface flow in variably saturated porous media (i.e., Richards' equation). The routing scheme derives from a discretization of the kinematic wave equation based on the Muskingum-Cunge, or matched artificial dispersivity, method. Surface runoff is propagated through a 1D drainage network of rivulets and channels automatically extracted by a digital elevation model (DEM)-based preprocessor and characterized using hydraulic geometry scaling relationships.

The distinction between overland and channel flow regimes is made using threshold-type relationships based on, for instance, upstream drainage area criteria. Lakes and other topographic depressions can be identified and specially treated as part of the DEM preprocessing procedure.

The subsurface solver is based on Galerkin finite elements in space, a weighted finite difference scheme in time, and linearization via Newton or Picard iteration. A boundary condition switching procedure is used to partition potential (atmospheric) fluxes into actual fluxes across the land surface (infiltration or exfiltration) and changes in surface storage. This scheme resolves the coupling term in the CATHY equations that represent the interactions between surface and subsurface waters.

The main model inputs are atmospheric forcing (rainfall and potential evaporation), topography, and surface and subsurface flow parameters (e.g., Gauckler-Strickler conductance coefficients, saturated hydraulic conductivity, and soil retention curves based on the Van Genuchten (1980) and Brooks and Corey (1964) formulations. Topographic input data is obtained from a DEM and analyzed in a preprocessing step that discretizes the surface dividing each cell to form two

triangles. Then, a three-dimensional subsurface grid is generated, as the triangles are projected on the layers to form tetrahedra. The model has several different options for vertical layering and for the base of the domain to be flat, to be parallel to the surface, or to be provided as an input (e.g., a map of the bedrock topography). If the model is run in subsurface mode only, the horizontal discretization can be nonuniform as well.

The atmospheric inputs are handled as a time-varying boundary condition that can alternate between a Neumann (flux) condition and a Dirichlet (prescribed head) condition according to the saturation (for rainfall) or dryness (for evaporation) status of the soil surface (Sulis *et al.*, 2010).

The model outputs include spatially distributed quantities (e.g., moisture content, surface, and subsurface flow velocities, groundwater levels, and hydraulic heads) and integrated quantities (e.g., streamflow at the catchment outlet and total groundwater storage) (Camporese *et al.*, 2015).

4.5 Previous models in the study area

A number of studies have recently focused on the Fox Creek area, which covered a very large region (approximately 22,000 km^2) as part of a series of geoscience products published by the Alberta Geological Survey (AGS), including a hydrogeological study by Smerdon *et al.* (2019).

As part of these studies, Corlett *et al.* (2019) first mapped 49 geological surfaces, including regional unconformities, between the top of the bedrock surface and the Precambrian basement, for an even larger study area (43,141 km^2). Wireline logs, drill cores, and previous work published in the area were collected and used in ArcMap, then in Petrel to obtain a 3D bedrock geological model. This model identified important horizons and provided information about complex stratigraphic relationships and on paleotopography throughout geological time in this region.

A 3D geological model for the Paleogene−Quaternary sediments was developed by Atkinson and Hartman (2017). This Paleogene–Quaternary model is based on information on lithology, stratigraphic and topographic position, genesis, and depositional setting found from multisource boreholes and field data. The Paleogene−Quaternary sediments were classified into five stratigraphic units (SU): gravel deposits associated with benchlands (SU1); gravel deposits associated with plains (SU2); sand or gravel associated with buried valleys and discrete meltwater channels (SU3); broadly distributed glaciogenic diamict of varying grain size (SU4a); fine grained sediments associated with deposition in major glacial lakes (SU4b); and sand or gravel confined to modern valleys and glaciofluvial drainage-paths, and eolian deposits (SU5) (Atkinson & Hartman, 2017). Each of these units presents a description that can be correlated to

hydrogeological properties, as well as geometrical properties such as thickness and extent. Stratigraphic correlations based on this information allowed the construction of a 3D geological model.

Babakhani *et al.* (2019) developed and documented a 3D model of sandstone abundance for the Upper Cretaceous–Paleogene bedrock formations (namely the Lea Park, Wapiti, Battle, Scollard, and Paskapoo) at the regional scale (1:100 000) (Figure 4.3), partly based on the work of Corlett *et al*. (2019). The model displays the sandstone abundance that was established based on a combination of gamma-ray logs of oil and gas wells and water well lithological descriptions. It presents the net sandstone to gross interval thickness (referred to as net-to-gross ratio: NGR), which is very useful to infer permeability, and thus to define hydrostratigraphy. The NGR data were estimated for the Lea Park, Wapiti, Battle, Scollard, and Paskapoo Formations. The authors partitioned these geological formations into a series of slices, for which they estimated the sandstone abundance, then grouped them and used geostatistical methods to establish the NGR. This model shows that a wide variation in sandstone abundance is present. It also allows the identification of zones likely to act as aquifers within the surrounding siltstone–mudstone sedimentary rocks.

Interesting findings have emerged from the development of the model by Babakhani *et al.* (2019): 1) the presence of a nearly continuous sandstone unit (~230 m) at the bottom of the Wapiti Formation and a discontinuous mudstone shale dominated unit (~200 m) at the top; 2) the absence of a sandstone unit at the bottom of the Paskapoo Formation, but the confirmation of abundant yet heterogenous sandstone in its upper part; and 3) a general dominance of NGR values of about 0.4 for all these bedrock formations.

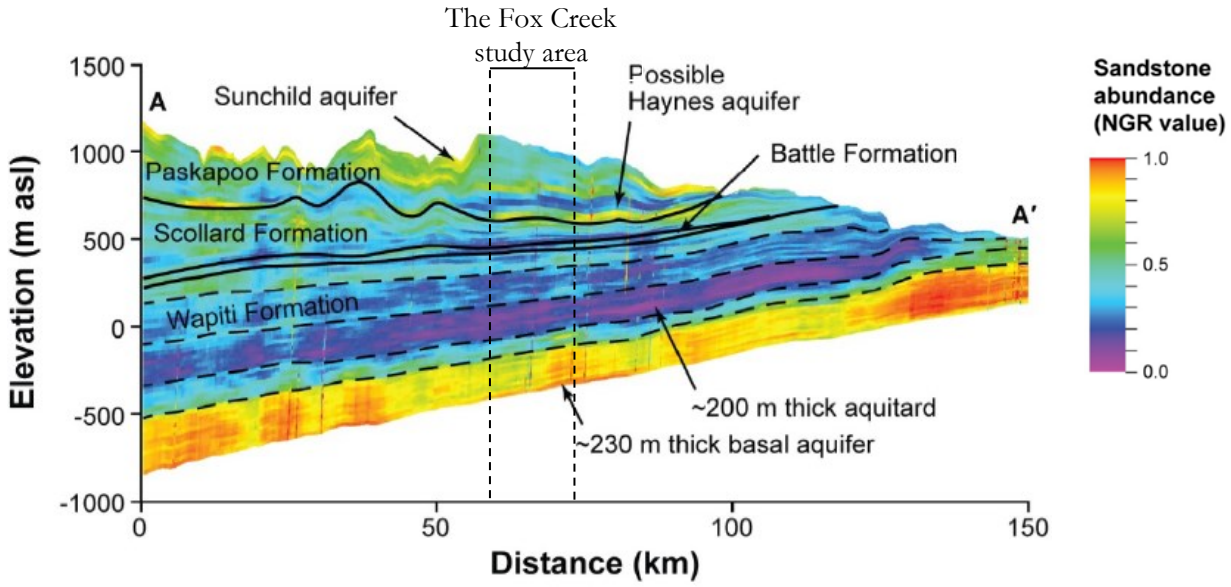

Figure 4.3. Bedrock hydrostratigraphy showing the distribution of sandstone on cross-sectional A-A' illustrated in Figure 2.5 (a) from Babakhani *et al.* (2019). The location of the Fox Creek study area is also shown.

Within the framework of these provincial studies, three shallow boreholes (121-150 m) were drilled in 2015 into the upper part of the Paskapoo Formation near Fox Creek, in which downhole geophysical logs were carried out (Smerdon *et al.*, 2016). The boreholes intersect lithologies that are typical of the Sunchild aquifer and Lacombe aquitard. In two of them, vibrating wire piezometers were installed to measure hydraulic heads at four depths to obtain vertical gradients. The data indicated that the Little Smoky River is in a localized groundwater flow system that is nested within a larger-scale system. This suggests that recharge conditions (downward vertical gradient) could generally occur in the Paskapoo Formation, except close to streams (which are generally discharge zones) in this area.

In the regional hydrogeological characterization by Smerdon *et al.* (2019), a conceptual hydrogeological model was developed to enhance the understanding of the hydrogeological framework, circulation of groundwater, and interactions with surface water in the Fox Creek area. Previous work related to the geological models by Atkinson and Hartman (2017) for the unconsolidated sediments and by Babakhani *et al.* (2019) for the bedrock formations were integrated to define regional hydraulic pathways. Hydrogeological properties for the bedrock units were taken from Hughes *et al.* (2017b) for the Paskapoo Formation and from AccuMap for the Wapiti Formation, while values were inferred from lithological units for the unconsolidated sediments as they are generally unknown. As part of the study, four wells were sampled and three rivers were sampled at 18 different locations, including the Little Smoky River. A water surplus

value of 70 mm/y was reported for the region near the Town of Fox Creek from ClimateNA gridded data, estimated from precipitation and reference evaporation. Water sampling indicates that groundwater recharge is sourced primarily from snowmelt and that there is large spatial variation in groundwater discharge to river systems. This study showed that streams receive an appreciable amount of baseflow only where they are in close proximity to the bedrock containing abundant sandstone. Two conceptual models were developed, one for high topographic relief where sandstone is abundant and the other for low topographic relief, where mudstone prevails (less-resistant bedrock). As expected, recharge, groundwater circulation, and stream discharge is promoted in the former. The use of environmental tracers indicated that rivers contain very young groundwater (<10 years).

Chunn *et al.* (2019) developed a coupled groundwater-surface water model using SWAT–MODFLOW in the Little Smoky River watershed covering 11,494 km^2 to study the potential impacts of climate change (2010-2034 period) and groundwater withdrawals on SW-GW interactions at a regional scale. Their simulations showed that total average discharge into the rivers should not be significantly impacted by climate change. Nonetheless, while SW-GW exchange also did not appear to be substantially affected by climate change, the introduction in the model of 21 supply wells with a pumping rate deemed representative of what the oil and gas industry would need in the future (54 L/s) suggests that localized river flow rates could be considerably impacted.

Singh and Nakevska (2019) developed a piezometric map for the Wapiti/Belly River formations, considering them as a single hydrostratigraphic unit. They interpolated the available hydraulic heads using simple kriging. A total of 603 oil and gas wells and 463 water wells were used (Figure 4.4). This map shows that in the vicinity of the study area, groundwater flow in the Wapiti Formation is to the north. However, on a regional scale, it is influenced by a major topographic high to the northeast of the study area. As can be seen from this figure, very little data are available in the Fox Creek area.

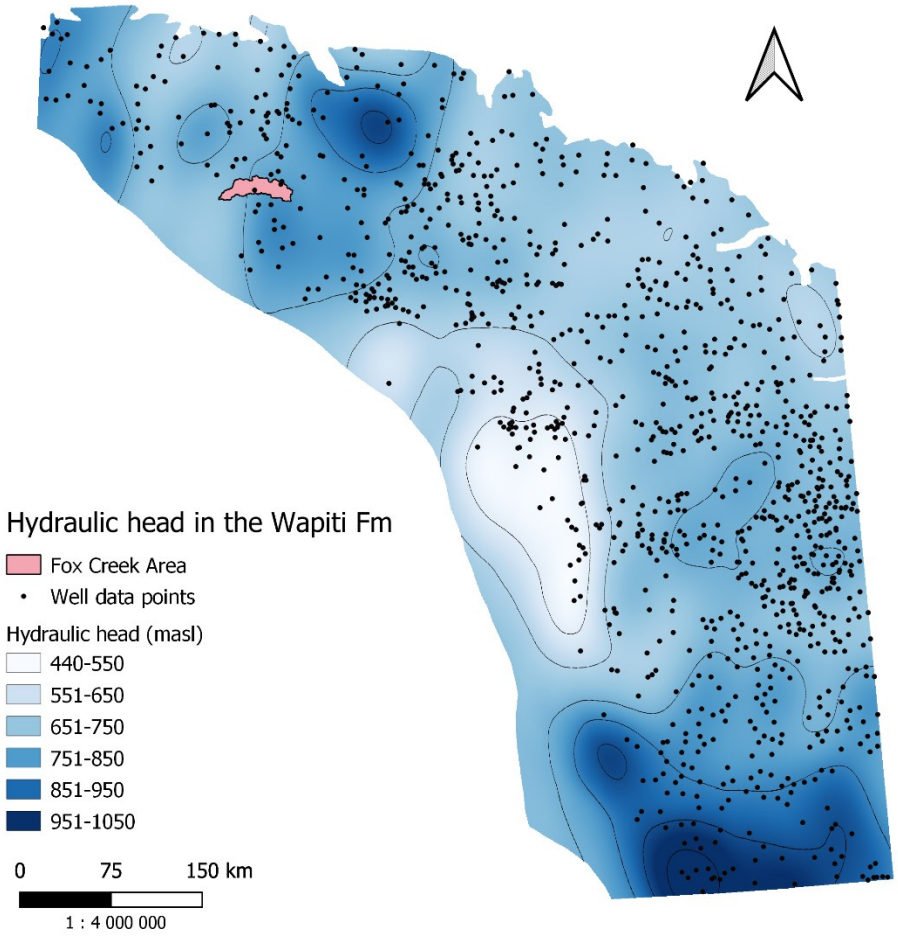

Figure 4.4. Distribution of hydraulic head in the Wapiti / Belly River hydrostratigraphic unit (Singh & Nakevska, 2019). The Fox Creek study area is shown in pink. Hydrogeological properties provided by previous studies

Several studies have provided values of hydraulic properties for the Paskapoo Formation, mostly focusing on the southern part of Alberta. Grasby *et al.* (2007) estimated porosity and permeability values using thin sections from 56 samples (53 in sandstone and 3 in mudstone) collected from six drill cores (0-45 m in depth), from the Red Deer and Calgary region. As earlier work had indicated that outcrop samples were not reliable indicators of subsurface properties, mostly because weathering significantly affects cementation near the surface, this study focused on the examination of cored holes. Estimated permeability of the matrix from air permeametry was in general quite low, with a mean value of 1.4 x 10^{-12} m^2 (translating into 10^{-5} m/s in hydraulic conductivity). A bimodal distribution was observed, representative of higher permeability coarse-grained sandstones and lower permeability fine-grained sandstones and mudstones.

Grasby *et al.* (2008) used data from the provincial databases, in particular pumping test data and results from the mini-permeameters on cores from five wells, and provided a statistical (log-normal) distribution of transmissivity values ranging from 10^{-12} to 10^{-2} m^2/s, with an average 10^{-8}

m^2/s. They also noted that the sandstone ratio decreases to the south of this formation and that fracture density shows a strong inverse relationship to bed thickness, such that fracture flow becomes more important for thinner sandstone beds.

Riddell *et al.* (2009) obtained values for the northern part of the Edmonton–Calgary corridor (between Red Deer and Edmonton) as part of a drilling program from AGS. Continuous cores with a diameter of 7.5 cm (3 inches) were obtained from 12 wells (129 m to 151 m in depth) located in 5 different geological units (Paskapoo, Scollard, Battle, Whitemud, and Horseshoe Canyon formations), which all have sandstone and mudstone successions. Over the 172 analyzed samples, 57 were from the Paskapoo Formation (33%). The latter showed the largest range in grain size of the bedrock formations encountered. Riddell *et al*. (2009) estimated hydraulic conductivity from air-permeameter analysis on core plugs. The values obtained range from 10^{-10} to 10^{-9} m/s for low-permeability claystone or mudstone to 4.9×10^{-5} m/s for very coarse-grained, uncemented sandstones. While mudstone units showed little variation in permeability, sandstone units showed a variation of several orders of magnitude. Such large variation was attributed to grain size distribution and degree of cementation. The differences between horizontal and vertical permeability values observed with core samples were not large: the anisotropy ratio (K_H:K_V) usually showed a 2:1 ratio for sandstone units and close to unity for mudstone units, although anisotropy ratios up to 10 were found.

Hughes *et al.* (2017a) determined hydraulic conductivity values using air permeametry on seven core samples from wells located between Hinton and Fox Creek. As part of the provincial hydrogeological characterization of the Fox Creek area, this study focused on the northwestern portion of the Paskapoo Formation, while the other studies had mostly focused on the lower and southern portions. In their summary of hydraulic conductivity values, Hughes *et al.* (2017b) also analyzed pumping test data using the Cooper-Jacob method from 50 water wells for which records were publicly available in the northernmost portion of the Paskapoo Formation and included air permeametry analysis from two additional core samples. Hydraulic conductivity values from air permeameter tests ranged from 1.1×10^{-10} m/s to 3.0×10^{-5} m/s, with a slight bimodal distribution about a mean value of 7.6×10^{-7} m/s. A mean value of 1.3×10^{-6} m/s was found for sandstone units. *K* values from pumping tests were found to range between 2.5×10^{-6} m/s and 1.0×10^{-3} m/s, with a mean of 2.3×10^{-4} m/s, interpreted as being representative of sandstone units in the uppermost 80 m. The mean transmissivity was found to be 2.3×10^{-3} m^2/s. No significant variation with geographical location was found, and no significant correlation was found with depth. These values show a broad range again in hydraulic conductivity values,

typically much lower for values obtained using core samples than those estimated with pumping tests, since the latter includes larger scale heterogeneity (e.g., fractures).

The results from these studies confirm that the Paskapoo Formation is an extremely heterogeneous system, with hydraulic conductivity values varying over several orders of magnitude. Table 4.1 summarizes the hydraulic conductivity values from Grasby *et al.* (2007), Riddell *et al.* (2009), Hughes *et al.* (2017a), and Hughes *et al.* (2017b), while Figure 4.5 illustrates with boxplots the distribution of the values obtained. Figure 4.6 presents the location of the samples or wells from previous studies within the Paskapoo Formation.

Table 4.1. Median hydraulic conductivity (*K*) values for the Paskapoo Formation obtained from previous studies.

Reference	Location	Number of values	*K* Median (m/s)	*K* Sandstone (m/s)	*K* Mudstone (m/s)
Grasby *et al.* (2007) from air-permeameter (mostly sandstone)	Red Deer and Calgary region	160	5.98×10^{-9}	-	-
Riddell *et al.* (2009) from air-permeameter	Edmonton-Calgary corridor	57	1.77×10^{-6}	4.9×10^{-5}	10^{-10} to 10^{-9}
Hughes *et al.* (2017a) from air-permeameter	Between Hinton and Fox Creek	214	5.79×10^{-9}	1.3×10^{-6}	4.4×10^{-9}
Hughes *et al.* (2017b) from pumping tests	Northern part of the Paskapoo Formation	50	1.54×10^{-4}	-	-

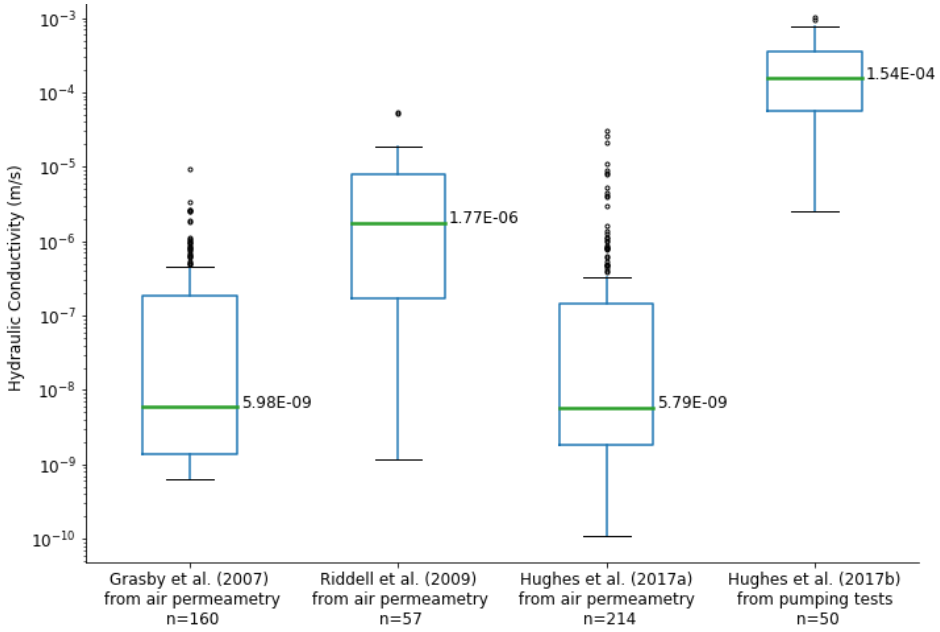

Figure 4.5. Box plot distribution of hydraulic conductivity in the Paskapoo Formation (including 431 values from air permeameter and 50 values from pumping tests). The blue box corresponds to the 1st and 3rd quartiles and the green line to the median, while the black lines correspond to the minimum and maximum values. The black dots are considered as outliers.

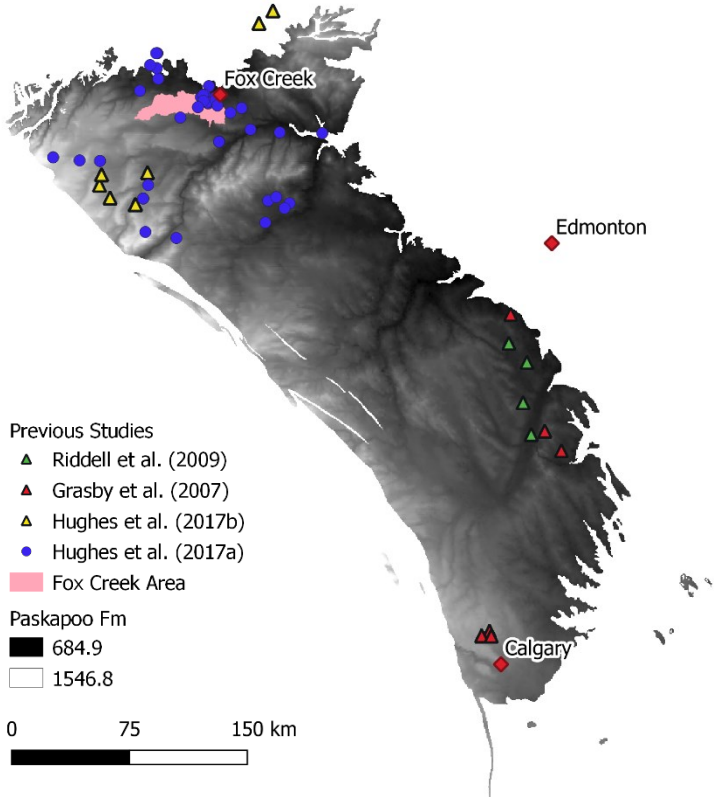

Figure 4.6. Locations of air-permeameter and pumping test measurements from previous studies with symbols colour-coded to match. Elevation of the Paskapoo Formation top is shown as a background (Lyster & Andriashek, 2012).

Chen *et al.* (2007b) estimated 1114 transmissivity values from short "pumping tests" (during well development) that lasted more than 2 hours. Three methods were used for their interpretation: Cooper-Jacob recovery method, truncated Theis solution, and Cooper and Jacob graphic approach. The transmissivity values ranged from 2.3 x 10^{-6} to 3.2 x 10^{-1} m^2/s with a mean value of 2.97 x 10^{-3} m^2/s and a median value of 3.84 x 10^{-4} m^2/s, indicating a skewed distribution, typical for this parameter. As part of a request to obtain a term license for the pumping of 10 water source wells (76 m – 97.5 m deep) for supporting the Kaybob Duvernay unconventional resource development, Chevron estimated 16 values of transmissivity in the Fox Creek area. Long-term (72 hours) pumping tests had been carried out in previous studies and their interpretation was made using the Cooper-Jacob approximation using the AQTESOLV software (Chevron Canada Limited, 2017). Transmissivity values from 1.1 x 10^{-3} to 1.3 x 10^{-2} m^2/s were obtained with a median of 4.8 x 10^{-3} m^2/s. Values of storativity (S=0.05 and 0.002) were also estimated from two observation wells.

As for porosity values in the Paskapoo Formation, the study of Chen *et al.* (2007a) reported in Grasby *et al.* (2007) used 600 log curves from 208 oil and gas exploratory wells and 56 samples (including 53 in sandstone and three in siltstone/mudstone) from five cored stratigraphic test wells between Calgary and Red Deer. Although oil and gas wells do not target the upper 200-500 m, these analyses were used to characterize deeper portions of the Paskapoo Formation. The resulting porosity values range from 4.8 to 32.5%, with an average of 19.2%. Due to the depths investigated, these values may not be representative of the near-surface aquifers. However, both studies found no clear trend with depth. According to Grasby *et al.* (2007), three types of porosity are presented: intergranular porosity (being dominant), secondary porosity, and micro-porosity. The evolution of the pore system appears to be controlled by mechanical and chemical alteration/dissolution of rock fragments and compaction, and by common diagenetic phases encountered in the Paskapoo sandstones including authigenic chlorite, kaolinite, calcite, and pyrite. Hughes *et al.* (2017a) reported a mean porosity of 23.2% from a previous study from the private sector, obtained from nine cores from the Paskapoo Formation. Hughes *et al.* (2017a) also found, on a subset of three drill cores (a total of 25 samples) containing sandstone, siltstone, and mudstone units, a wide interval ranging from 0.01 to 15.3% with an average of 4.8%, with sandstone units practically spanning the whole range. This value is much smaller than the two other mean values reported here, confirming again the strong heterogeneity of the Paskapoo Formation. No significant trend was observed between porosity and depth.

Hydraulic property values of the Scollard and Battle formations, estimated using a mini-permeameter on core plugs have been presented in Riddell *et al.* (2009). Hydraulic conductivity for the Scollard Formation ranges from 9.53 x 10^{-10} to 3.54 x 10^{-6} m/s, while the Battle Formation shows values from 7.37 x 10^{-10} to 1.34 x 10^{-7} m/s. Very little data are available for these formations, and the few data points available are located in the Edmonton–Calgary corridor, north of Red Deer from relatively deep cores (wells from 129 to 150 m deep), passing through each of the major bedrock formations. Khidir and Catuneanu (2010) also determined permeability and porosity for the Scollard-age formations (that include the Scollard, Coalspur, and Willow Creek) from 53 sandstone samples (of which 28 come from the Scollard Formation) from 23 outcrops and 156 conventional core samples (with depths ranging from 355 to 663 m) from Scollard sequence sandstones. Porosity in the latter is considered to be both primary and secondary in origin, and the sandstone secondary porosity was associated with partial dissolution of soluble constituents. Sandstones from outcrops had permeability values ranging from 0.14 mD to 40 mD (average of 7.8 mD, corresponding to 7.7 x 10^{-15} m^2), with a difference for samples containing more or less than 5% calcite cement (8 versus 2 mD). The permeability of the Scollard sequence sandstones measured in core samples (at depth) was higher (less cemented), ranging from 0.06 mD to 92 mD (equivalent to 4.5 x 10^{-10} and 6.9 x 10^{-7} m/s when converted for fresh water at 10°C, salinity being unknown) and averages 40 mD (corresponding to 3.0 x 10^{-7} m/s for the same assumptions). Porosity values from the thin sections for the Scollard sandstones were found to range from 1% to 16% with an average of 7%, while conventional, plug-type porosity analysis generally provided slightly higher results ranging from 0.2% to 25% with an average of 11.2%. The differences in the values obtained between these methods were considered to be caused by the existence of microporosity (associated with the clay minerals) in the Scollard sandstones.

For the Wapiti formation, Smerdon *et al.* (2019) used values obtained from plug measurements (air permeability) reported in the AccuMap database (IHS Markit, 2018). The maximum permeability values were converted to hydraulic conductivity and grouped based on two depth intervals to differentiate parts of the Wapiti Formation that may interact with surface water and be available for typical non-saline applications. This database provided a median hydraulic conductivity value of 2.6 x 10^{-6} m/s for the upper 500 m and 2.6 x 10^{-8} m/s for the 500 m below and mean porosity values of 22% for the 0 to 500 m depth interval and of 19% for the 500 to 1000 m depth interval. Similar to hydraulic conductivity values, the median porosity for the uppermost 500 m was higher than for the lower half (500 to 1,000 m depth), suggesting a positive relationship between porosity and hydraulic conductivity.

Table 4.2 and Table 4.3 summarize the available hydraulic conductivity and porosity values for the Paskapoo, Scollard, Battle, and Wapiti formations.

Table 4.2. Summary of the range of hydraulic conductivity (K) values obtained for the Scollard, Battle, and Wapiti formations in the literature.

Formation	*K* (m/s)	Median value	Reference
Scollard	$9.53 \times 10^{-10} – 3.54 \times 10^{-6}$	1.1×10^{-8}	From mini-permeameter (Riddell *et al*., 2009)
Battle	$7.37 \times 10^{-10} – 1.34 \times 10^{-7}$	2.9×10^{-9}	From mini-permeameter (Riddell *et al*., 2009)
Wapiti (0 – 500 m)	-	2.6×10^{-6}	(IHS Markit, 2018) in Smerdon *et al.* (2019)
Wapiti (0 – 1000 m)	-	2.6×10^{-8}	(IHS Markit, 2018) in Smerdon *et al.* (2019)

Table 4.3. Summary of available porosity values for the Paskapoo, Scollard, Battle, and Wapiti formations in the literature.

Formation	Porosity	Reference
Paskapoo	0.02 – 32.5%	(Hughes *et al*., 2017; Chen *et al*., 2007a/Grasby *et al*., 2007)
Scollard	1 – 25%	(Riddell *et al*., 2009; Khidir & Catuneanu, 2010)
Battle	13%	(Riddell *et al*., 2009)
Wapiti (0 – 500 m)	26%	(IHS Markit, 2018) in Smerdon *et al.,* (2019)
Wapiti (0 – 1000 m)	18%	(IHS Markit, 2018) in Smerdon *et al.,* (2019)

Smerdon *et al.* (2017) compiled the permeability measurements done on core samples from the Horseshoe Canyon, Battle, Scollard, and, mainly, Paskapoo formations between 2004 and 2015 using the air-permeameter. They also provided a conversion into hydraulic conductivity. Figure 4.7 presents the statistical distribution using boxplots and a logarithmic scale for the hydraulic conductivity values of the three upper formations. The Paskapoo Formation shows a very wide range of *K* values, as expected for a very heterogeneous formation (sandstone, siltstone, and mudstone) and a high number of available values. However, although not mentioned in the compiled table itself, the vast majority of these samples should correspond to sandstone units, based on the reports and papers from which they were taken. Therefore, the texture (fine, medium, and coarse-grained) and the percentage of pore-filling matrix of these sandstones likely play a major role. The Scollard Formation is also expected to be heterogeneous, but only 21

values are available. Interestingly, its median and statistical distribution are very similar to that of the Paskapoo (the statistical distribution is narrower. However, due to the limited number of values; there are only 4 values available for the Battle formation). Nonetheless, the statistical distribution suggests its mudstone-dominated composition, showing lower values than the two other overlying formations (by about an order of magnitude).

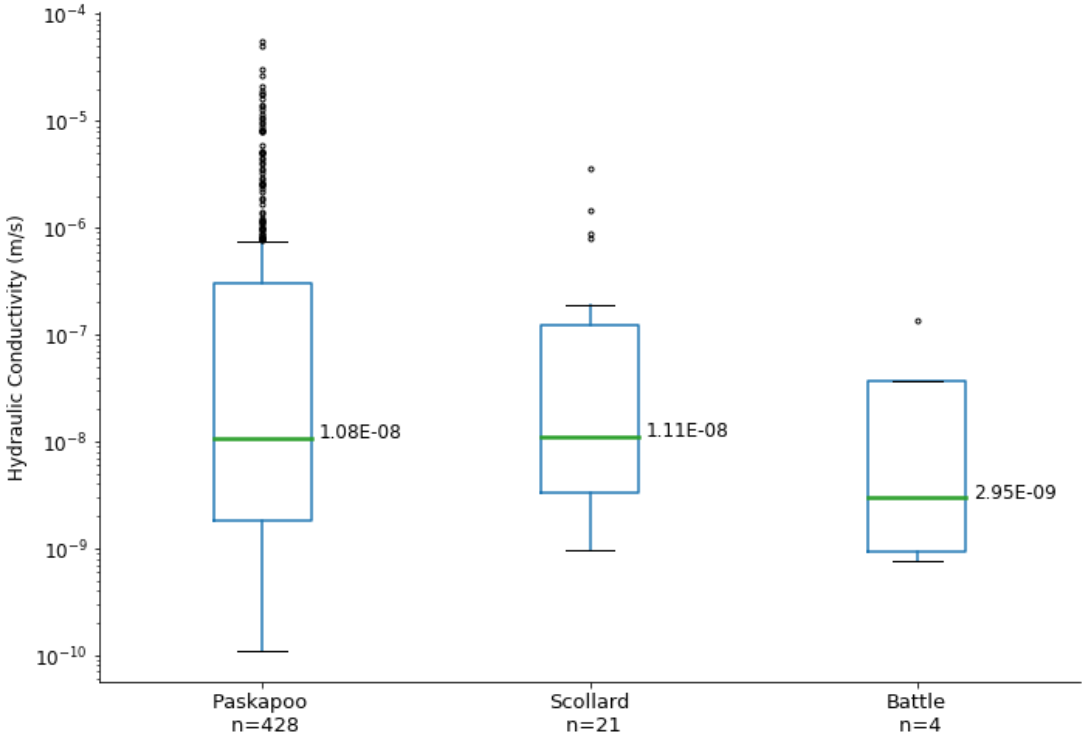

Figure 4.7. Box plot distribution of hydraulic conductivity values for the Paskapoo, Scollard, and Battle formations determined from air-permeameter measurements on core samples (values taken from the compilation done by Smerdon *et al.* (2017) including data from Grasby *et al.* (2007), Riddell *et al.* (2009), and Hughes *et al.* (2017b)). The blue box corresponds to the 1st and 3rd quartiles and the green line to the median. The number of values for each formation (n) is also indicated.

5 METHODOLOGY

To better understand and characterize the groundwater flow system in the Fox Creek area, existing data and field data acquired specifically for this project were used to assess the hydraulic conductivity and aquifer recharge. A description of these data sets is provided below.

5.1 Estimation of specific capacity and development of a piezometric map using available well data

To establish a preliminary understanding of the hydrogeological setting, a review of hydrogeological data found in relevant reports and databases was conducted. The provincial databases (AWWID, Alberta Environment and Parks (2018)) and a report by Chevron (Chevron Canada Limited, 2017) provided data on 455 wells located within the study area. Shallow water wells in the study area have been drilled since the 1960's, essentially by the oil and gas industry for water supply (notably in the last 10-12 years for hydraulic fracturing purposes). All the wells are completed in the Paskapoo Formation.

Available well data have undergone a preliminary verification to make sure that water levels are above the well depth and that each well has a valid geographical coordinate. When two or more wells had the same coordinates, the average value was retained and set as the single value for those coordinates. Most of the wells with the same coordinates in the database seemed to be duplicates (or very close), as the values were similar; the duplicates were then removed. Wells with pumping information during its development went through an additional screening process to select wells with appropriate information to estimate specific capacity values. Wells have been excluded if: 1) the pumping rate or the static and final dynamic water levels were incomplete; 2) they were under flowing artesian conditions; or 3) the screen/perforated casing information was not provided.

Specific capacity values (C_s), considered good estimates of transmissivity values when no pumping tests have been conducted in a well, were calculated using the reported pumping rate during the well development divided by the final drawdown (equation (7)).

$$C_s = \frac{Q}{H_{final} - H_{static}} \tag{7}$$

where Q is the pumping flow rate [L^3/T], H_{final} is the water level at the end of the well development period [L], and H_{static} is the static water level [L], so that the denominator $(H_{final} - H_{static})$

corresponds to the total drawdown. Hydraulic conductivity values were then obtained by dividing these C_s values by the open section of the well b ($K = T/b \approx Cs/b$). Indeed in this case, b, the saturated thickness, corresponds to the open section, hence to the screen or the perforation length.

For the piezometric map, developed as part of the CGC project, a total of 249 static water levels were used and groundwater elevations were obtained from ground surface elevation minus these static water levels in wells. The DEM used for the study area is based on the Canadian Digital Elevation Model (CDEM, 2015), whose spatial resolution is 0.75 arc seconds. The elevation (z) has a precision varying between 5 and 10 m for this region. A preliminary map was first developed using ordinary kriging. However, since data are scarce in many zones of our study area, the resulting map did not appear representative in these zones. To assess whether topography could help improve the piezometric map in areas where no data are available, groundwater elevations were plotted versus ground surface elevations for the available wells (Figure 5.1).

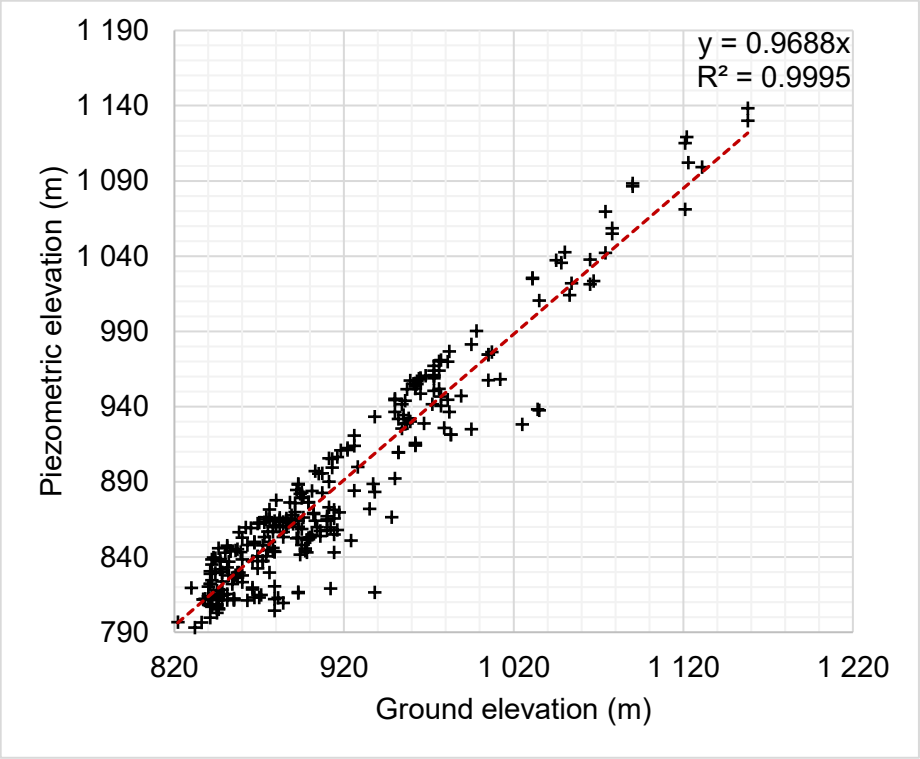

Figure 5.1. Relationship between elevations of the water levels in wells and the ground surface. The dotted red line represents the linear regression.

A strong relationship was indeed found (R^2 = 0.99), indicating that groundwater flow is strongly controlled by topography and that the latter can be used as a secondary parameter to help improve the piezometric map. A refined map was thus created using kriging with an external drift,

using groundwater elevations as the primary parameter and topography as the secondary parameter. Desbarats *et al.* (2002) demonstrated that the use of additional information from topography in regions where topography controls the water table levels considerably reduced the interpolation errors.

5.2 Additional data from fieldwork

The initial plan was to acquire additional data through fieldwork, to supplement the existing database and support model calibration. Nine observation wells were drilled in the fall of 2020 (their locations are presented in the following chapter, in Figure 6.4). Drill cutting samples were obtained and sent to both GSC-Calgary and provincial core facilities. Two monitoring wells (MW6C and MW6D) are twin wells located about 6 meters apart, but at different depths. Well MW10A is located on an active pad of an oil and gas operator. Because the Paskapoo Formation is very friable, wells had to be cased, and screens were installed at their bottom. As the general GSC project aims to study potential impacts of oil and gas activities on groundwater, screens were installed in shaly intervals to sample more evolved water (i.e., older water) than could potentially be found in sandstone intervals. Borehole geophysical logging was conducted immediately following the drilling, prior to casing and screen installation. These wells were developed using air, as they were expected to be poorly permeable. The borehole logging interpretation is underway at the GSC.

Pressure transducers equipped with temperature sensors were installed in these observation wells to obtain continuous data for pressure (hydraulic head) and temperature. Two barometers were also installed. Permeability testing (slug tests) in these monitoring wells had been planned for fall 2020, but had to be postponed to fall 2021 due to the pandemic. For the same reason, limited groundwater samples were collected in fall 2020, mainly to see if they contained dissolved hydrocarbons. The full suite of groundwater samples was collected in the fall of 2021. Monitoring will continue throughout the duration of the Fox Creek project, thus until March 2024. In addition, since no hydraulic conductivity values were available for unconsolidated sediments in the study area, permeameter tests had been planned, but could not be performed until fall of 2021. Grain-size analyses are currently underway, and *K*-values will be derived using various formulas. A gauging station was also installed near the outlet of Tony Creek in fall of 2020. However, an animal damaged the pressure transducer cable (apparently only a few weeks after installation), and it was carried a few meters, likely by ice at the end of winter in this shallow stream. Another setup was carefully planned and deployed in the fall of 2021.

5.3 Recharge assessment

Groundwater recharge is a key component in any water resources management plan. Because recharge is challenging to estimate reliably, the use of multiple methods is recommended (Rivard *et al.*, 2014; Scanlon *et al.*, 2002). Several recharge assessment methods are available, including approaches based on water table fluctuations, river hydrograph separation, water budget, soil moisture balance, stable isotopes, and numerical modeling.

Due to the fact that data from the gauging station and monitoring wells in the study area were not available in time for this project, assessment methods based on hydrograph separation and 7-day low-flows, and well hydrographs could not be used. Nonetheless, a rough estimate was first obtained based on water surplus estimated by subtracting reference evapotranspiration from precipitation for the 2016-2019 period using data from the nearby Tony Auto and Pass Creek Auto weather stations. In addition, recharge values were also obtained from a water budget method and using numerical modeling. A range of recharge rates was obtained from these different approximations.

5.3.1 Water budget method

Water budget methods are based on the water-budget equation (see section 4.1.1). Scanlon *et al.* (2002) presented a very detailed equation for a watershed (equation (8) below). In this equation, water flow in and out the site are written as the sum of surface flow, interflow, and groundwater flow, and evapotranspiration (*ET*) is distinguished on the basis of the source of evaporated water (surface, unsaturated zone, or saturated zone). Water storage occurs in snow, surface water reservoirs, the unsaturated zone, and the saturated zone. All components correspond to rates (mm/d).

$$P + Q_{in}^{sw} + Q_{in}^{gw} = ET^{sw} + ET^{uz} + ET^{gw} + Ro + Q_{off}^{gw} + Q^{bf} + \Delta S^{snow} + \Delta S^{sw} + \Delta S^{uz} + \Delta S^{gw} \qquad \textbf{(8)}$$

where P is precipitation; Q_{in} and Q_{off} are water flow into and out the site, respectively, from surface flow (*sw*) and groundwater flow (*gw*); ET is evapotranspiration; Ro (runoff) is surface-water flow off the site; Q^{bf} is baseflow and ΔS represent the change in water storage; superscript *sw* is for the surface, *uz* for the unsaturated zone, and *gw* for the saturated zone.

Groundwater recharge (R) includes any infiltrating water that reaches the water table and thus comprises the following terms:

$$R = Q_{off}^{gw} - Q_{in}^{gw} + Q^{bf} + ET^{gw} + \Delta S^{gw} \quad \textbf{(9)}$$

Equation (9) states that all water arriving at the water table either flows out of the basin as groundwater flow, is discharged to the surface, is evapotranspired, or is retained in storage (Scanlon *et al.*, 2002).

The most common way of estimating recharge by the water-budget method is the indirect or "residual" approach, whereby all of the variables in the water-budget equation except recharge (*R*) are measured or estimated, and *R* is set equal to the residual. Substituting equation (9) into equation (8) produces the following version of the water budget:

$$R = P + Q_{in}^{sw} - Ro - ET^{sw} - ET^{uz} - \Delta S^{snow} - \Delta S^{sw} - \Delta S^{uz} \quad \textbf{(10)}$$

However, several of these components are difficult to estimate, and the simplified following equation is often used:

$$R = P - Ro - ET \pm \Delta S \quad \textbf{(11)}$$

Typically, a water budget is estimated over a grid (e.g., 500 m x 500 m) using GIS tools for weekly or monthly values using equation (11). For this study, precipitation (*P*) data have been obtained from available hydrologic data from nearby weather stations (see section 2.2). Evapotranspiration *(ET)* was estimated using the Thornthwaite empirical equation (Thornthwaite, 1948), which uses the average temperature, the latitude of the measurements, and the length of the day. Potential evapotranspiration is zero during winter when the average daily temperature is below zero. Snow sublimation has not been taken into account because no data were available to incorporate this factor. Runoff *(Ro)* was calculated with the SCS method (USDA, 1985), this method predicts the volume of runoff after a rainfall event by determining the curve number defined by the dominant soil (Soil Landscapes of Canada Working Group, 2010) and the land use (Government of Canada, 2015). The CN is a dimensionless parameter ranging from 0 to 100, representing the soil retention capacity and thus the rainfall that can become runoff. If the water budget is estimated over several years, the water storage (ΔS) is often considered negligible.

The different maps for this study were prepared using the raster calculator and interpolation methods in GIS. Since very short series and limited data for each station are available in the study area, different stations with short or no overlap were used for the water budget estimate, including a gap-filling treatment.

5.3.2 2-D numerical groundwater flow model

Recharge can also be estimated using numerical modeling. In this project, the ratio of annual aquifer recharge and hydraulic conductivity was first obtained using a 2D model with saturated and steady-state conditions (FLONET, see section 5.4). Subsequently, transient simulations with CATHY using a model integrating surficial sediments and unsaturated hydraulic value functions provided monthly values of recharge for the study area. CATHY computes recharge by summing the downward vertical component of Darcy velocities across the water table. The water table at any given time step is located by interpolating, for each vertical profile in the discretized domain and proceeding from the bottom layer to the top, the position between successive grid nodes where the pressure head changes from a positive value to a negative value (Gauthier *et al*., 2009). The recharge flux is zero for any profile that becomes completely saturated.

5.4 Conceptual, groundwater, and coupled surface water/groundwater models

A 2D conceptual model was developed using the available data for the different geological formations and general knowledge gained on this hydrogeological system from the literature review (see sections 4.5 and 4.6). To simplify the hydrogeological system, several hypotheses were made. One of the main hypotheses is to use a transect along a flow path based on the piezometric map, for which transverse flow (i.e., perpendicular to the transect) is considered negligible. Since the selected transect is perpendicular to equipotentials (isocontours) and thus parallel to the hydraulic gradient, it is considered representative of the regional flow direction.

A first 2D cross-section numerical model of the selected transect was constructed using a hydrogeological model in fully saturated, steady-state conditions (FLONET, Molson and Frind (2017)), based on the provincial geological model and maps, the average value of recharge, and hydrogeological properties found in literature (see section 4.7) and the piezometric map. This model aimed to reproduce the observed hydraulic heads and to produce a map of groundwater velocities.

The transect was chosen in the Tony Creek subwatershed, not too far from the outlet (see section 6.5). The four upper formations of the sedimentary succession, spanning a thickness of almost 1000 m, were included in this model. Although hydrocarbon activities take place at much greater depths (3.5 km), we wanted to develop a model that would provide insight into the hydrodynamics of the upper 1 km, before adding several potentially unnecessary units. Hydraulic conductivity, porosity, and thickness values for the Paskapoo, Scollard, Battle, and Wapiti formations found in previous studies, and notably from Table 4.2 and Figure 4.7, were used. The thin, permeable

surficial sediment cover was first neglected for the FLONET saturated simulations since it is typically unsaturated. The Paskapoo Formation was divided into two sections: an upper 100 m was used to take into account the more permeable rock due to sub-horizontal fractures. For this 13 km transect, the fractured aquifer is represented as an equivalent porous medium. The median *K* value from pumping tests, then from estimated *Cs* were used for this more permeable layer, as almost all (>99%) wells in the provincial database in this region are less than 100 m deep. The lower part of the Paskapoo Formation was assigned the median value obtained from all core plugs (i.e., from all three studies, see section 4.7), considering that fractures are mostly closed at this depth due to the weight of the overlying rock matrix. For the Battle and Scollard formations, the median value of mini-permeameters was used (Riddell *et al.*, 2009), while for the Wapiti Formation, the hydraulic property data estimated by Smerdon *et al.* (2019) were used. The Wapiti Formation was also divided into two equal sections based on previous work (Babakhani *et al.*, 2019; Smerdon *et al.*, 2019), assigning a much higher value to the upper half. The mesh used in the 2D model was generated using the GRID extension of the FLONET model.

The objective of the model calibration process was to minimize the differences between the simulated and interpolated (extracted from the piezometric map) hydraulic head values along the profile. Interpolated heads were used in this case since there are very few water wells along the transect. Calibration therefore consisted in finding the right parameter combination (*K* and recharge values) within the previously defined ranges, which would minimize the difference between simulated and interpolated hydraulic heads, using a regular interval. These differences were evaluated using the root mean square error (RMSE) calculated with values every 500 m along the cross-section, based on the DEM resolution. The calibration of this preliminary model consisted in manually adjusting the hydraulic conductivity, keeping values within the range established in previous studies (section 4.6), while maintaining a fixed recharge rate and a constant anisotropy ratio (*K*h:*K*v). The calibration process also allowed the identification of the most sensitive parameters. In addition, since the Battle Formation is thin and discontinuous, different scenarios were developed to study its influence on the model response. Finally, a sensitivity analysis of the calibrated model to the most sensitive parameters was carried out by varying these parameters while keeping all other parameters constant. The most sensitive parameters were increased and decreased using increments, remaining within the plausible ranges presented in section 4.7.

Different scenarios and boundary conditions were also tested to investigate various hypotheses, including the possibility of flow interconnectedness between shallower and deeper formations.

Once satisfactory results were obtained for the FLONET simulations, the next step was to build a more complex 2D model of the same cross-section incorporating unsaturated and transient conditions, using CATHY (Bixio *et al.*, 2000). Within the scope of the simplified configuration considered in this study (a 2D transect rather than an entire watershed), only the subsurface module of this code was used. Surface runoff and subsurface return flow (to the surface) are nonetheless simulated (it is just the overland routing component that is not used). The model is driven by rainfall and potential evaporation inputs, which get partitioned into infiltration, runoff, and actual evaporation. Results and knowledge gained from the first hydrogeological modeling were used to develop the second hydrogeological model.

Long-term simulations in CATHY had to be developed to reproduce as much as possible the FLONET conditions, which means seeking a steady-state. Thus, the implementation of these two very different models represented an opportunity to investigate the flow system extensively. Furthermore, these two models embody complementary aspects, such as time dependency (steady and unsteady state) and treatment of the saturated/unsaturated interface (free surface boundary condition and vadose zone). Thus, while FLONET characterizes the average conditions of the study area at a larger scale, CATHY allowed a more detailed investigation of the flow system. Table 5.1 presents the data sources for the different parameters required in CATHY.

Table 5.1. Required parameters for the implementation of the CATHY model and their source.

Parameter	Source
Atmospheric Forcing	
Precipitation	Daily data from weather stations
Potential evapotranspiration	Daily data from weather stations
Topography	
Digital terrain data	Canadian Digital Elevation Model (CDEM, 2015) and provincial geological model (Corlett *et al.*, 2019)
Subsurface properties	
Horizontal hydraulic conductivity	Previous studies (see section 4.7)
Vertical hydraulic conductivity	Anisotropy from previous studies (see section 4.6)
Porosity	Previous studies (see section 4.7)
Specific storage	Previous studies (see section 4.7)
Van Genuchten or Brooks-Corey retention curves	From literature, derived from soil type and grain size distribution

Five-year simulations were initially used due to their high computational cost. Once the model was calibrated, these simulations were extended up to 100 years to reach near-stable (steady state) conditions.

The van Genuchten and Brooks-Corey soil retention curves, widely used in physically based models, describe the relationship between pressure and saturation in an unsaturated medium (Brooks & Corey, 1964; Van Genuchten, 1980). These relationships use the residual water content (θr), the air entry pressure head (Ψs), and an empirical parameter related to the pore size distribution (n).

Several van Genuchten parameters were evaluated using 5-year simulations, representative of various soil types, from a finer and thus low permeable soil to a permeable sandy soil. Figure 5.2 shows the pressure head as a function of the hydraulic conductivity and the moisture content for three markedly different soil types (clay, silty loam and sandy loam). The parameter values used in this study were taken from the literature (Carsel & Parrish, 1988). The van Genuchten relationships illustrated in (a) show smoother transitions at the capillary fringe than the Brooks-Corey relationships shown in (c), and were thus preferred for this study. The van Genuchten parameters corresponding to the dominant soil type over the study area (silty loam) were used for the CATHY model.

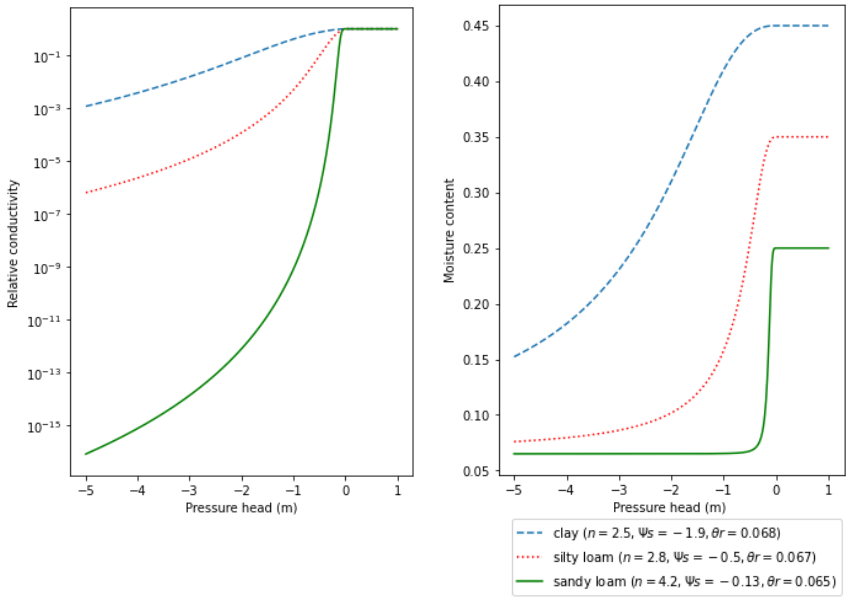

(a)

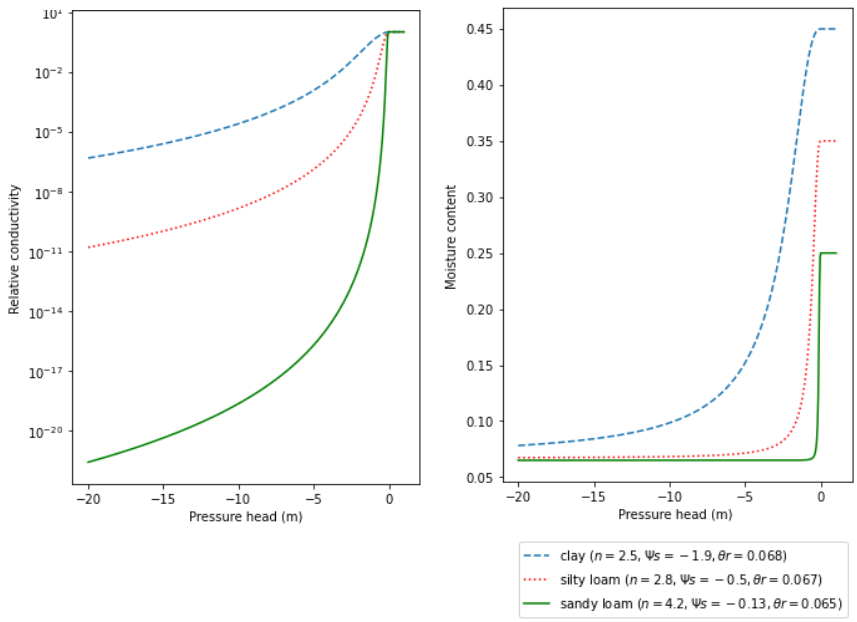

(b)

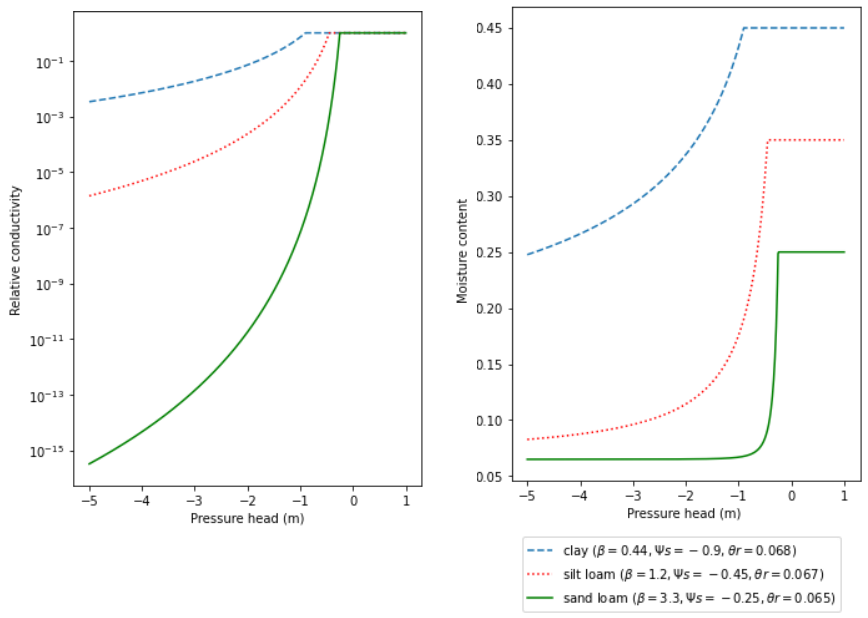

(c)

Figure 5.2. Retention curves representative of three soil textures: clay, silty loam and sandy loam a) using van Genuchten curves for pressure heads between -5 and 1 m, b) using van Genuchten curves for pressure heads between -20 and 1 m and c) using Brooks-Corey curves for pressure heads between -5 and 1 m.

Hypotheses tested in FLONET provided information on the number of geological formations to include in the model and the minimum level of heterogeneity required to avoid an unnecessarily increased computational cost. For the CATHY modeling, the depth of the cross-section and its heterogeneity were defined based on the FLONET results. The first CATHY setup aimed to

reproduce the same conditions as those implemented in FLONET. Therefore, the surficial sediments were neglected and the same boundary conditions were assigned. The mesh used in the CATHY model was generated using a refined DEM at 20 m in the horizontal direction for the Paskapoo Formation, based on the delineation of this unit by Corlett *et al.* (2019).

Since CATHY is a 3D model, two cells were used in the direction transverse to the transect to emulate a 2D domain, so as to use the line of nodes at the interface between these two cells as the simulation transect. The other two lines of nodes, forming the outer boundary for each of the two cells, were assigned no-flow boundary conditions, thereby guaranteeing a 2D flow setup: along the transect and in the vertical direction. A three-dimensional subsurface grid was automatically generated with variable layer thicknesses increasing with depth. Each layer was parallel to the surface except for the last one at the base of the model domain (i.e., the bottom of the bedrock aquifer), in this case, the Scollard Formation (the model is illustrated later, in section 7.3). To compare results between these two hydrogeological models, the nearly steady-state conditions in CATHY were also evaluated by comparing simulated heads with the interpolated water table from the piezometric map. The RMSE was also calculated for CATHY results, but in this case, every 20 m along the transect.

Later, the thin permeable surficial sediment cover was included, obtained from the Paleogene–Quaternary sediment units defined in the 3D geological model by Atkinson and Hartman (2017). As hydraulic properties for the unconsolidated Paleogene–Quaternary sediments are generally unknown, the description of the various units was qualitatively correlated to hydrogeological properties, as suggested by (Smerdon *et al.*, 2019).

Different scenarios and hypotheses were tested, including different boundaries and initial conditions. The model outputs examined include spatiotemporal patterns of overland flow, return flow (groundwater that returns to the surface), streamflow, groundwater levels, recharge, and surface saturation fraction.

Meteorological data for the 2007-2010 period were later included in the model as rainfall minus evapotranspiration (estimated in section 6.5.2). This period was selected because it presents one of the most complete records and an accumulated total precipitation rate similar to the atmospheric conditions initially used. Initial conditions for the water table were estimated from the difference between topography and the simulated FLONET water table.

All precipitation input to CATHY is considered as rainfall. Therefore, the simple “degree-day” method (USDA, 1985) was used to reproduce snow accumulation and melting. The snow melting

rate and the threshold snow melting temperature were selected based on the land cover in the cross-section B-B' corresponding to 35% deciduous forest, 37% coniferous forest, and 26% mixed forest (Soil Landscapes of Canada Working Group, 2010).

The snow module was applied using three different values 1) for the snow melting rate (7.76 mm/day°C for deciduous forest, 1.56 mm/day°C for coniferous forest, and 2.74 mm/day°C for mixed forest) and 2) for the snow melting temperature threshold (2.10°C for deciduous forest, 2.32°C for coniferous forest, and 2.22°C for mixed forest) (USDA, 1985).

Results from the degree-day method were compared with historical snowpack water equivalent data obtained from a provincial model based on the Versatile Soil Moisture Budget (VSMB) (Akinremi *et al.*, 1996), which uses daily temperatures, precipitation, and Julian day for each township (Figure 2.4). Figure 5.3 presents the calculated and simulated (based on VSMB) snowpack water equivalent, showing a good correspondence in peak heights over time. These calculations are thus assumed to represent actual conditions since snowpack observations are not available in the area.

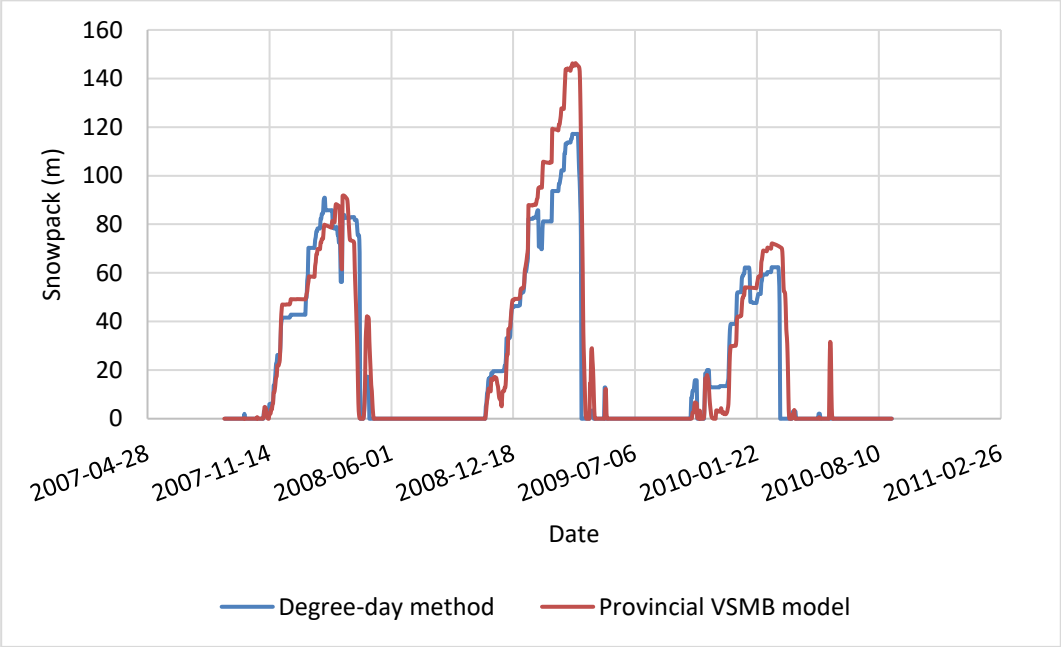

Figure 5.3. Calculated and observed snowpack water equivalent for the 2007-2010 period

6 HYDROGEOLOGICAL CHARACTERIZATION RESULTS

6.1 Water well data from the provincial database

The number of available data from the provincial database after the screening process for the 700 km^2 watershed are presented in Table 6.1. Well depth varies from 6 to 200 m with a median value of 60 m, while the static water level ranges between 7 and 74 m with a median value of 24 m. Based on the available lithological data, these wells appear to contain slightly more fine-grained rocks (including mudstone, siltstone and shale, 52%) than sandstone (46%) in the study area, but these percentages vary widely by well. The proportion of rock types in available wells are shown in Figure 6.1. The Paskapoo Formation is known to be soft (i.e. only weakly consolidated) and friable. Therefore, these water supply wells are typically cased, and screens are installed in the most permeable strata.

Table 6.1. Available water well data from the provincial database in the 700 km^2 study area.

Data	Number of available values after screening	Range (m)	Median value (m)
Lithology from well logs	250	-	-
Total well depth	329	6 – 200	60
Static water level	235	7 – 74	24
Dynamic water level and pumping rate during well development	151	-	-

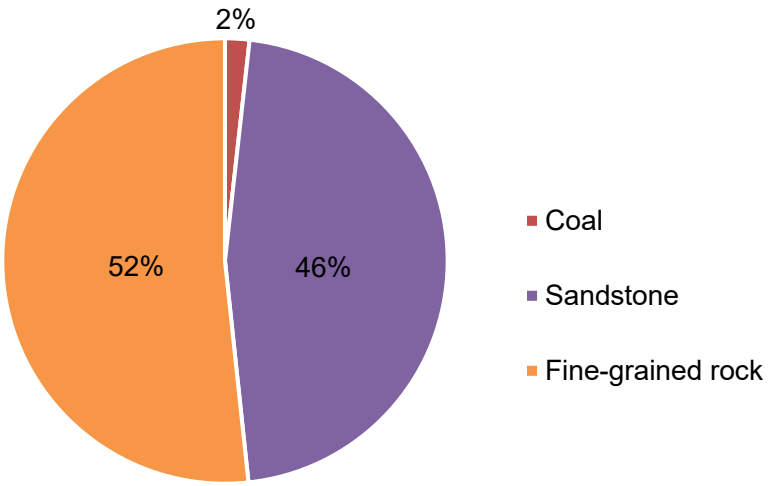

Figure 6.1. Proportions for the different rock types based on the well description of shallow wells located inside the Fox Creek study area (lithology from the provincial database).

The spatial distribution of the available wells is shown in Figure 6.2. The eastern part of the study area presents a higher density of wells, especially the north-eastern portion close to the Town of Fox Creek and Smoke Lake (not visible on this figure).

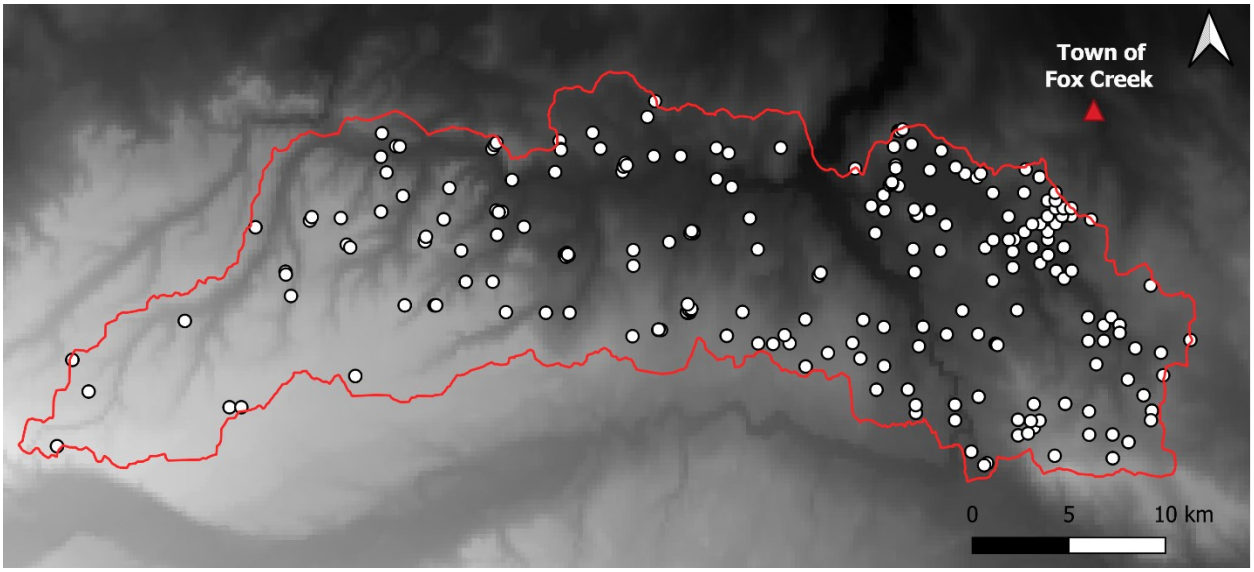

Figure 6.2. Spatial distribution of water wells inside the 700 km^2 study area.

The Sunchild aquifer, located in the Paskapoo Formation, is known to be more permeable due to the higher percentage of sandstone present than in the rest of the formation. However, its thickness in the study area ranges from 0 m to 100 m, with a median value of 59 m (Lyster & Andriashek, 2012), as illustrated in Figure 6.3. The provincial wells located within the Sunchild

aquifer in the study area only show a slightly higher percentage of sandstone (55%) than outside of it (48%). This likely suggests that the Sunchild aquifer zone in the study area is probably not more permeable than the rest of the Paskapoo Formation or simply that these wells are not actually completed in the Sunchild aquifer.

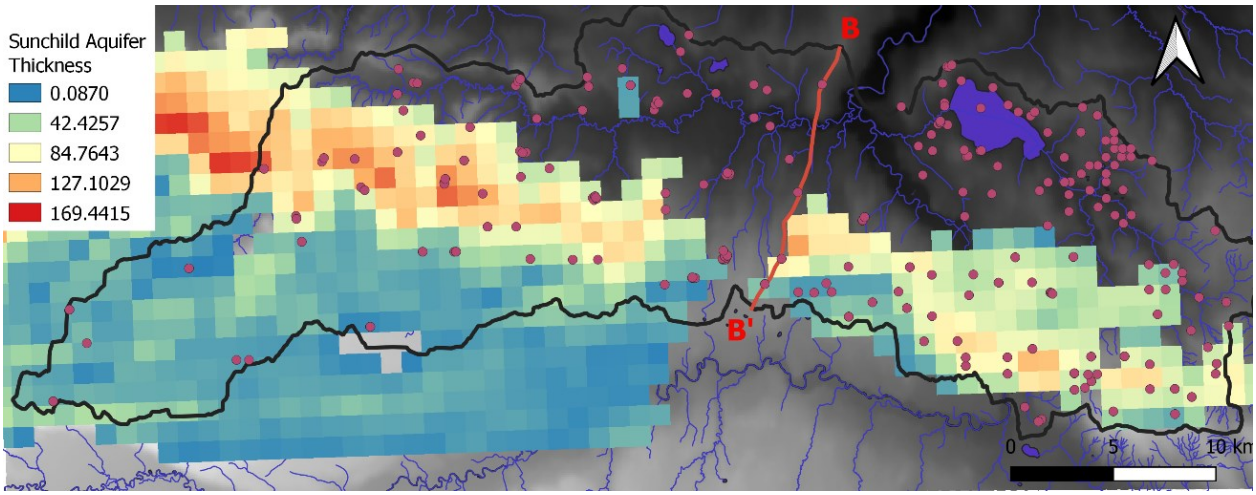

Figure 6.3. Sunchild aquifer thickness and wells logs over the study area

6.2 Well data from fieldwork

Some additional data come from the nine monitoring wells that were drilled in the Paskapoo Formation at various locations in the study area (Figure 6.4). Due to delays caused by the pandemic, the data available for this thesis only include groundwater levels in these wells and their geological descriptions.

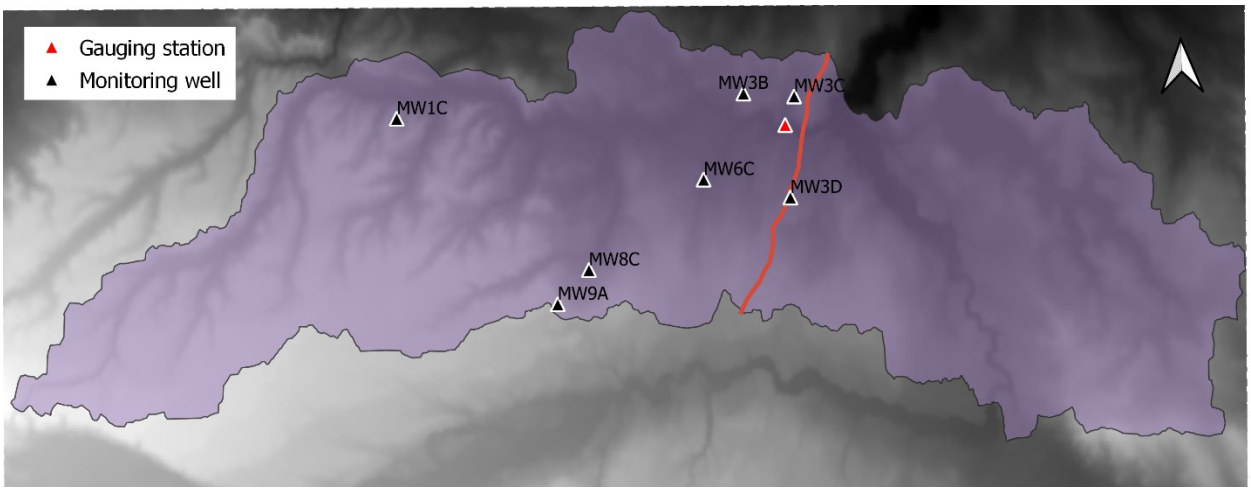

Figure 6.4. Location of the 8 monitoring wells drilled on Crown land. Well MW-10A was drilled on an active well pad and its location cannot be shown yet. The location of the gauging station is also shown.

Well depths vary from 35 to 90 m, with an average of ~50 m (Table 6.2), while the static water level ranges from 3.6 to 54.6 m, with a median value of 29 m. Groundwater generally follows the topography, showing the same behavior as the wells from the provincial database.

Table 6.2. Basic information on the nine monitoring wells

Site	Lat (WGS84)	Long (WGS84)	Z[1] (m)	Total drilled depth (m)	Overburden thickness (m)	Top of screen (depth in m below TOC) [2]	Static water level (m below TOC) [2]	% fine-grained rocks	% sandstone
MW-1C	54.36	-117.381	955	51.1	4.1	46.75	38.9	22.7	74.2
MW-3B	54.3783	-117.118	869	51	12.2	42.6	9.3	35.6	63.7
MW-3C	54.3769	-117.079	852	51.4	8.3	42	44.3	61.2	38.7
MW-3D	54.3322	-117.082	883	90	29.1	79.4	54.6	80	19.65
MW-6C (twin)	54.3403	-117.148	858	35	9.8	28	17.1	19.3	80.7
MW-6D (twin)	(next to MW-6-C)	(next to MW-6-C)	858	51	9.8	44	18.1	37.15	62.85
MW-8C	54.3005	-117.235	935	52	6.5	44.7	29.3	33.5	64.05
MW-9A	54.2854	-117.259	1049	52	13.9	40.6	28.2	61	35.65
MW-10A	On an active well pad		838	56	38	46.5	3.6	18.1	81.1

[1] Poor precision, in the order of 5 to 10 m.
[2] TOC: Top of casing (m)

The surficial sediment thickness varies from 8.3 to 38 m, with a median value of 12 m. The bedrock sections of these wells are generally dominated by sandstone (the percentage of sandstone is above 60% in 6 of them), but the percentage of fine-grained rock (shale, siltstone, and mudstone) varies from 18 to 80%. Figure 6.5 shows the rock types distribution in the nine monitoring wells.

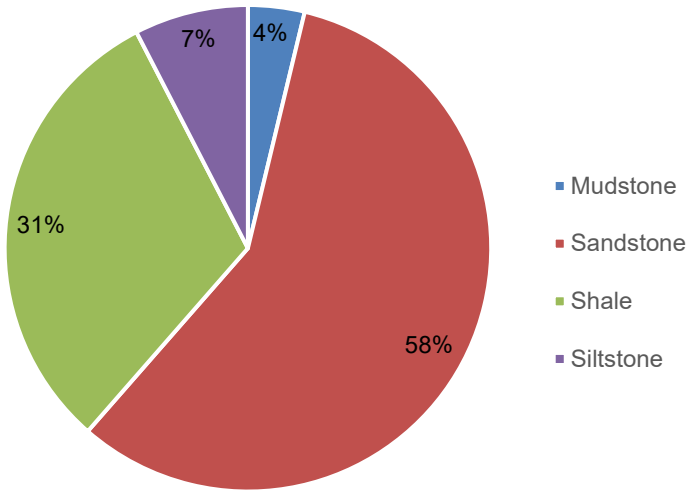

Figure 6.5. Percentage of rock types in the monitoring wells

6.3 Additional transmissivity and hydraulic conductivity values for the bedrock aquifer inferred from specific capacity values

In addition to the transmissivity (*T*) and hydraulic conductivity (*K*) values found in previous studies for the Paskapoo Formation (see section 4.7), specific capacity (*Cs*) values were calculated for the 151 water wells located within the study area for which static and dynamic water levels were available, as well as the pumping rate during well development. *Cs* represents an approximation for transmissivity and has the advantages of being simple to calculate and provide estimates for many wells, especially in areas where no, or only a few, *T* and *K* data are available.

Estimated *Cs* values range from 6.1 x 10^{-6} to 1.7 x 10^{-2} m^2/s, but most values lie between 7.8 x 10^{-5} and 2.1 x 10^{-4} m^2/s, with a median of 1.4 x 10^{-4} m^2/s. This range is narrower than that reported by Chen *et al.* (2007b), who used short pumping tests from wells located in the Calgary–Red Deer corridor (to the south of our study area) to estimate 1114 transmissivity values. Nonetheless, values obtained from *Cs* values compare well with those found by Chen *et al.* (2007b), as illustrated in Figure 6.6 using boxplots. The larger spread of the latter, as well as the important numbers of outliers, is likely due to a large extent to the much higher number of available data (1114 versus 151). This figure thus suggests that the *Cs* values found correspond to an acceptable approximation for transmissivity values for the study area.

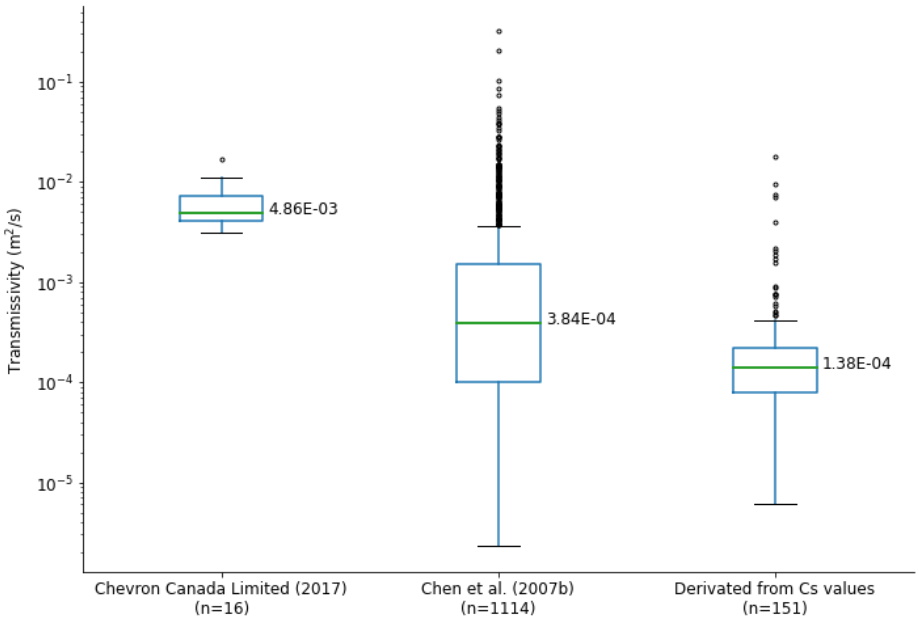

Figure 6.6. Comparison of transmissivity values derived from specific capacity (*Cs*) with values from Chevron Canada Limited and Chen *et al*. (2007b). Both Cs and Chevron values are representative of wells located in the study area, while Chen *et al*. (2007b) values

Figure 6.6 also shows *T* values from the 72 h pumping tests reported in the Chevron Canada Limited (2017) report. The Chevron wells show a much higher median value than the others (by an order of magnitude). This is certainly partly due to the fact that they contain more sandstone (~62%) than the average (~46% for all wells in the study area). Also, these wells have likely been selected for a pumping test because they had shown especially good yields during their drilling, while other wells with smaller yields may have been put aside (and thus, not tested).

A map showing the spatial distribution of available *Cs* values is presented in Figure 6.7. Three classes for the *Cs* values have been used to visualize its variability. The highest *Cs* values are found in the eastern part of the study area, and especially the north-eastern portion near the watershed outlet, while the lowest values seem to be found in the southwest, although very few values are available in this part of the study area.

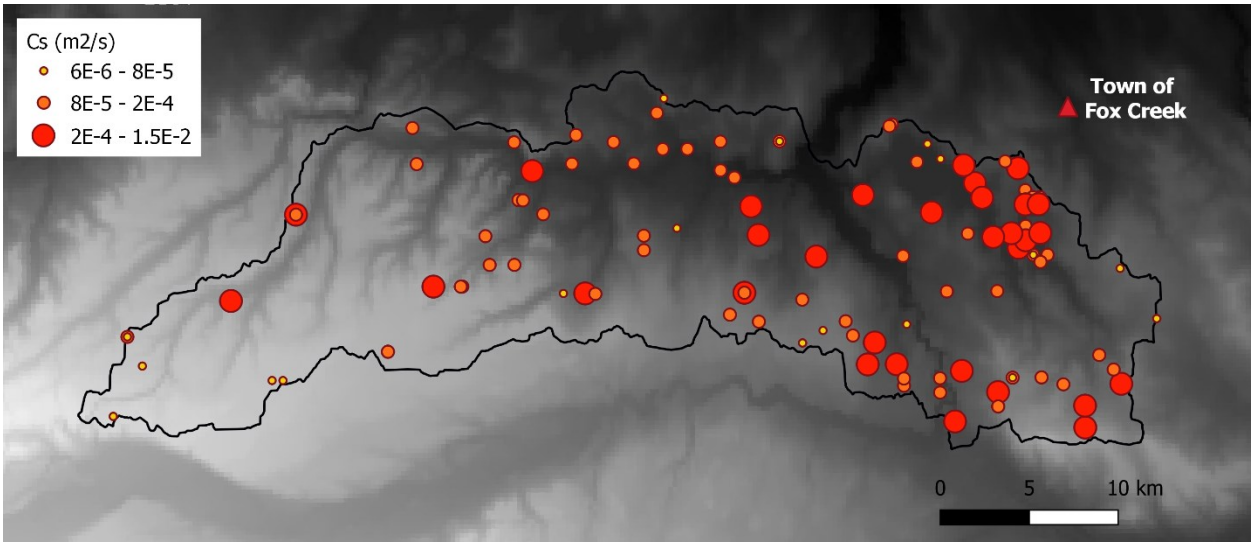

Figure 6.7. Spatial distribution of specific capacity (*Cs*) values.

Data from the provincial (AWWID) database show that the well-completion field for wells located in the study area mostly contains information on perforations (there are very few indications of screen installation). Perforation lengths range from 1.5 to 36 m with a median value of 5.8 m. Values in the 5-10 m range are by far the most frequent (Figure 6.8). This is not surprising since the maximum screen length is currently 7.6 m. Data on perforations were thus used to convert these transmissivity values into hydraulic conductivity values (using $K=Cs/b$).

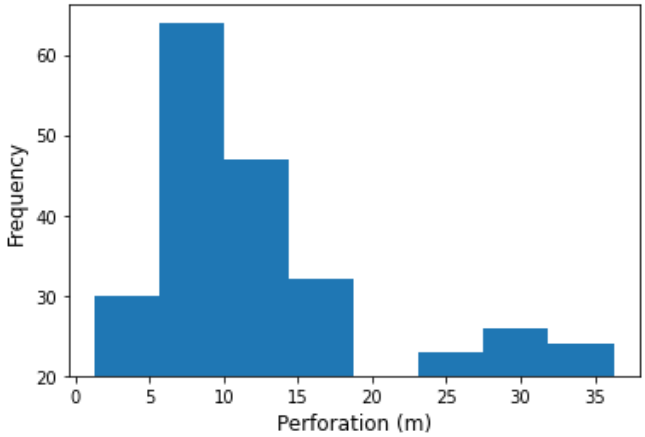

Figure 6.8. Histogram of lengths of perforated intervals.

Hydraulic conductivity values (inferred from specific capacity) range from to 3.4 x 10^{-7} m/s to 3.4 x 10^{-3} m/s, but most values lie between 9.2 x 10^{-6} and 2.4 x 10^{-5}, with a median of 1.4 x 10^{-5} m/s. In Figure 6.9, these *K* values are plotted against those obtained from 50 pumping tests by Hughes *et al.* (2017b) and from converted *T* values reported in the Chevron Canada Limited (2017) report. Values inferred from *Cs* spread over a larger interval (over four orders of magnitude) than those

obtained from pumping tests, likely due to the larger number of available data (151 versus 50 and 16). Nonetheless, they show a much smaller range between the 1st and 3rd quartiles (25-75 percentiles) than those from Hughes *et al.* (2017b), indicating less variable values for at least half of the available values. The lower median value found using *Cs* values (by at least an order of magnitude) probably reflects the fact that only "promising" wells (i.e., those that showed promising yields during drilling) underwent long-term pumping tests. Water wells in this region are indeed used primarily for hydraulic fracturing activities, which require high yields.

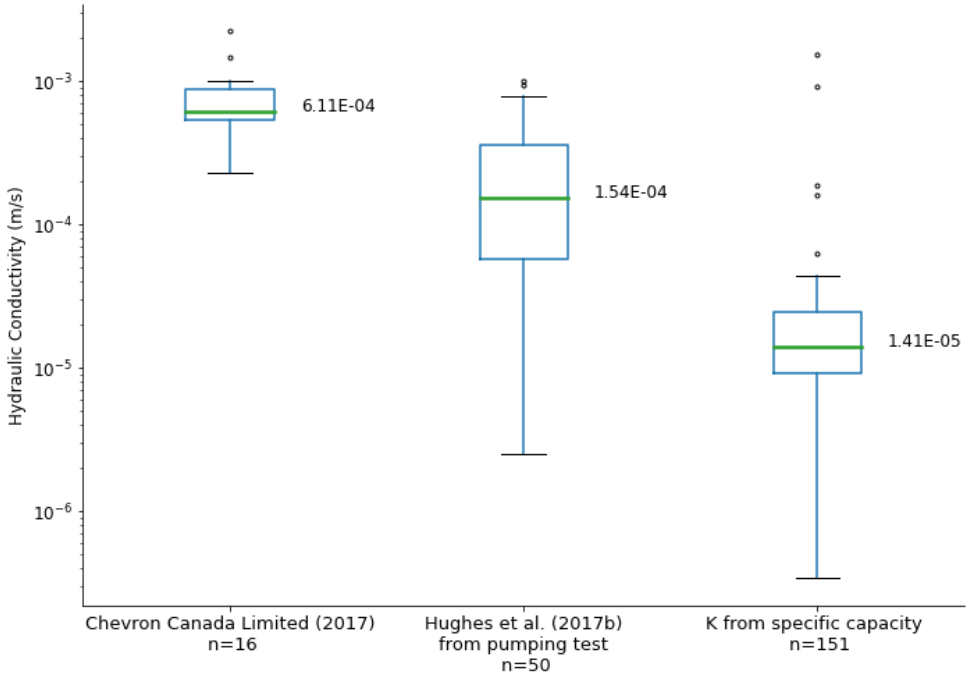

Figure 6.9. Hydraulic conductivity values available for the study area inferred from *Cs* compared to those found using pumping tests by Hughes *et al.* (2017b) and Chevron Canada Limited (2017). Although wells used by Hughes *et al.* (2017b) are located in the northern part of the Paskapoo Formation (Figure 4.6), only 18 fall within or very close to the study area.

Figure 6.10 shows the spatial distribution of hydraulic conductivity values presented in Figure 6.9. Three classes for the *K* values have been used. As expected, the *K* values inferred from *Cs* present the same behavior as *T* values from which they were derived (shown in Figure 6.7), with the highest values being in the eastern part of the study area. The *K* values from Hughes *et al.* (2017b) also show elevated values in the northeastern part, but very few data are available within the study area. The 16 *K* values from Chevron wells are clustered around three small areas in the center part of the study area.

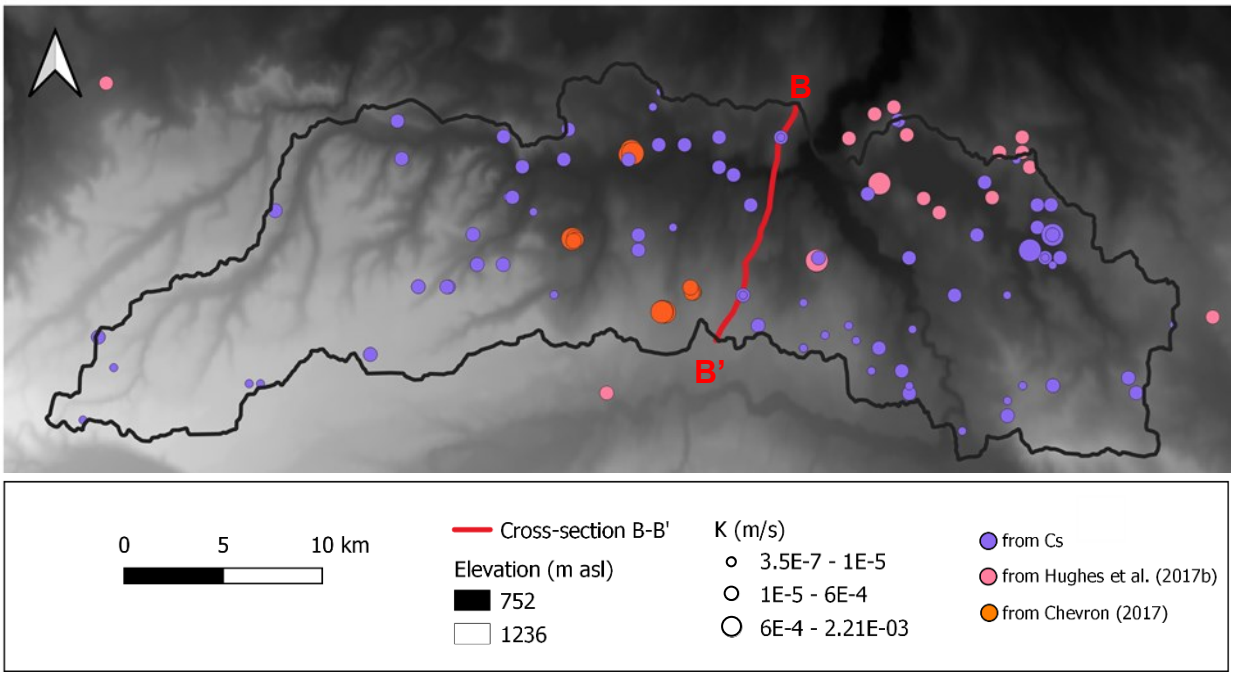

Figure 6.10. Spatial distribution of hydraulic conductivity values available for the study area (presented in Figure 6.9), i.e. inferred from specific capacity (*Cs*), from *T* values reported in Chevron Canada Limited (2017) and from pumping tests by Hughes *et al.* (2017b). Cross-section B-B' is the transect used for the 2D numerical model. The DEM is shown as a background.

6.4 Piezometric map

Figure 6.11 presents the piezometric map for the Paskapoo aquifer obtained using kriging with an external drift, derived from 249 water levels and using topography as the secondary variable. As expected, it shows that groundwater mostly flows from south to north in the Tony Creek sub-watershed towards the stream, closely following topography. Due to the interpolation method used, the estimated groundwater elevations are likely overestimated in some areas, such as in higher topographic areas. Nonetheless, it is strongly believed that this map provides a much more representative portrayal of real conditions than the first map that had been obtained using only groundwater elevations. There are different sources of uncertainty associated with this piezometric map, including the uncertainty in the water levels in the provincial database (which could comprise measurement errors and/or erroneous levels taken too soon after the well was drilled), the accuracy of the DEM (which is 5-10 m, see section 5.1), and the fact that the data were collected over several decades and various seasons. The piezometric map is considered representative of the study area scale, but likely contains an uncertainty of about 10 m (± 10 m). Therefore, it cannot be considered reliable at the local scale.

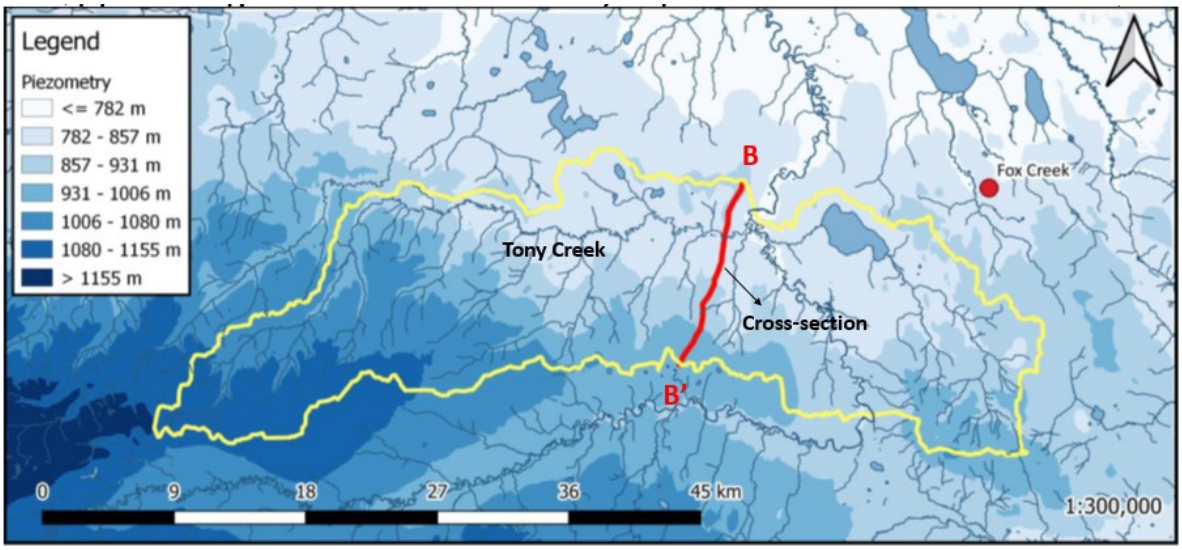

Figure 6.11. Piezometric map obtained using kriging with an external drift, based on available water levels in wells and topography. Cross-section B-B' is the transect used for the 2D numerical models.

6.5 Recharge

6.5.1 Preliminary water budget

The estimation of a first, very simplified water budget was attempted early in the project based on measurements of potential evapotranspiration from nearby weather stations and interpolated total precipitation data, to obtain an order of magnitude of the annual recharge rate in this study area. Only four years (2016-2019) of data are available for potential evapotranspiration for a grass reference surface. However, only rain data are available for these stations. The weighted average was calculated for the 2016-2019 period from townships to obtain total precipitation (see section 2.2). Different data sources are far from ideal, but provided a quick indication of the recharge for the study area.

Table 6.3 presents the weighted average total precipitation, mean evapotranspiration and the estimated water surplus for the available period (obtained from total precipitation minus potential evapotranspiration). This table suggests that recharge is quite small (even zero, in the case of the negative value of water surplus estimated for 2018) and highly variable from one year to another in this region.

Table 6.3. Water surplus in the Fox Creek study area with average total precipitation (Ptot) and evapotranspiration (ET).

Year	Ptot (mm/y)	ET (mm/y)	Water surplus (mm/y)
2016	768.6	693.3	75.3
2017	763.2	712.1	51.1
2018	621.1	685.7	-64.7
2019	749.9	596.6	153.3

6.5.2 Assessment of recharge using a water budget

The different components of the water budget, presented in the simplified water balance equation (11), were computed over a grid of 100 m x 100 m with GIS tools. The water budget was estimated on a monthly basis for a 20-year period. The 1991-2011 period was selected based on the availability of the measurements for precipitation and temperature. Because many types of data are scarce, a range of values for aquifer recharge was obtained from this water budget and previous studies.

6.5.2.1 Precipitation and temperature

Precipitation and temperatures for the assessment of the water budget was obtained from the Fox Creek Junction weather station (Government of Canada, 2020), based on its proximity to the study area and the fact that only about 7% of the data were missing (Table 6.4). However, data are only available for the 1991-2011 period (Table 6.4). Only one weather station, located 90 km from the town of Fox Creek, includes recent precipitation data from 2000 to 2020.

Table 6.4. Data from 1991 to 2011 (20 years) for the Fox Creek Junction weather station

Weather variable	T_{max}	T_{min}	T_{mean}	P_{tot}
Days with missing data	596	523	588	515
	-7.40%	-6.50%	-7.30%	-6.40%

Data from this station were processed using the GWHAT software (Gosselin *et al.*, 2017) to fill in the gaps using neighboring stations. To do this, neighboring stations with good correlation coefficients and similar time series were identified (Table 6.5). The gap-filling procedure in GWHAT is performed via an automated algorithm using the least-absolute-deviations method according to different selected criteria. In this case, the criteria include three meteorological stations with a maximal distance of 50 km from the Fox Creek Junction station and a maximum

elevation difference between the two stations of 350 m. Table 6.5 shows that the Meekwap, Pass Creek Lo, and Kaybob 3 stations fulfilled the distance and elevation difference criteria (although Pass Creek Lo slightly exceeds it by 6 m). Temperatures presented very good correlation coefficients, but not precipitation, with correlation coefficients below 0.7.

Table 6.5. Characteristics of neighboring weather stations to the Fox Creek Junction station. Data obtained from GWHAT.

Neighboring Stations	ΔAlt. (m)	Dist. (km)	Data	Correlation Coefficients			
				T_{max}	T_{min}	T_{mean}	P_{tot}
Meekwap	7	26.3	1989-2011	0.961	0.865	0.953	0.655
Pass Creek Lo	306.4	18.9	1954-2011	0.959	0.781	0.933	0.637
Kaybob 3	173.8	34.5	1973-2011	0.97	0.931	0.973	0.600
Eagle Lo	213.4	27	1958-2011	0.951	0.793	0.937	0.581

Figure 6.12 presents monthly values for rain, snow, as well as minimum and maximum temperatures for the selected 20-year period obtained with the Fox Creek Junction station complemented with the neighboring stations. An annual precipitation of 552 mm and an average annual temperature of 2.4 °C were obtained.

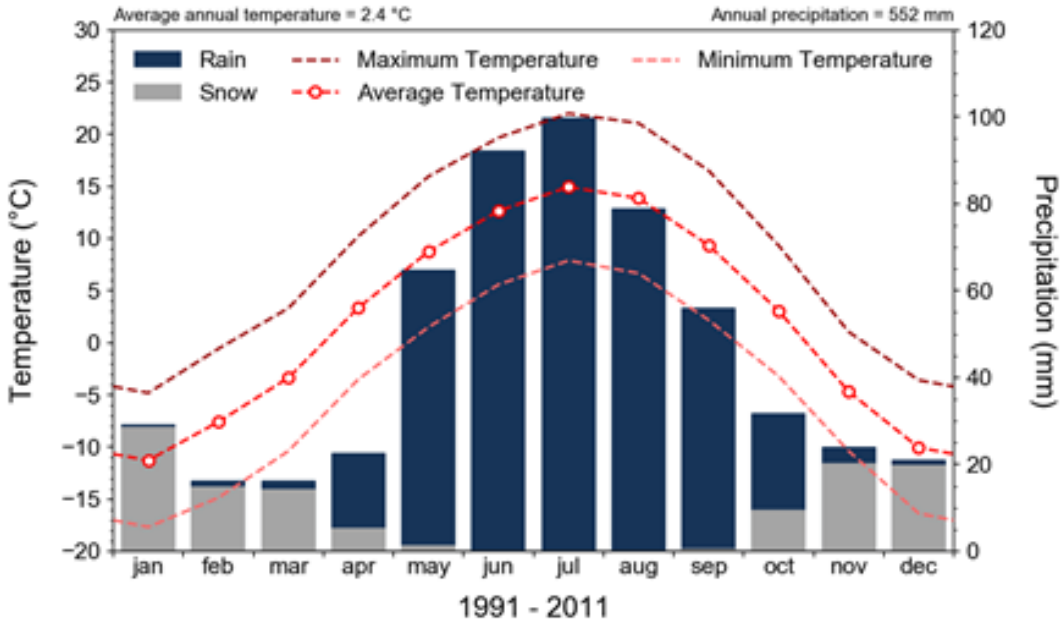

Figure 6.12. Gap-filled data series for precipitation and temperatures for the Fox Creek Junction station between 1991 and 2011. Data come from the Government of Canada (2020) and were processed using GWHAT software (Gosselin *et al.*, 2017) to fill in the gaps (graph taken directly from GWHAT)

These monthly precipitation rates were considered uniformly distributed over the watershed due to the lack of data, which likely underestimates precipitation up to 15% based on Figure 2.3. Precipitation from November to March was assumed to accumulate as snow on frozen ground (since their mean monthly temperature is below 0°C) ($P_{delayed}$) and to thaw in April, when mean daily temperatures are above zero, in order to estimate more realistically monthly values for recharge. Figure 6.13 shows the monthly values for rain, snow, precipitation, and delayed precipitation ($P_{delayed}$) used for the water budget.

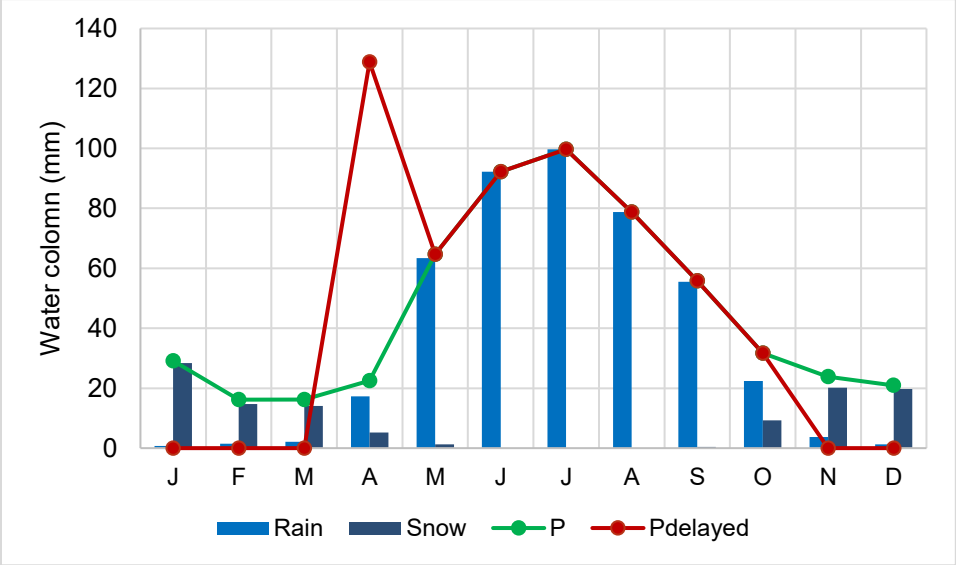

Figure 6.13. Accumulated and measured precipitation for the gap-filled Fox Creek Junction station. The delayed precipitation dataset was used for the water budget.

6.5.2.2 Evapotranspiration

Potential evapotranspiration (*ET*) was calculated with the Thornthwaite empirical method on a monthly basis (Thornthwaite, 1948), using the gap-filled data for average temperature. An annual value of 495 mm was found for evapotranspiration. A single value was used for the water budget since mereological stations had shown very little difference when temperature data were available. This evapotranspiration value seems to be high compared to precipitation. However, this value corresponds to potential *ET*. The Alberta Climate Information Service (2013) estimated that the evapotranspiration rate in Alberta is on average about 74% of the precipitation and can even be higher than precipitation, notably in the boreal plains (Devito *et al.*, 2005). For this study area, the average evapotranspiration corresponds to 90% of the annual precipitation (495 mm/y versus 552 mm/y of total precipitation). Due to its importance in the water budget of this region and the fact that very little information is available, evapotranspiration will be measured using four stations as part of another MSc thesis within the GSC project.

6.5.2.3 Runoff

Runoff was calculated using the SCS curve number method (USDA, 1985). The soil type map confirms that the dominant soil types are B and D, corresponding to a provincial classification of sand, clay, and silt percentages. The western part of the study area is dominated by soil type D, containing more permeable soils, while the eastern part appears to be less permeable (soil type B). The land cover in the study area is dominated mainly by forests: needleleaf, broadleaf, and mixed forest cover 80% of the watershed.

The CN numbers for the study area vary from 55 to 93, with a median value of 64 (Figure 6.14). There is a marked difference between the western and eastern parts of the study area, for the CN numbers and hence for the runoff values, due to the distribution of soil types B and D. An annual overall runoff rate of 151 mm was found for the entire Fox Creek area (Figure 6.15). However, these high values for runoff are very unlikely since evapotranspiration is high, leaving little water available for runoff or sub-runoff. The general SCS curves should ideally be adapted to a given region (as Monfet (1979) did for Quebec), but this has not been done for the Canadian Prairies to our knowledge. We thus believe that runoff (including sub-runoff) is significantly less than the values found here.

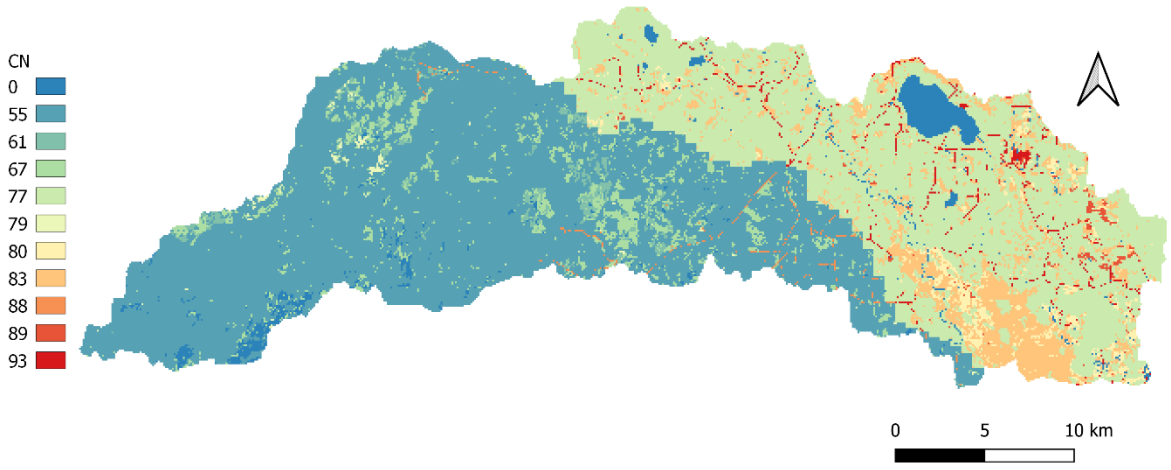

Figure 6.14. Curve number for each cell of the study area.

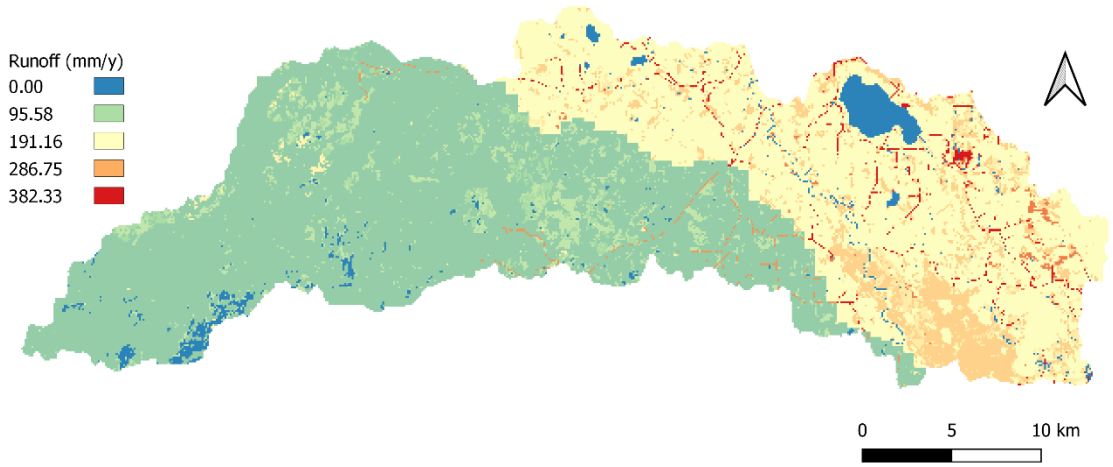

Figure 6.15. Potential runoff map of the study area.

Figure 6.16 shows a summary of total precipitation, evapotranspiration, and runoff obtained from the water budget for the 1991-2011 period. The sum of evapotranspiration and runoff exceeds total precipitation, to varying degrees.

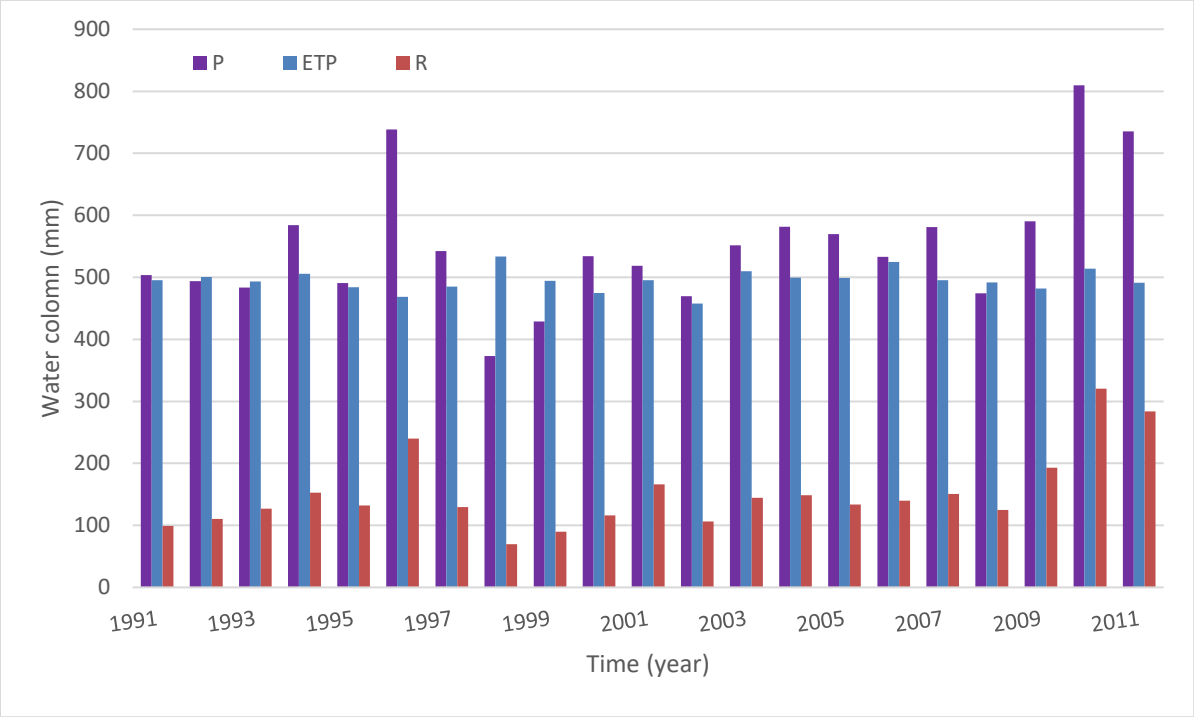

Figure 6.16. Precipitation, evapotranspiration, and runoff for the 1991-2011 period.

Table 6.6 presents three different sets of annual values for the water budget components, based on different assumptions. The first value of recharge (70 mm/y) corresponds to the estimate from the provincial study that used weather data from the Town of Fox Creek and considered runoff to be negligible (Smerdon *et al.*, 2019). The second value (57 mm/y) comes from the water budget

estimated here, also considering the runoff to be negligible. The third value uses the same water budget estimates, but this time considering runoff. Since recharge rates were often negative when using the spatially distributed values found via the SCS curves, a zero-recharge scenario is also deemed possible, and hence a recharge range from 0 to 70 mm was retained. These values are within the range of previously identified recharge values for the Canadian Prairies (from 0 to 65 mm/y in the northern part of the Edmonton-Calgary corridor, with the greatest values for the western portion of the corridor, decreasing towards the east) (Barker *et al.*, 2011). Figure 6.17 shows the monthly distribution of recharge values with and without runoff. Recharge is zero from May to September since the evapotranspiration is higher than the precipitation, which appears to be quite common for this region.

Table 6.6. Mean values for the different water budget components for the Fox Creek area, including recharge rates.

	Precipitation (mm/y)	Evapotranspiration (mm/y)	Runoff (mm/y)	Recharge (mm/y)
Smerdon *et al*. (2019)	595	525	-	70
Water budget without runoff	552	495	-	57
Water budget including runoff	552	495	151	0

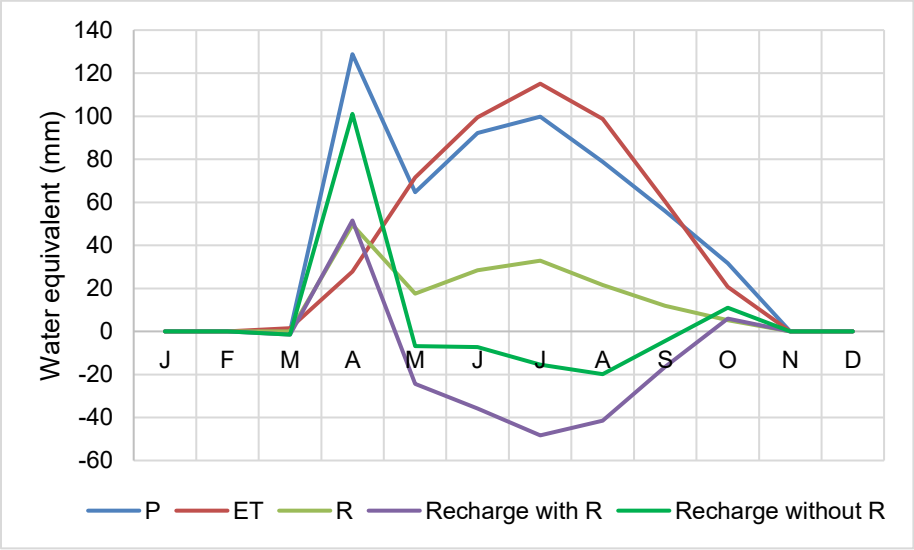

Figure 6.17. Monthly values for P (total precipitation), ET (potential evapotranspiration), R (potential runoff), and recharge from the water budget. Recharge is considered to be zero when plotted as negative.

7 MODELING RESULTS

7.1 Conceptual model

Figure 7.1 presents the 2D conceptual model that was later used for the numerical models. The vertical boundaries on each side of the cross-section B-B' (see its location in Figure 6.11), corresponding to the watershed physical limits, were assigned a no-flow type boundary in the Paskapoo, Scollard, and Battle formations. In the Wapiti formation, a fixed head was assigned on each side based on values from the piezometric map developed by (Singh & Nakevska, 2019). At the location of Tony Creek, a fixed hydraulic head was assigned to represent this small stream based on topography. Finally, a recharge rate of 70 mm/y, based on the value reported in Smerdon *et al*. (2019), was assigned to the top layer. The modeled cross-section is approximately 13 km long with a maximum depth of 1.2 km.

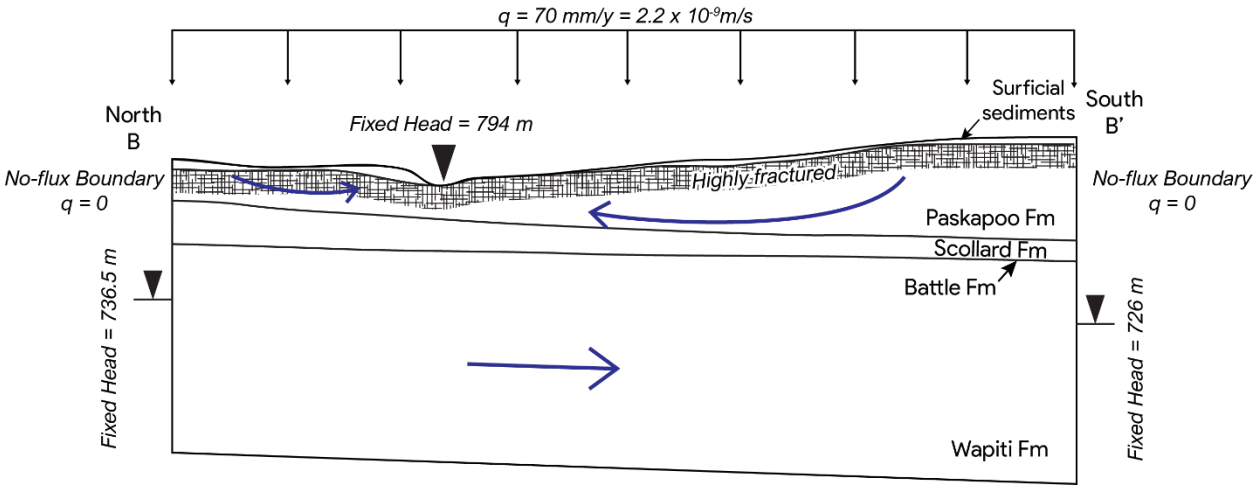

Figure 7.1. 2D conceptual model for the B-B' cross-section. The location of the cross-section within the Fox Creek watershed is shown in Figure 6.11.

The topography (top and bottom) of the bedrock formations for the B-B' cross-section modeled in FLONET and then in CATHY was extracted from Corlett *et al.* (2019) and is shown in Figure 7.1 and Figure 7.2. Note that the surficial sediment cover, which is generally thin and permeable, was not considered in the FLONET model.

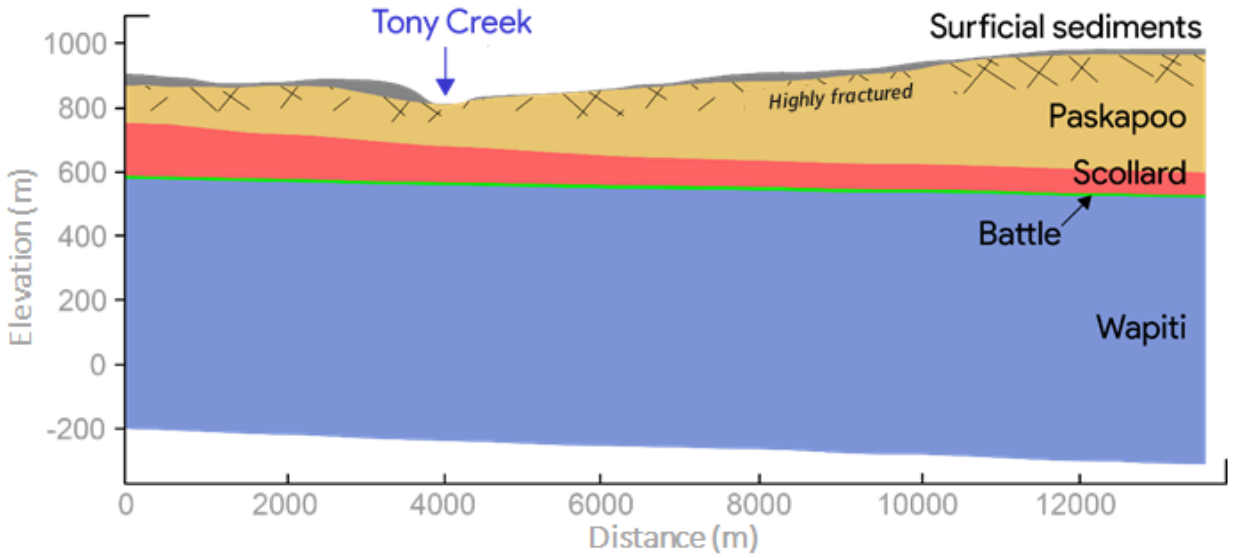

Figure 7.2. Cross-section B-B' in the Fox Creek study area (adapted from Corlett *et al.*, 2019). Note: surficial sediments are not included in the FLONET model.

7.2 FLONET model

7.2.1 General model description and preliminary calibration

The mesh for the FLONET simulations, generated using the GRID auxiliary program, is composed of 23,001 deformable elements (Figure 7.3). The size of the elements gradually increases vertically with depth to avoid disproportionate mesh and numerical instabilities. The initial vertical element size varies from 3 m close to the top of the model to 50 m at its base. The horizontal width was fixed to ~30 m, except for the cells close to Tony Creek, where the mesh width was refined to 10 m (Table 7.1). Nonetheless, the deformed final mesh presented smaller size elements in the vertical direction than those initially assigned. These smaller cells are generated during the simulation since they are allowed to deform vertically to account for any hydraulic head difference between iterations. The minimum possible size, in the vertical direction, was set at 0.1 m. The smallest vertical cell size achieved during the simulation is 0.15 m and is located at Tony Creek. The model is discretized into 51 layers and 451 rows.

Smaller mesh sizes for the top layer were also tested to investigate the influence of the mesh in the modeling. However, as cells are allowed to deform until 0.1 m, the deformed mesh did not present a significant change.

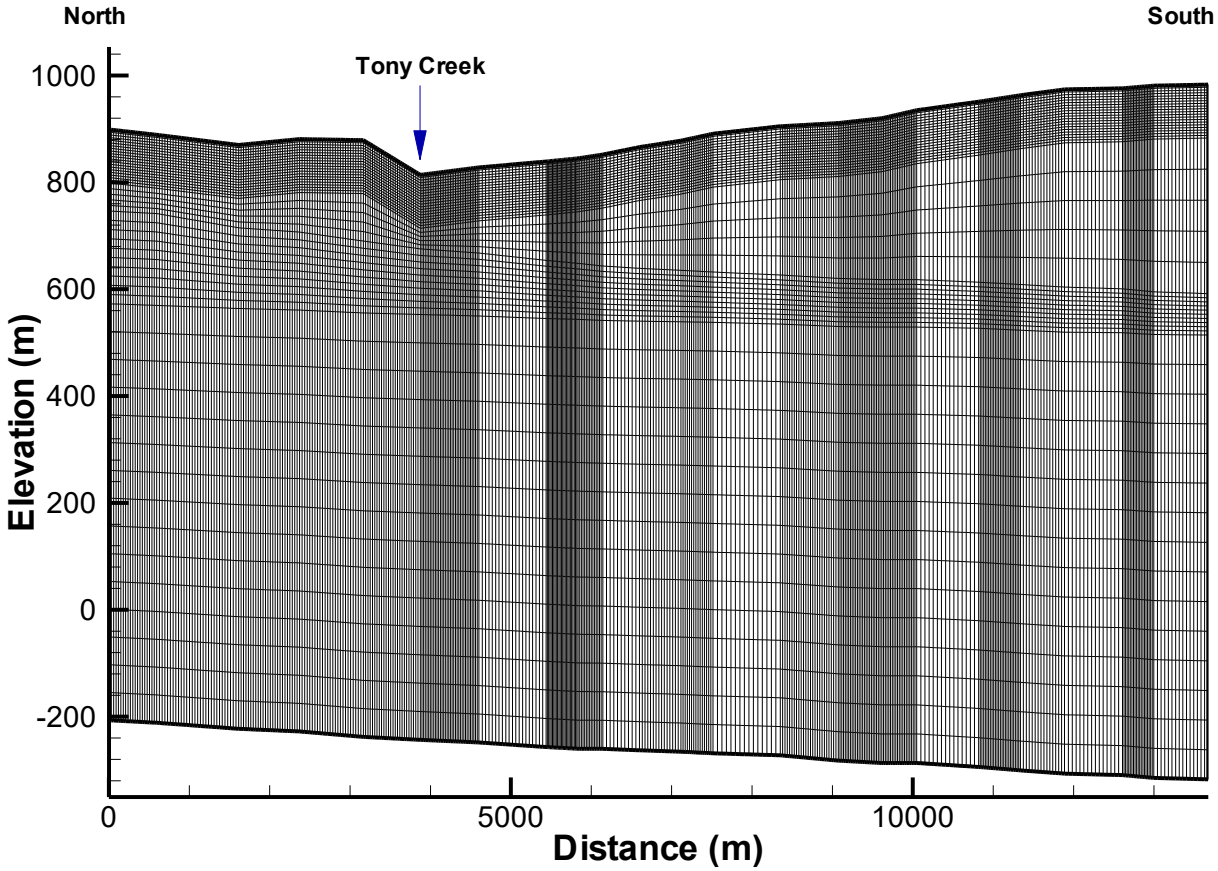

Figure 7.3. Representation of the FLONET mesh for cross-section B-B'.

Table 7.1. Characteristics of the 2D FLONET model mesh.

Bedrock formation	Number of layers	Vertical element size (m)	Horizontal element size (m)*
Paskapoo 1 (0-100 m)	18	~3	~30
Paskapoo 2 (>100 m)	10	~5	~30
Scollard	7	~10	~30
Battle	1	~10	~30
Wapiti 1 (0 – 500 m)	8	~50	~30
Wapiti 2 (500 – 1000 m)	7	~50	~30

*Except close to Tony Creek

The mean hydraulic conductivity values assigned initially to each unit are shown in Table 7.2, along with their reference. As mentioned in section 5.44, the Paskapoo Formation was divided into two sections, referred to here as Paskapoo 1 and Paskapoo 2, to consider the more fractured zone in the first 100 m. Similarly, the Wapiti Formation was divided into an upper and a lower unit, based on its known characteristics. Values for the Scollard, Battle and Wapiti formations correspond to those presented in Table 4.2. An anisotropy ratio of Kh/Kv=10 was assigned to the upper part of the Paskapoo Formation to take into account the presence of sub-horizontal fractures (section 4.7).

Table 7.2. Initial hydraulic conductivity used for the 2D FLONET model.

Formation	*K* value (m/s)	Reference
Paskapoo 1 (0-100 m)	2.4×10^{-4}	Median from pumping tests (Hughes *et al.* 2017b) (see Figure 4.6)
Paskapoo 2 (>100 m)	1.08×10^{-8}	Median found using mini-permeameters (Hughes *et al.*, 2017a; Riddell *et al.,* 2009; Grasby *et al.,* 2007) (see Figure 4.7)
Scollard	1.1×10^{-8}	Median found using mini-permeameters (Riddell *et al.,* 2009)
Battle	2.9×10^{-9}	Median found using mini-permeameters (Riddell *et al.,* 2009)
Wapiti 1 (0 – 500 m)	2.6×10^{-6}	From Smerdon *et al.* (2019)
Wapiti 2 (500 – 1000 m)	2.6×10^{-8}	From Smerdon *et al*. (2019)

At first, when using for the upper part of the Paskapoo Formation the median value obtained from pumping tests, the simulated water table was too low compared to the interpolated water table (obtained from the piezometric map) across the transect. To increase the simulated water table, the *K* value for Paskapoo 1 was then decreased to the median value found using the specific capacity values (K=1.4 x 10^{-5} m/s, see Figure 6.9), which is nearly an order of magnitude lower. It can be argued in fact, that this value is more representative of this specific region than a value derived from 50 pumping tests conducted in more promising wells across the northern part of the Paskapoo Formation (see Figure 4.6). While the simulated water table was now closer to the interpolated one in the southern portion of the transect, it was still slighty below the interpolated water table in the northern part. The *K* value for Paskapoo 1 was thus decreased to the first quartile value found using specific capacity (K=9.5 x 10^{-6} m/s). The water table became too high in the southern part and still a little too low in the northern part. Different anisotropy factors were

assigned while keeping the initial horizontal hydraulic conductivity value. However, the model showed little sensitivity to this parameter (see section 7.2.2.2).

Therefore, it was decided to divide the upper portion of the Paskapoo Formation (Paskapoo 1) into two zones (Paskapoo 1.1, south to Tony Creek, and Paskapoo 1.2, north to Tony Creek; see Figure 7.4), based on the fact that the southern part is within or very close to the Sunchild aquifer (see Figure 2.5 (b)), which is characterized by more sandstone and should thus be more permeable than the northern part. This is also suggested by the logs of two wells and their *K* values inferred from *Cs* close to cross-section B-B' (see Figure 6.10), both north and south of Tony Creek.

For Paskapoo 1.1 (to the north), the *K* value was decreased to 7.1 x 10^{-6} m/s, which corresponds to a value slightly lower than the first quartile derived from *Cs,* but remains within the range of plausible values (see Figure 6.9). Paskapoo 1.2 (to the south) was assigned a *K* value of 1.15 x 10^{-5} m/s, a value between the median and the first quartile obtained from *C*s values, which provided a better match with the interpolated water table.

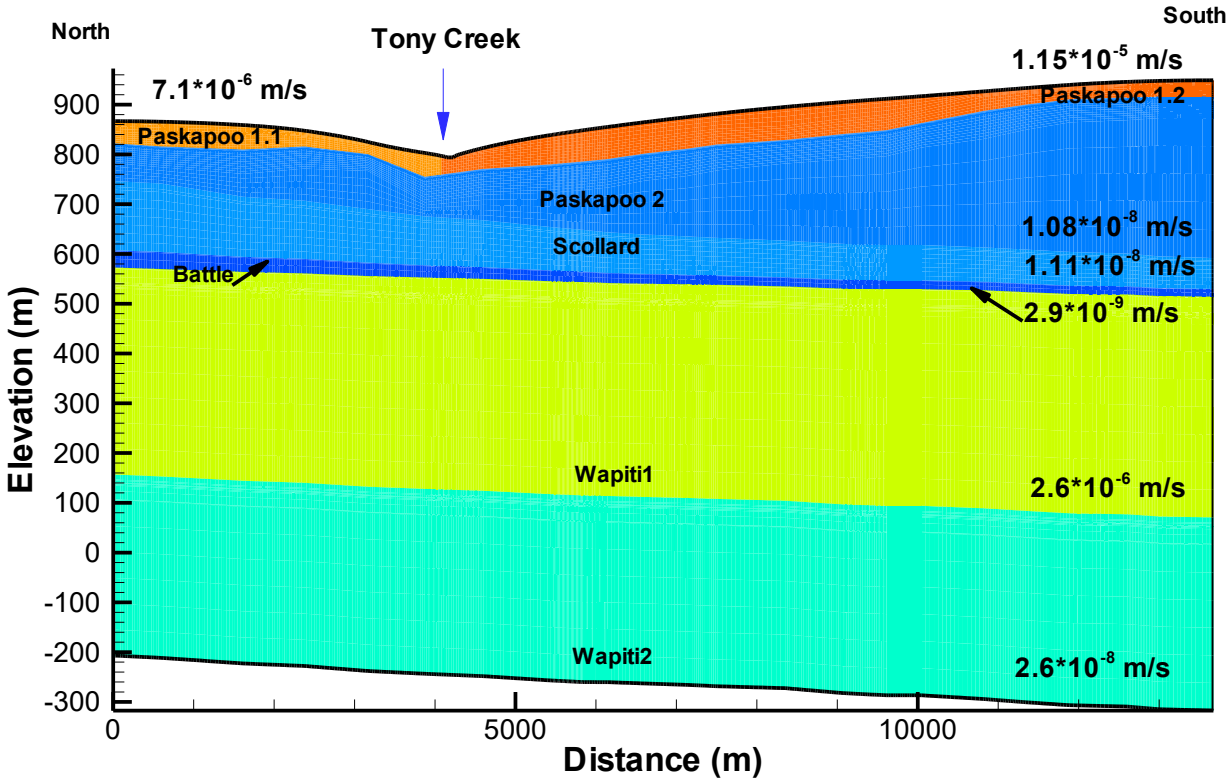

Figure 7.4. Hydraulic Conductivity values *(K)* in the B-B' transect after preliminary calibration with two sections in the upper part of the Paskapoo Formation.

A relatively good match for the water table was found using the values shown in Figure 7.4, while the rest of the formations were kept unchanged (corresponding to the values from Table 7.2). Figure 7.5 shows that the modeled water table is either slightly higher or lower in the southern part than the interpolated water table (and even above the ground surface at the 6 km distance).

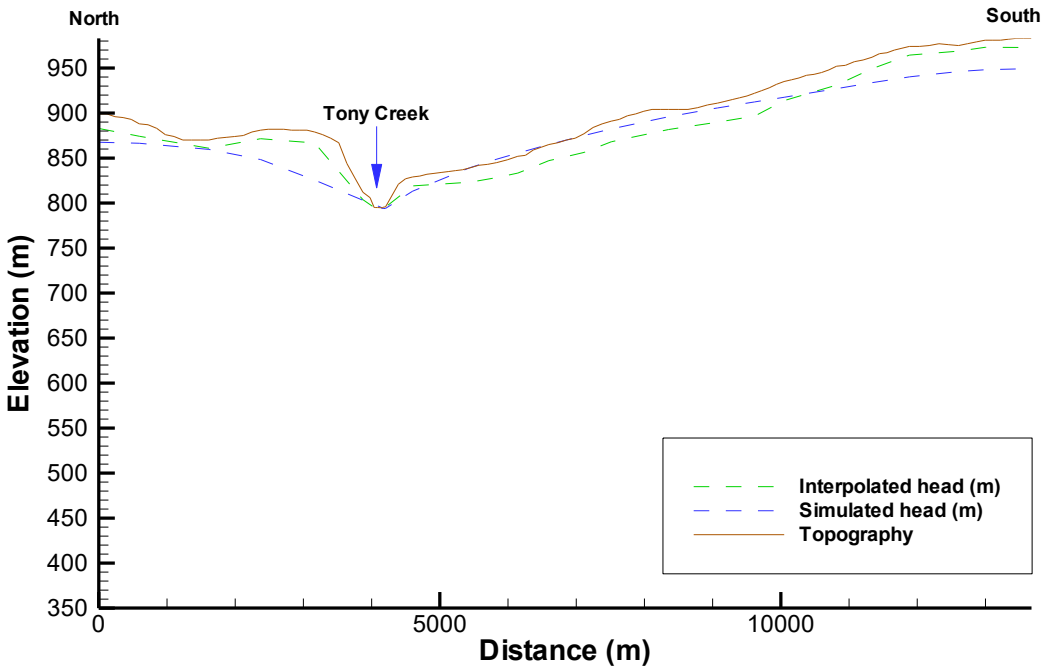

Figure 7.5. Comparison of the simulated hydraulic heads obtained after the preliminary calibration process using values shown in Figure 7.4 with those extracted from the piezometric map along the B-B' profile. Note that in the simulated case, a fixed hydraulic head was assigned at Tony Creek at the top of the first layer

The root mean square error (RMSE) between the simulated and interpolated hydraulic heads was 15.85 m, corresponding to 8.9% of the difference between the maximal and minimal water table elevations along cross-section B-B' (hydraulic heads varying between 795 to 973 m, thus having a difference of 178 m). Note that the RMSE obtained is relatively high, mostly due to the local mound just north of Tony Creek. However, as mentioned in section 6.4, the actual water table is probably lower than what is shown in Figure 7.5 since the interpolation method used (kriging with an external drift using topography as the secondary parameter) for the piezometric map likely overestimates the water table elevation, especially in topographic highs when very few or no wells are available. Excluding the mound north of Tony Creek, the RMSE decreases to 13.98 m, corresponding to 7.84%. Thus, the error on simulated heads is still slightly above the 5% acceptability threshold for groundwater models with hydraulic head calibration suggested by Anderson and Woessner (1992).

This preliminary calibration process showed, not surprisingly, that the hydraulic conductivity values of the Paskapoo Formation (especially those of Paskapoo 1) were the parameters with the greatest impact on the model response. In contrast, the model was not very sensitive to the hydraulic conductivities of the underlying formations (Scollard, Battle, and Wapiti).

Although the piezometric map is not considered flawless, an attempt was made to obtain a better match with the interpolated water table. To do so, a third section (Paskapoo 1.3) in the upper part of the Paskapoo Formation (Paskapoo 1) was introduced in the southernmost portion of the cross-section B-B' (Figure 7.6). A hydraulic conductivity of 5.5×10^{-6} m/s was assigned to this new section, allowing for improved RMSE. The use of this lower hydraulic conductivity (by about half an order of magnitude) is inconsistent with the presence of the Sunchild aquifer. Nonetheless, it can be justified by the fact that four well logs from the provincial database, along this short section, have a much lower percentage of sandstone than those located along the Paskapoo 1.2 and even Paskapoo 1.1 sections, even though Paskapoo 1.3 borders the Sunchild aquifer and should thus theoretically have higher values. Figure 7.7 presents the location of the four wells over the cross-section, with their percentage of sandstone and fine-grained rocks (shale, mudstone, and siltstone). Based on these data, the two northernmost wells have the highest percentage of sandstone (50 and 81%), while the two southernmost wells are dominated by fine-grained rock (53% and 75%). These percentages suggest, as in section 6.1, that the Sunchild aquifer may not be present in the study area or may simply be too shallow for these wells to be representative of this permeable aquifer.

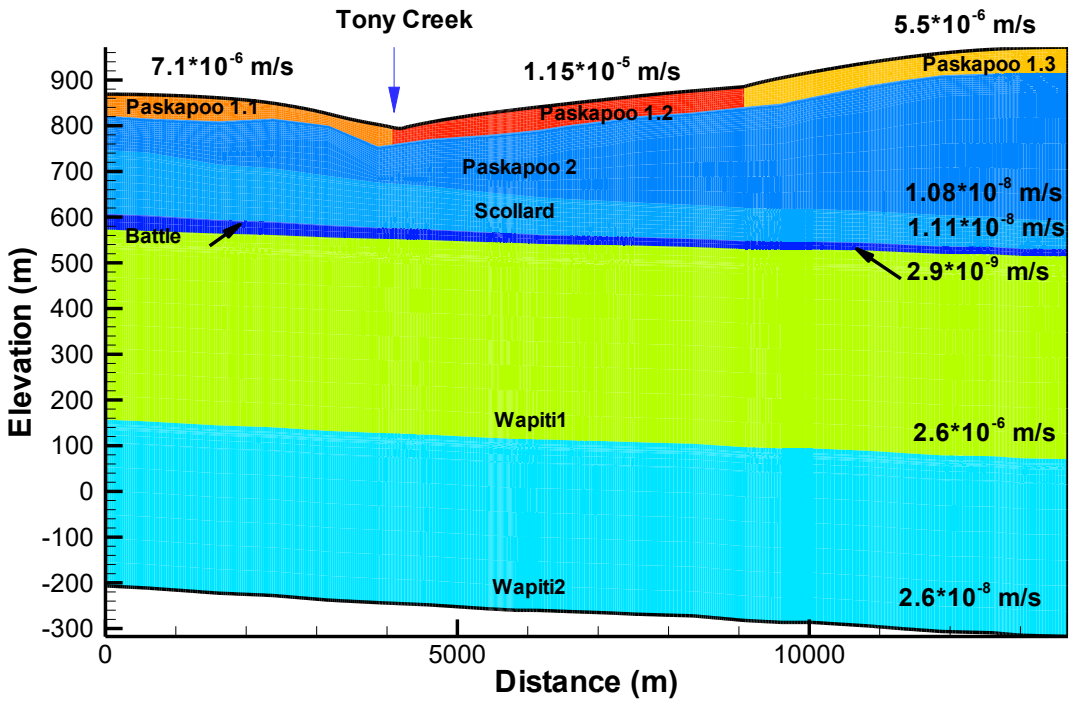

Figure 7.6. Hydraulic conductivity values (*K*) in the B-B' transect with three sections (Paskapoo 1.1, 1.2, and 1.3) in the Paskapoo 1 for the preliminary calibration.

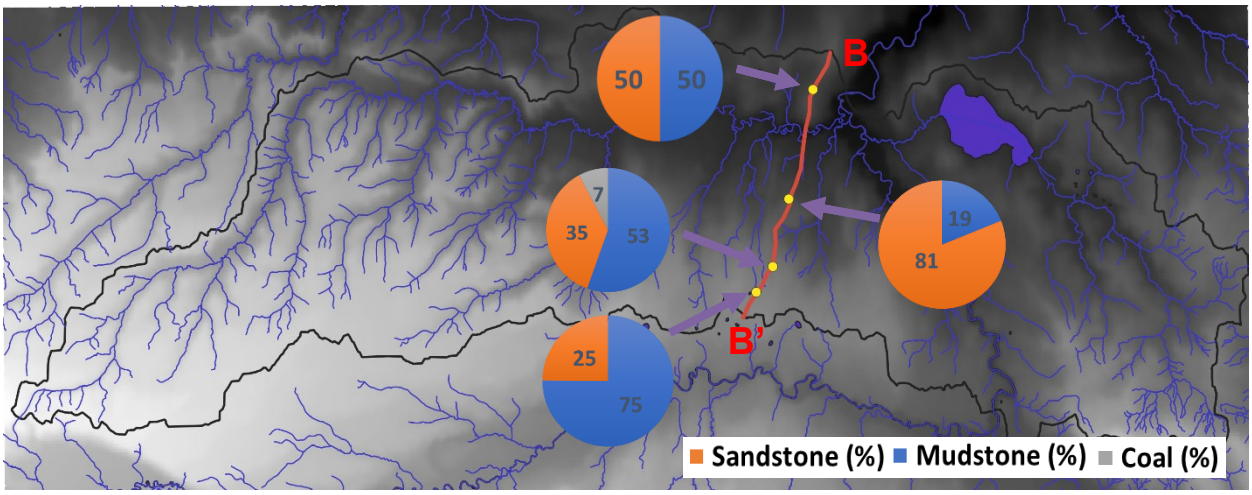

Figure 7.7. Rock types from wells located along the cross-section B-B'.

Using these three sections (Paskapoo 1.1, 1.2, and 1.3, see Table 7.3) reduced the RMSE to 13.57 m, a non-negligible improvement of nearly 15%. The other *K* values (for the underlying formations) remained unchanged. This scenario corresponds to 7.6% of the total difference between the maximum and minimum hydraulic head elevations over the cross-section.

Table 7.3. Hydraulic conductivity (*K*) obtained after the preliminary calibration, using three sections in the Paskapoo upper part (Paskapoo 1)

Formation	*K* value (m/s)	Reference or justification
Paskapoo 1.1	7.1×10^{-6}	Plausible values within the range of *K* values inferred from *Cs* values (see section 6.3)
Paskapoo 1.2	1.15×10^{-5}	
Paskapoo 1.3	5.5×10^{-6}	
Paskapoo 2	1.08×10^{-8}	From mini-permeameters (Grasby *et al.*, 2007; Hughes *et al.*, 2017b; Riddell *et al.*, 2009)

To investigate other possible combinations of hydraulic conductivities and recharge rate, simulations were performed using recharge rate values ranging from 0 to 70 mm/y, considered the plausible range for this region (see section 6.5). Hydraulic conductivity values had to be decreased significantly compared to the previous scenarios to increase the water table when using a value lower than 70 mm/y for the simulated hydraulic heads to be close to the interpolated water table. Results showed that for a recharge of 10 mm/y, the *K* values of the Paskapoo Formation had to be decreased by an order of magnitude, while for a recharge of 40 mm/y, they had to be decreased by half an order of magnitude. However, the *K* values found previously for a recharge of 70 mm/y are already slightly below the 1st quartile of the values obtained with *Cs*, shown in the boxplot of Figure 6.9. Therefore, these scenarios using lower recharge rates were discarded because it seemed difficult to justify using even lower *K* values.

Different boundary conditions were initially tested, including fixed hydraulic heads assigned to each side of the model along the Paskapoo and Scollard formations, based on values from the surficial piezometric map (Figure 6.11). The results of these simulations showed a good match between the simulated and interpolated water table. However, these results were not very sensitive to changes, such as increasing or decreasing *K* values, clearly indicating that the model was too constrained. Therefore, a no-flow boundary condition was assigned to the Paskapoo, Scollard, and Battle formations for all the simulations presented in this chapter.

7.2.2 Optimal scenario using a sensitivity analysis

A systematic sensitivity analysis was performed to try to decrease further the RMSE and to study the impact of the different input parameters on the flow model response quantitatively. A one-at-a-time (OAT) sensitivity analysis, in which one input parameter is varied while the others are fixed, was implemented.

First, each hydraulic conductivity value of the Paskapoo Formation was changed by a small percentage compared to the base case scenario (corresponding to the scenario that provided the minimum RMSE previously discussed), while all the other parameters were kept at their previously “calibrated” values, since hydraulic conductivity is the parameter with the most significant impact. Then, different anisotropy ratios were investigated. The sensitivity of the model was evaluated using the corresponding change in the magnitude of the calculated RMSE between the simulated and interpolated hydraulic heads.

The preliminary calibration process had identified the most sensitive parameters of the flow model, which are, in decreasing order of importance: hydraulic conductivity (*K*) of the Paskapoo 1.2, 1.3, and 1.1 sections, and *K* in the Paskapoo 2 section. The input recharge rate was also tested.

7.2.2.1 Hydraulic conductivity of the Paskapoo Formation

The hydraulic conductivity values of the three sections of the upper part of the Paskapoo Formation were changed by a certain percentage to find the local minimum RMSE value. The Paskapoo 1.2 and 1.3 sections were optimized first since they showed a much higher sensitivity than the Paskapoo 1.1 section to the north of Tony Creek during the preliminary calibration. Hydraulic conductivity values for Paskapoo 1.1 and 2 were investigated in a second step.

i. Paskapoo 1.2

For the Paskapoo 1.2 section, located just south of Tony Creek, simulations using ranges from 70% to 190% of the "calibrated" *K* value (K= 1.15 x 10^{-5} m/s) were performed. Figure 7.8 shows the RMSE values obtained as a function of the different percentages (multipliers) used. The optimal *K* value for the Paskapoo 1.2 section was found to be 1.8 x 10^{-5} m/s, which corresponds to 157% of the initial value, with an RMSE error of 10.66 m (corresponding to 5.71% of the total elevation difference over the cross-section), which represents an improvement of over 20% compared to the base case (with an RMSE of 13.57 m).

Figure 7.8 shows that the errors (RMSE values) increase more rapidly when *K* values are reduced than when they are increased, likely due to the fact that although the same amount of water is present (same recharge rate), less water is able to flow (“drain”) towards Tony Creek, so the water table rises rapidly. Paskapoo 1.2 is the most sensitive segment due to its downstream position along the longest transect (southern side).

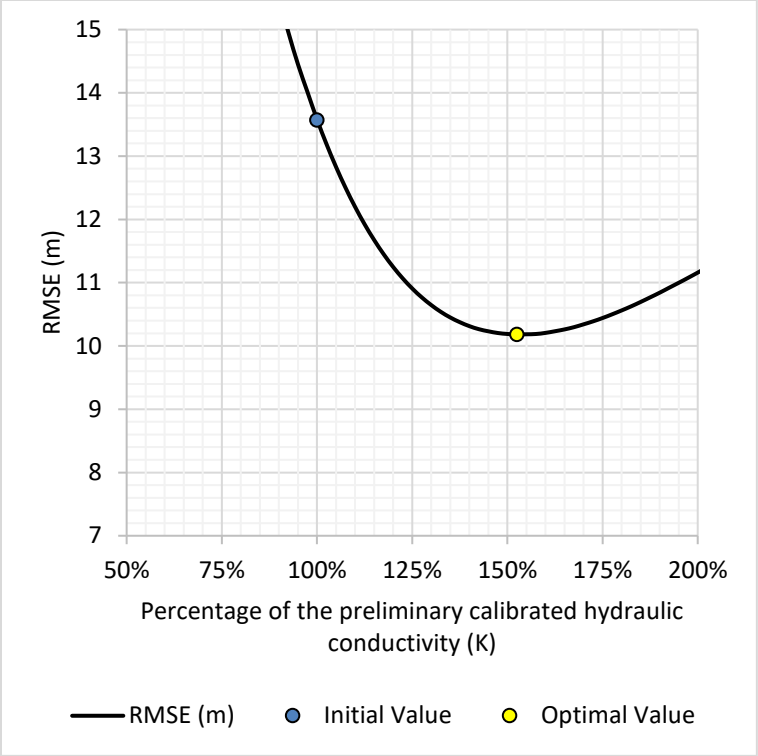

Figure 7.8. Results of the sensitivity analysis for the hydraulic conductivity of the Paskapoo 1.2 section. The yellow dot represents the optimal value, while the blue dot represents the preliminary calibrated value.

ii. Paskapoo 1.3

Simulations for the Paskapoo 1.3 section, located in the southernmost part of the cross-section, used a range from 50% to 185% of the "calibrated" value (K= 5.5 x 10^{-6} m/s). Figure 7.9 shows that the optimal value was 4.9 x 10^{-6} m/s, corresponding to 90% of the calibrated value, with an RMSE of 10.01 m (5.62% of the total hydraulic head elevation difference), for an overall decrease of 26% (compared to the base case).

Figure 7.9 shows again that the RMSE values increase more rapidly when K values are reduced than when they are increased, similar to Paskapoo 1.2. This figure also reveals that the model is in fact more sensitive to changes in hydraulic conductivity applied to the Paskapoo 1.3 section than to section 1.2 when the K value is above 100%, likely because its K value is lower than that of Paskapoo 1.2 and, hence, acts as a flow-limiting section.

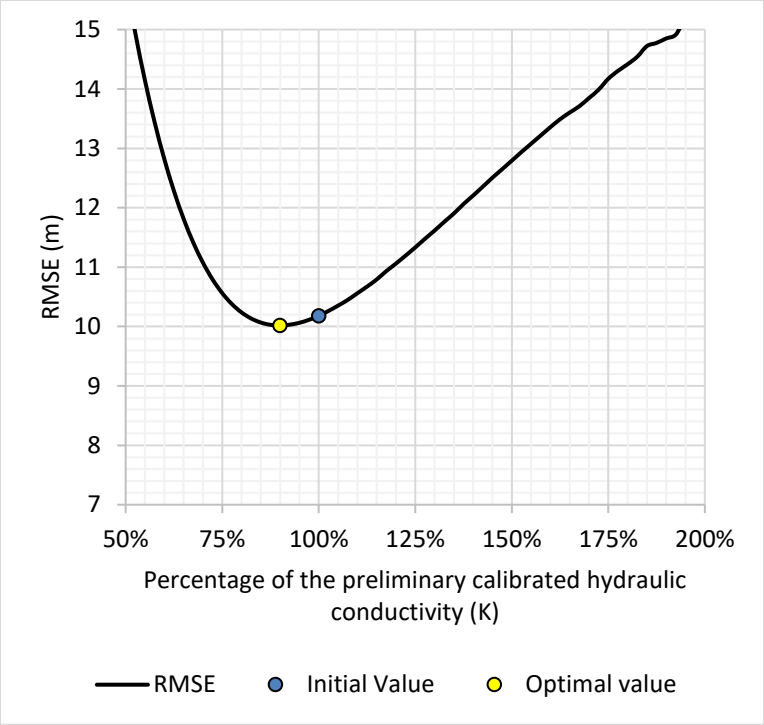

Figure 7.9. Results of the sensitivity analysis for the hydraulic conductivity of the Paskapoo 1.3 section. The yellow dot represents the optimal value, while the blue dot represents the preliminary calibrated value.

iii. Paskapoo 1.1

K values ranging from 25% to 125% of the preliminary calibrated value for section Paskapoo 1.1 (*K*= 7.1 x 10^{-6} m/s) were used in this case. For this section, the simulated water table is sometimes above the ground surface, and this is the case for the minimum RMSE value. Since this is highly unlikely for this area because none of the wells in the provincial database showed artesian flowing conditions in the study area, the actual optimal value was selected as 95% of the calibrated value (red dot, 6.75 x 10^{-6} m/s). This corresponds to the scenario for which the RMSE is the lowest while the water table is always located below the ground surface. An RMSE value of 9.67 m (5.42% of the total elevation difference) is then obtained, leading to an overall decrease of 28% (compared to the base case). Figure 7.10 shows again that RMSE values for the Paskapoo 1.1 increase more rapidly when *K* values are decreased than when they are increased compared to the base case scenario. Nonetheless, Paskapoo 1.1 is less sensitive than sections 1.2 and 1.3 because it covers only a small area to the north, with less topography than the southern sections, and thus less flow takes place.

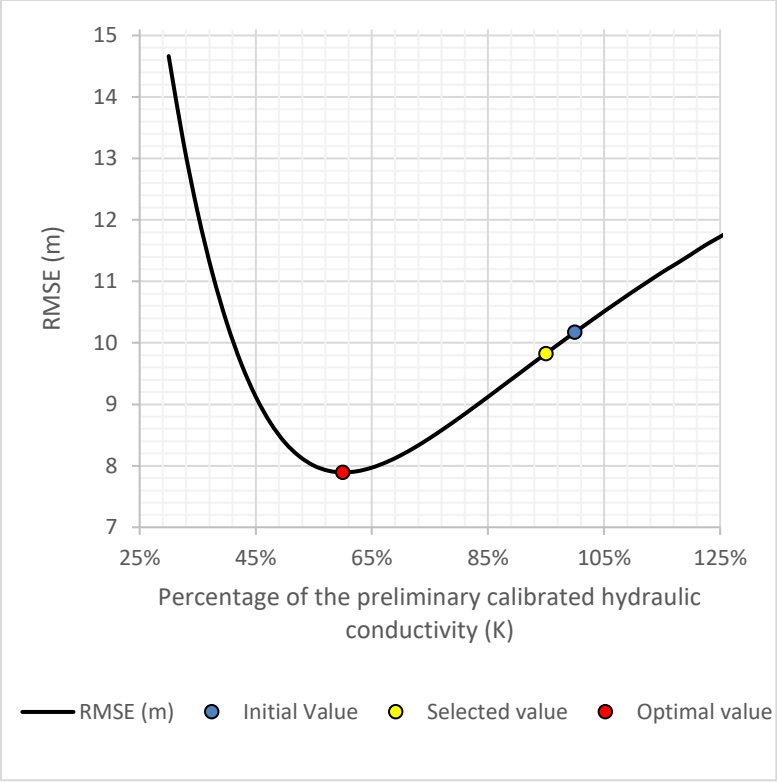

Figure 7.10. Results of the sensitivity analysis for the hydraulic conductivity of the Paskapoo 1.3 section. The yellow dot represents the actual optimal *K* value, which differs from the actual minimum value. Note that the x-axis scale differs from that in Figure 7.8 and Figure 7.9 to better show the results.

iv. Paskapoo 2

Similar to the Paskapoo 1.1 section, *K* values ranging from 10% to 185% of the preliminary calibrated value were used to test the sensitivity of the Paskapoo 2 unit. The optimal value for the Paskapoo 2 section is obtained with 50% of the initial value (K=1.08 x 10^{-8} m/s), thus corresponding to a hydraulic conductivity of 5.4x10^{-9} m/s and an RMSE of 9.65 m. However, this unit is insensitive to changes, as shown in Figure 7.11. Therefore, it would be questionable to significantly lower this *K* value to reduce the RMSE from 9.67 to 9.65 m, since the calibrated value corresponds to the median obtained using 458 core sample analyses from three studies (Figure 4.5). This insensitive behavior can be explained by the very small amount of groundwater flowing below the first 100 meters of the Paskapoo Formation (see below). Therefore, the *K* value for Paskapoo 2 was kept at 1.08 x 10^{-8} m/s.

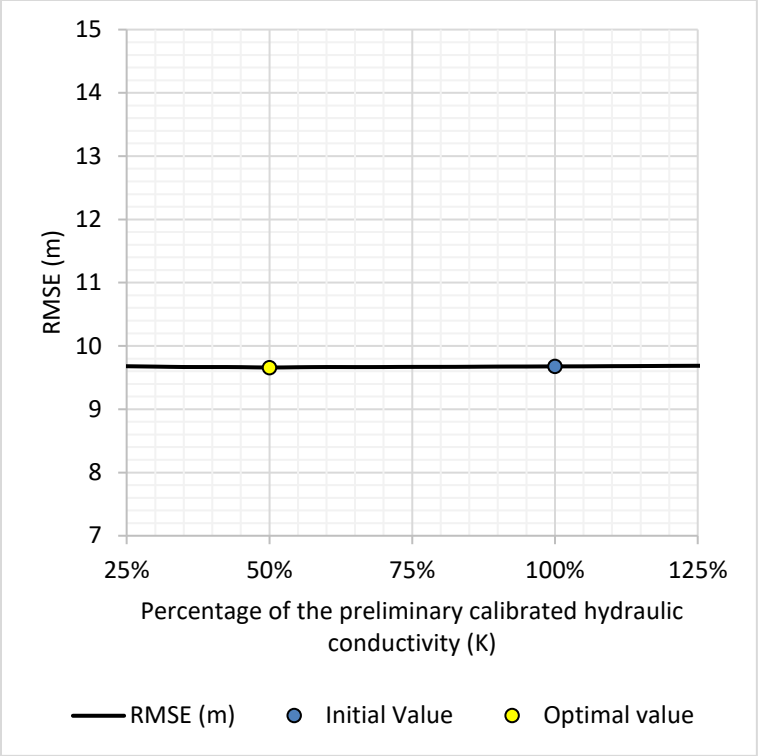

Figure 7.11. Results of the sensitivity analysis to hydraulic conductivity for the Paskapoo 2 section, showing an insensitive behavior. Although a slightly lower RMSE can be found (yellow dot), this insignificant reduction does not justify lowering the *K* value initially used for the base case scenario.

v. Optimal Scenario

Figure 7.12 presents the optimal scenario that includes all previously obtained optimal *K* values for the different units of the Paskapoo Formation, for which the RMSE is 9.67 m, corresponding to 5.42% of the difference between the maximal and minimal hydraulic head elevations along this cross-section. Figure 7.13 presents the graphical comparison between the simulated and interpolated hydraulic heads along cross-section B-B' for this optimal scenario. If the two values located in the topographic mound (circled in red in Figure 7.13) are excluded, the RMSE decreases to 5.09 m, or 2.86% of the total hydraulic head elevation difference (i.e., by almost half). The error is then well below the threshold of acceptability (5%) suggested by Anderson and Woessner (1992).

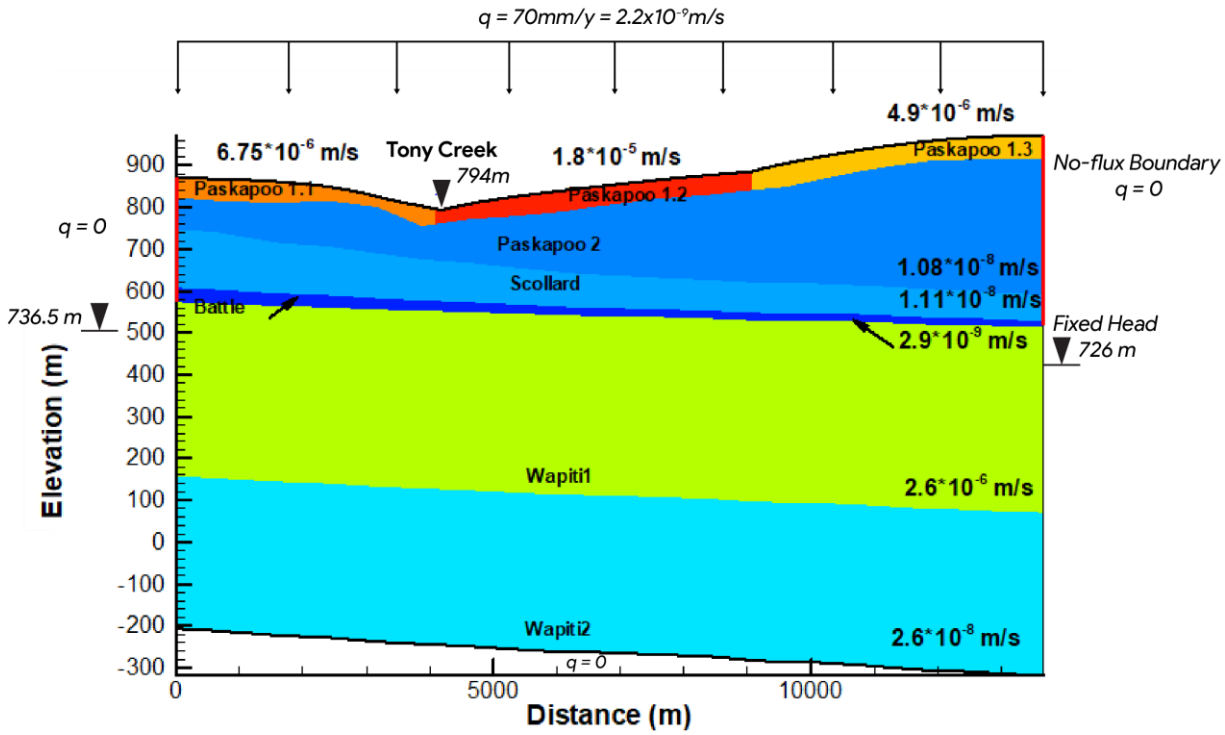

Figure 7.12. Summary of optimal *K* values for the different units of the Paskapoo Formation. The rest of the formations were kept unchanged (corresponding to values from Table 7.2).

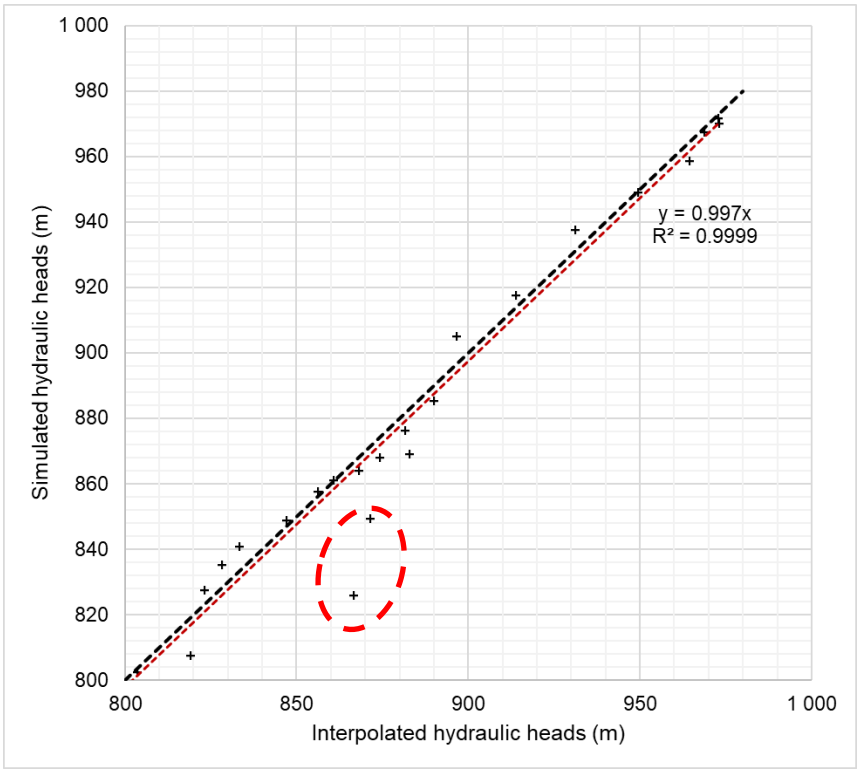

Figure 7.13. Comparison between interpolated and simulated hydraulic heads. The black dotted line represents the 1:1 slope, while the red dotted line represents the linear regression line. The values located in the vicinity of the mound, north of Tony Creek, are circled in red.

Figure 7.14 to Figure 7.16 present the results obtained for the optimal scenario. Figure 7.14 shows the location of the simulated versus the interpolated water table for this optimal scenario. Figure 7.15 shows the hydraulic heads and streamlines under steady-state conditions. As expected, flow is mostly concentrated in the upper part of the Paskapoo Formation, hence within the first 100 m, where a higher *K* value (by three orders of magnitude compared to Paskapoo 2) was assigned. Tony Creek acts as the primary discharge area for this shallow aquifer system. Figure 7.15 also shows that almost two distinct hydrogeological systems are present, separated by the nearly impermeable Battle Fm. A discharge value to Tony Creek of 2.86 x 10^{-5} m^2/s per meter of transverse width, which corresponds to **95.9%** of the total outflow, was found for this optimal scenario. Figure 7.16, which presents the uniform velocity vectors (i.e., showing only flow direction, not velocity magnitude), illustrates that groundwater flow is a few orders of magnitude higher in the upper 100 m zone than in the underlying layers. Final hydraulic conductivity values for the upper part of the Paskapoo Formation are located between the 20th and 50th percentile of specific capacity values (*Cs*) estimated in section 6.3.

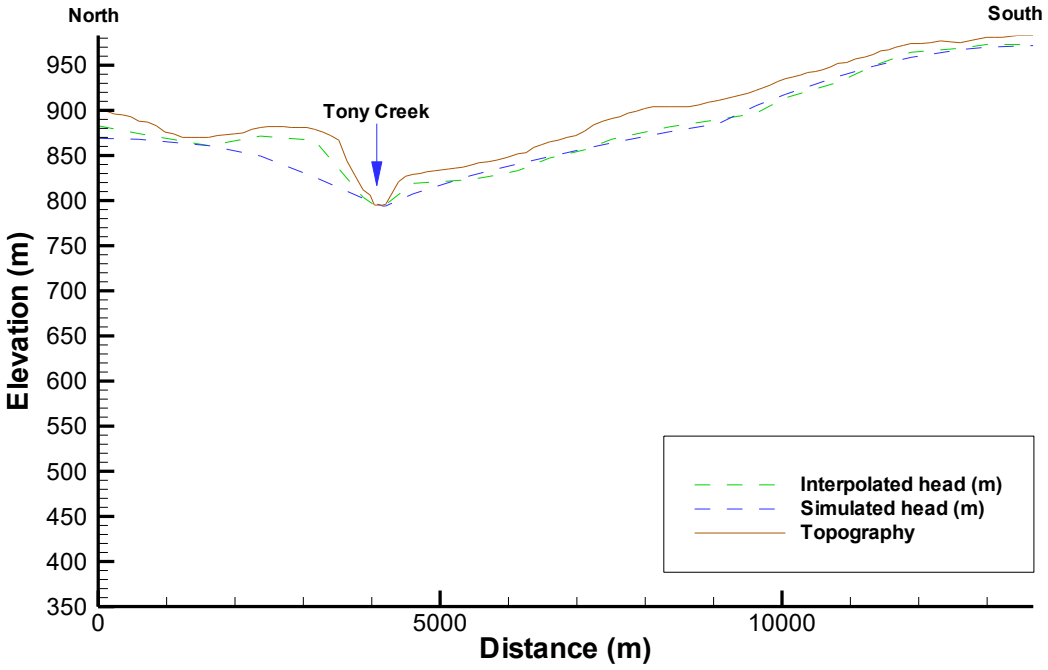

Figure 7.14. Simulated hydraulic heads obtained for the optimal scenario, along with the interpolated water table extracted from the piezometric map along the B-B' cross-section. Note: the water table at Tony Creek was assigned as a fixed head in the top of the Paskapoo Formation for the simulated case.

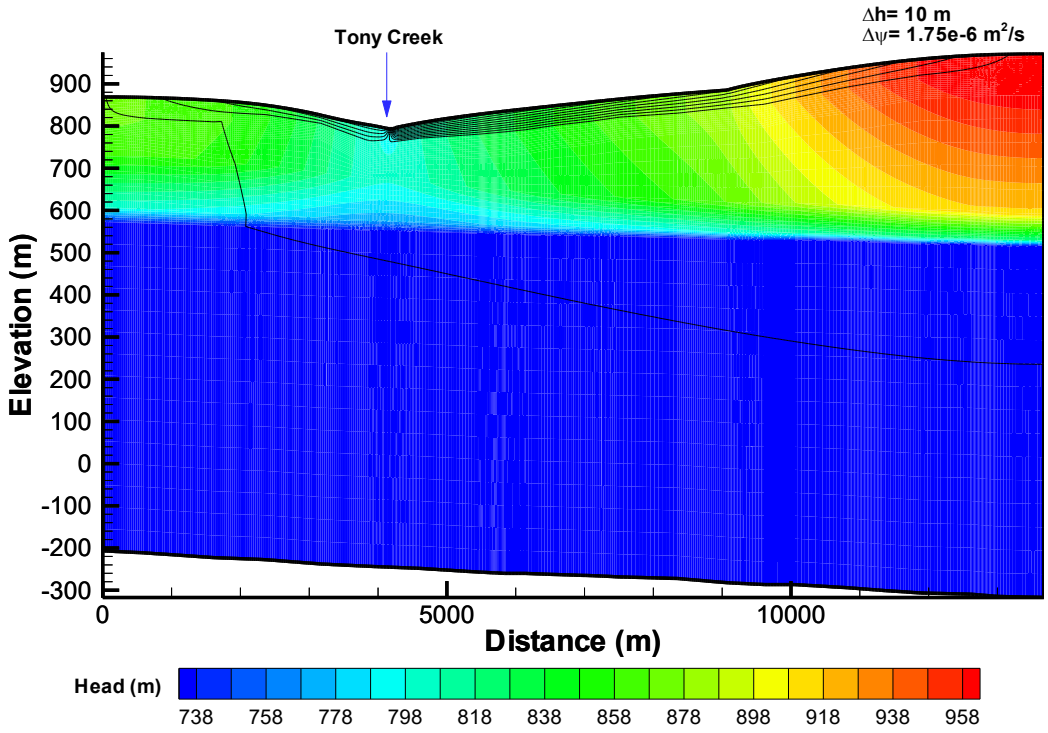

Figure 7.15. Hydraulic heads and steady-state flow lines over cross-section B-B' for the optimal scenario.

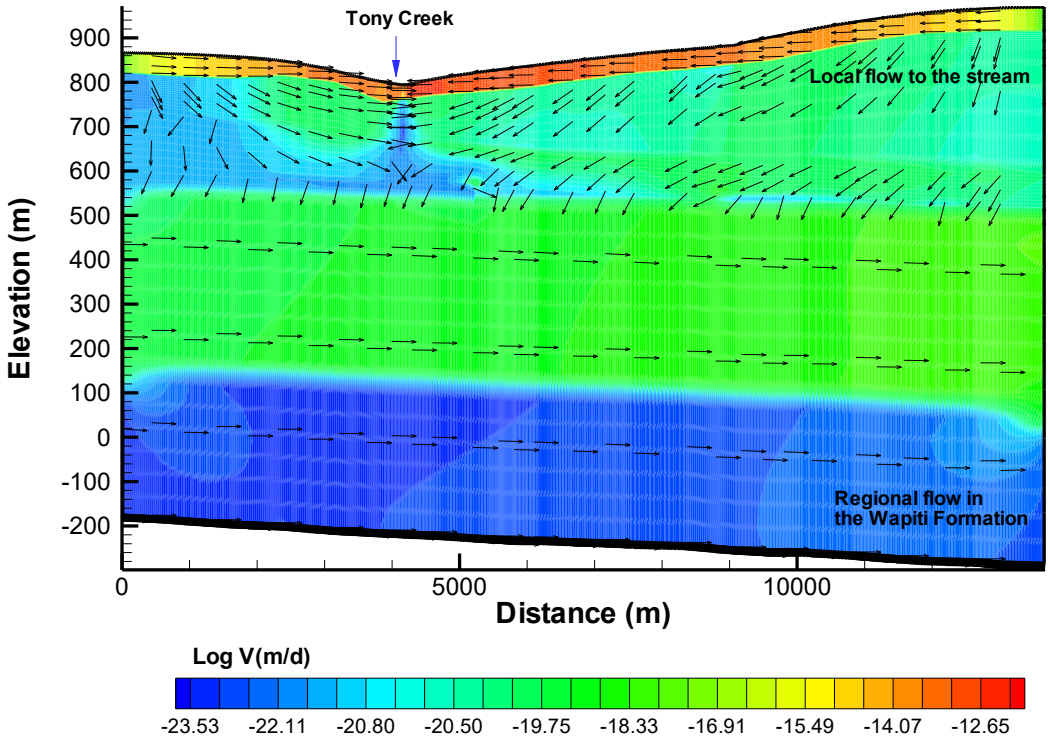

Figure 7.16. Groundwater velocities and steady-state flow lines over cross-section B-B' for the optimal scenario. A shallow system including Paskapoo 1.1, 1.2, 1.3 and 2 flows to Tony Creek, while a deeper system (part of the intermediate zone) consisting of the Scollard and Wapiti 1 and 2 units contributes to a more regional flow system.

7.2.2.2 Anisotropy

The anisotropy of the upper part of the Paskapoo Formation (where the active groundwater flow zone is located) was also investigated to evaluate its impact on the model response. Since the underlying units (Paskapoo 2 and below) were insensitive to hydraulic conductivities changes, this investigation was limited to the first 100 m. Riddell *et al.* (2009) suggested an anisotropy ratio (*K*h/*K*v) of 2 for the sandstone units of the Paskapoo Fm, but core samples have also shown Kh/Kv ratios up to 10, based on permeability measurements taken in both horizontal and vertical directions. Two other scenarios were also tested using higher anisotropy factors: *K*h/*K*v of 50 and 100 as the core sample measurements do not consider the presence of fractures. These four ratios were applied to all three sections (Paskapoo 1.1, 1.2, and 1.3) simultaneously using the optimal scenario of section 7.2.2.

Figure 7.17 presents the results obtained with these four values of anisotropy ratios for the upper part of the Paskapoo Formation (excluding again the values below the mound). It shows that the best RMSE value is obtained with *K*h/*K*v=10, the ratio assigned in the optimal scenario. The RMSE increases quite rapidly for the two largest anisotropy values tested, likely because the system becomes less permeable (since *K*v is decreased), producing a higher water table. The *Kh/Kv* ratio of 10 was thus kept to consider the presence of the fractures in the upper part of the Paskapoo Formation.

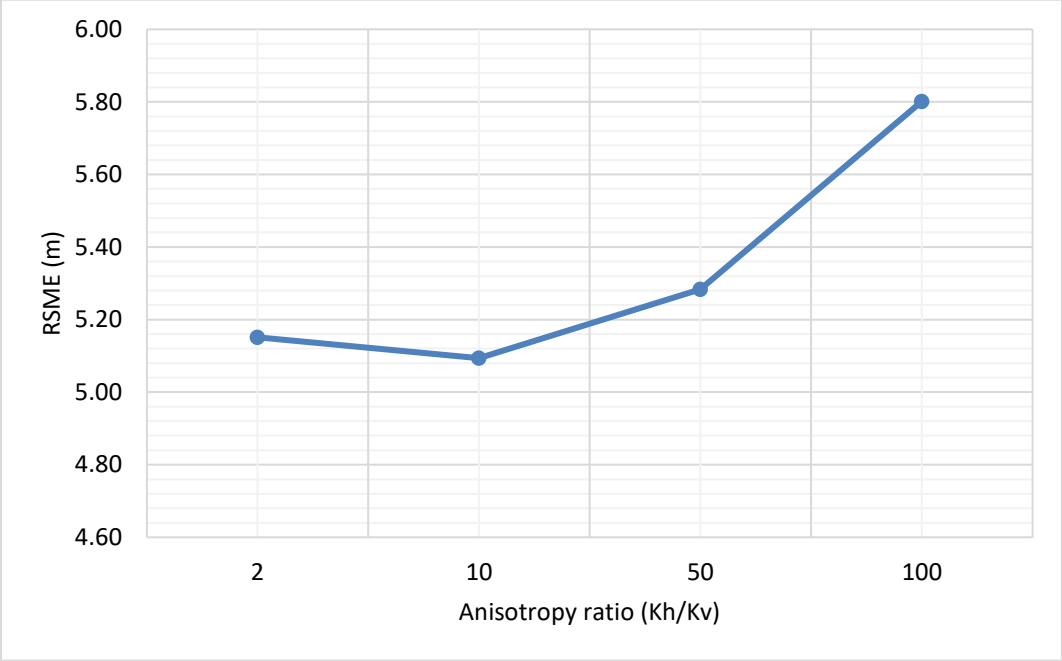

Figure 7.17. Summary of the results for the sensitivity analysis to anisotropy for the upper part of the Paskapoo Formation.

As expected, the model has the minimum error when *Kh/Kv* is equal to 10, since it was calibrated using this ratio. However, the various anisotropy factors result in minor changes in RMSE and, therefore, the model can be considered relatively insensitive to this factor, mainly because the active flow zone (located in the first 100 meters) is where the vast majority of the flow occurs and is primarily of a lateral nature towards Tony Creek.

7.2.3 Scenarios considering windows in the Battle Formation

As the GSC Fox Creek project aims to assess potential impacts of industrial activities carried out at depth on shallow aquifers, it was deemed important to study if upward flow can occur (or when, i.e., under which conditions) in this system. The simulations thus far (see for e.g., Figure 7.16) showed that there appear to be two distinct hydrogeological systems above and below the Battle Formation when the latter is considered continuous. Since the Battle Formation is thin and eroded entirely in some areas (Hathway, 2011), two scenarios were tested to investigate the impact of gaps (or “windows”) in the Battle Formation on a hydraulic connection between the Wapiti and Paskapoo formations.

To include realistic spatial discontinuity in the Battle Formation, three cross-sections within the Tony Creek watershed were extracted from the regional 3D geological model by Corlett *et al.* (2019). The thickness of the Battle Formation was extracted using GIS tools along these three cross-sections, which are located just west of the modeled 2D cross-section B-B', where a large window is located. Figure 7.18 shows the spatial distribution of the thickness of the Battle Formation and the location of these three cross-sections and two windows (in red). Figure 7.19 shows both the top of the Battle Formation and Wapiti Formation, illustrating the discontinuities in the Battle Formation and allowing the window size to be estimated along the cross-sections. These cross-sections show that windows range in length from 1 km to nearly 5 km in the study area.

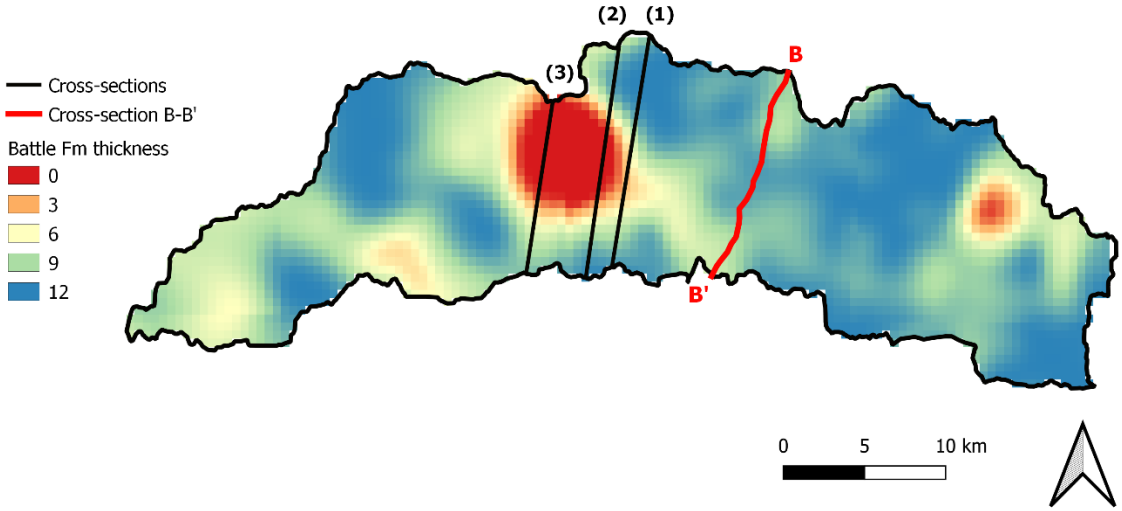

Figure 7.18. Thickness of the Battle Fm across the study area based on the 3D geological model of west-central Alberta by Corlett *et al.* (2019). The cross-sections (1), (2), and (3) (shown in black) are presented in Figure 7.19 (a) to (c) to illustrate the discontinuity of the Battle Formation.

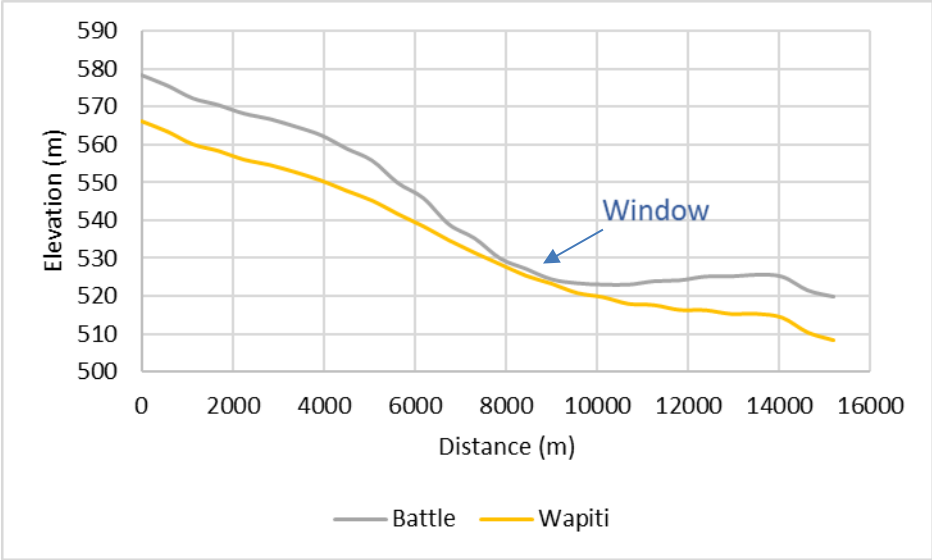

(a) Cross-section (1) shows a window between 8000 – 9000 m (1 km).

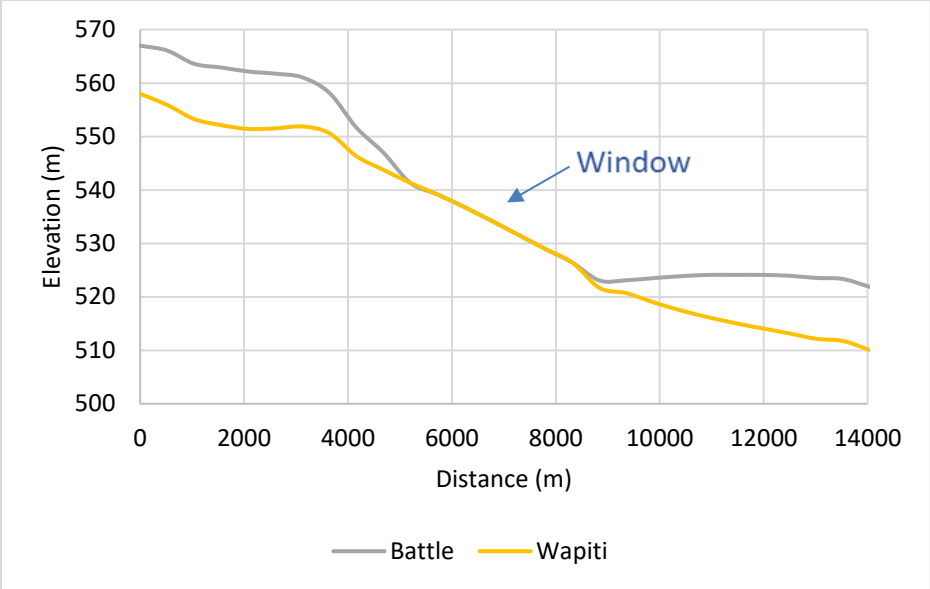

(b) Cross-section (2) shows a window between 5200 to 8800 m (3.6 km)

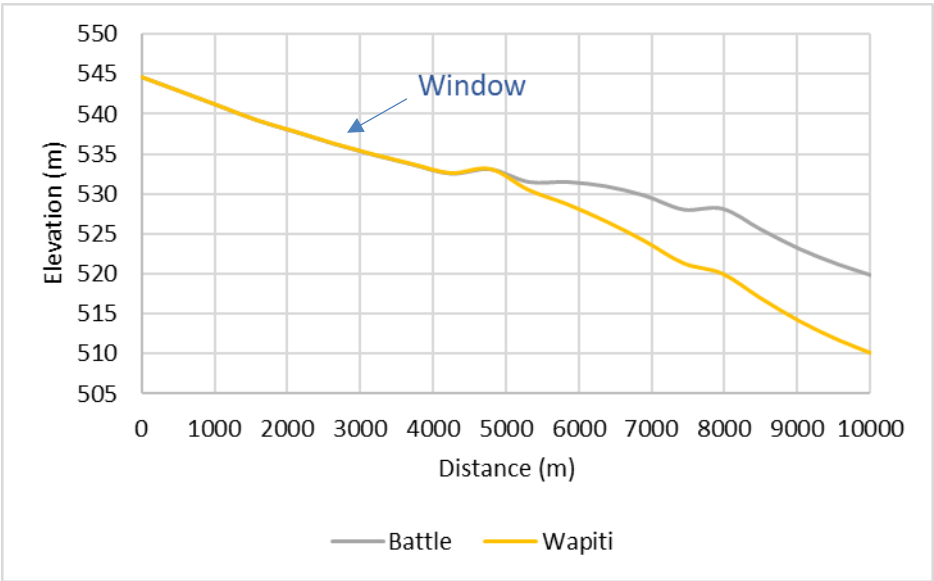

(c) Cross-section (3) shows a window between 0 to 4800 m (4.8 km)

Figure 7.19. Cross-sections extracted from the provincial 3D geological model (Corlett *et al.*, 2019) showing the top surfaces of the Battle and Wapiti formations.

Based on these cross-sections, three scenarios integrating a window in the Battle Formation, with different sizes and locations, were developed and simulated. The first window is 1 km long and is located 3 km south of Tony Creek; the second window is 3.6 km long and begins 1 km south of Tony Creek, while the third window is 4.8 km long and is located below and north of Tony Creek. The boundary conditions and parameter values are the same as those used in the optimal scenario. Figure 7.20 shows the hydraulic conductivities as well as the conceptualized windows for these three scenarios.

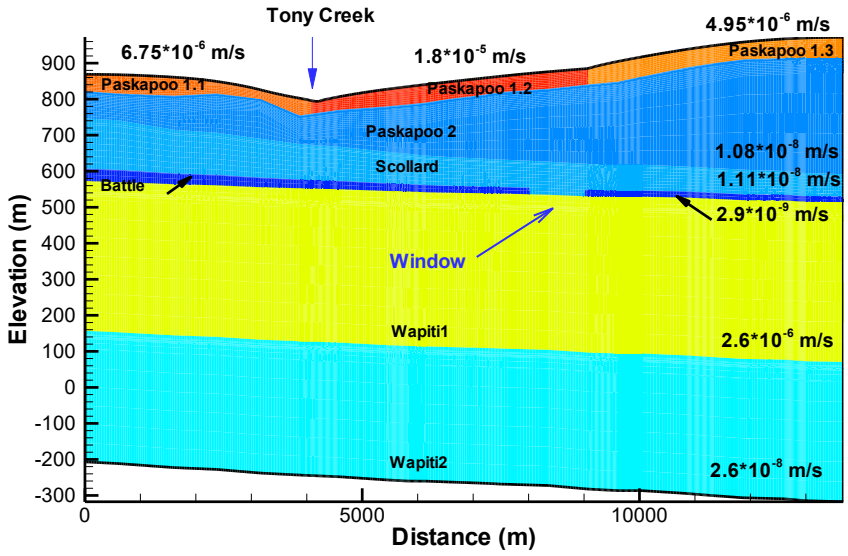

(a) 1 km window in the Battle Formation

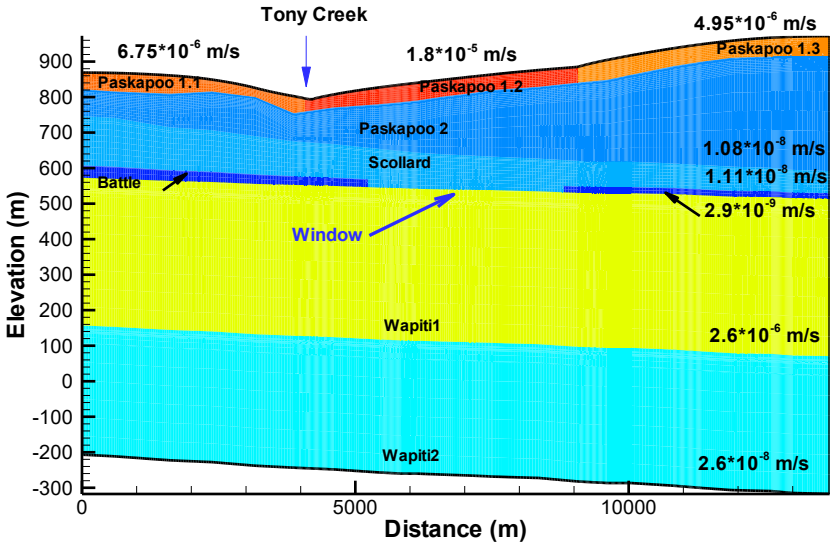

(b) 3.6 km window in the Battle Formation

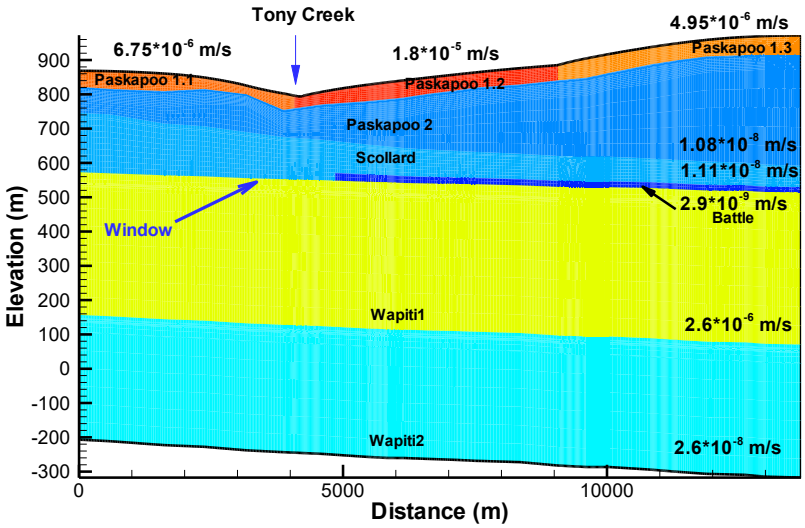

(c) 4.8 km window in the Battle Formation

Figure 7.20. Presentation of the three scenarios (a, b and c) used to study a potential hydraulic connection between deep and shallow formations when discontinuities are present in the Battle Formation. The conceptualized windows are indicated using a blue arrow.

The results for these three scenarios did not show a hydraulic connection between the upper part of the Paskapoo and Wapiti formations, even if the Wapiti Formation is under pressure (Singh & Nakevska, 2019), because the fixed hydraulic head assigned to Tony Creek is still higher than those in the Wapiti Formation. Figure 7.21 presents the results of these simulations. It shows that hydraulic heads below Tony Creek at the interface between the Wapiti and Battle formations are slightly higher than in the model without a window. Therefore, Figure 7.22, which presents the uniform velocity vectors (i.e., showing only flow direction, not velocity magnitude) for scenario b (3.6 km window), does not show the presence of an upward flow. Instead, it shows the presence of a preferential path through the window, where the " shallow" water migrates downward.

Although very little data are available for the deeper formations, scenarios considering various anisotropy ratios, with a *Kv* higher than *Kh* (with *Kv/Kh* = 2, 10 and 100), were also tested. They show, as expected, that as the anisotropy increases in the Scollard, Battle, and Wapiti formations, the downward flow is enhanced (not shown).

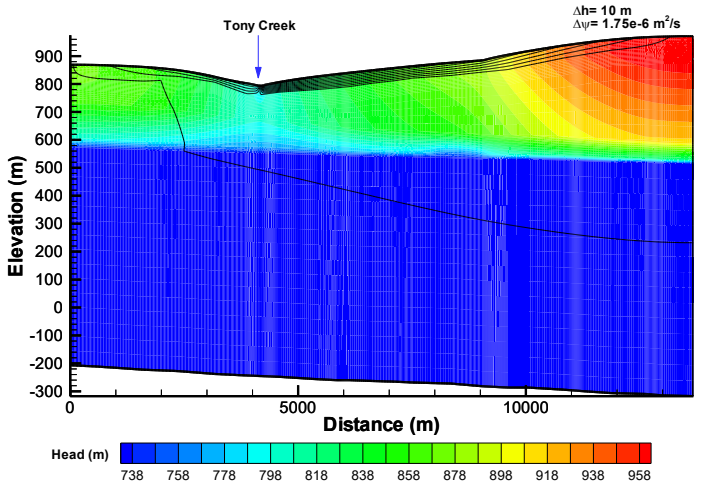

(a) 1 km window in the Battle Formation

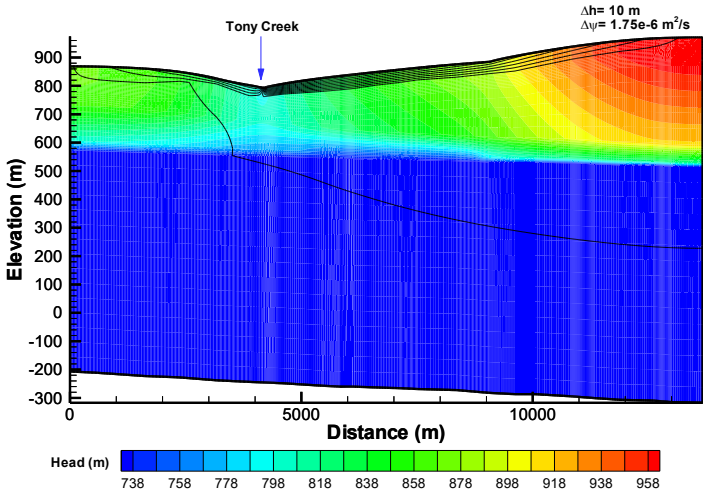

(b) 3.6 km window in the Battle Formation

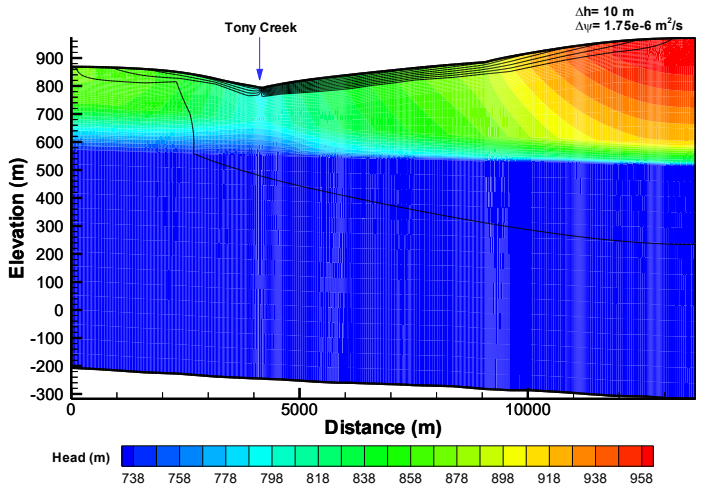

(c) 4.8 window in the Battle Formation

Figure 7.21. Hydraulic heads for the three scenarios including windows in the Battle Formation.

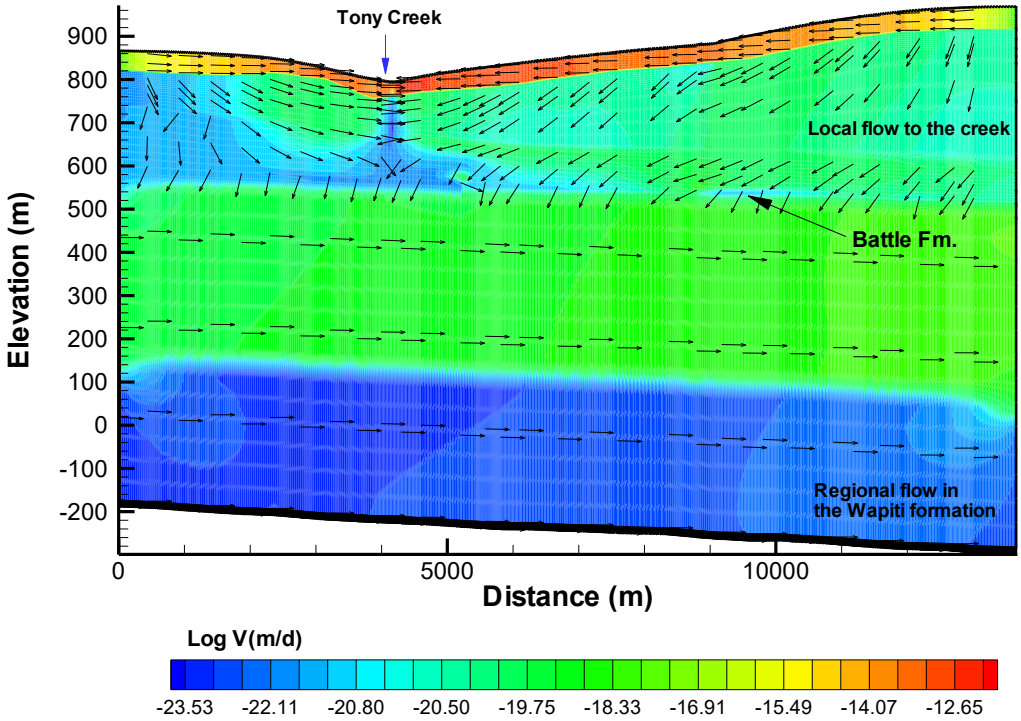

Figure 7.22. Uniform velocity vectors for scenario b (i.e., considering a 3.6 km window).

7.2.4 Scenarios testing the conditions required to have an upward flow

To study the conditions under which upward flow could occur, hydraulic heads in the Wapiti Formation were increased, based on plausible values shown on the piezometric map of this formation (Singh & Nakevska, 2019) not too far from our study area. As mentioned earlier, few data are available for deeper formations such as the Scollard, Battle, and Wapiti. Figure 7.23 shows that particularly few data are available in and around our study area. However, this piezometric map shows that much higher values (up to 900 m) than in our study area can be found just north of it. Therefore, new scenarios were developed using increasing values for the boundary conditions of the Wapiti Formation to investigate the possibility of upward flow from the Wapiti Formation to the surface.

Based on this piezometric map (Singh & Nakevska, 2019), the hydraulic heads in our study area lie between 726 and 735 m (Figure 7.23). Boundary conditions for three new scenarios were increased from 726 m to 795 m (slightly above the fixed hydraulic head at Tony Creek), then to 830 m, and then to a maximum value of 930 m on the south side of the model. Simulations showed that the hydraulic heads in the Wapiti Formation need to be increased by about 100 m (using values of 830 m on the south side and 850 m on the north side) compared to the base case to

actually see upward flow. Although the provincial piezometric map of the Wapiti Formation shows the possibility for such values northeast of our study area, this scenario seems quite unlikely. The fact that the water at this depth is saline and therefore denser, which has not been taken into account here, further reduces this probability. Nonetheless, this possibility cannot be completely ruled out.

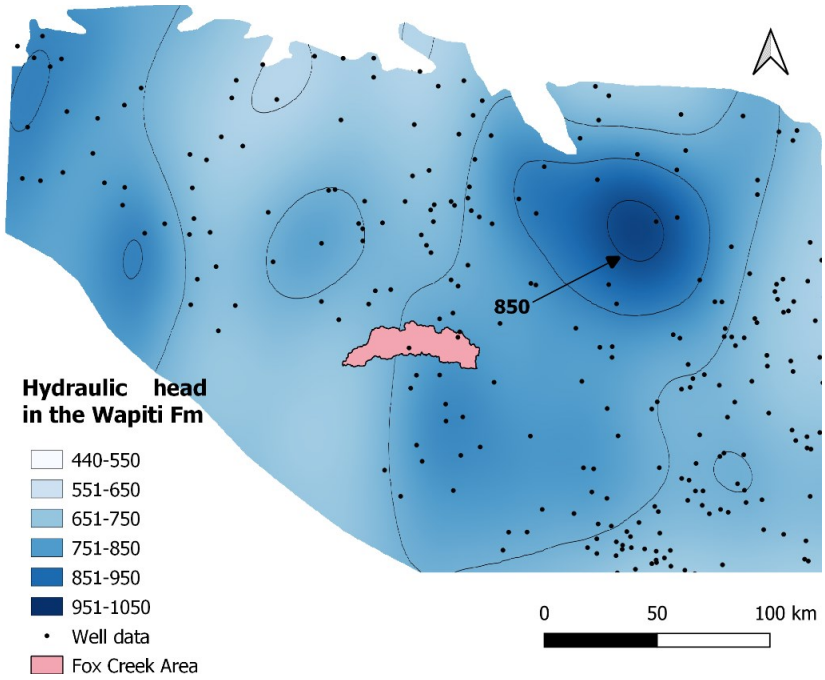

Figure 7.23. Zoom of the Wapiti piezometric map by Singh & Nakevska (2018) in the vicinity of the Fox Creek area. The darker blue area shows values > 900 m.

Figure 7.24 presents the uniform velocity vectors for the new scenario b, including a 3.6 km window in the Battle Formation, showing the presence of an upward flow below Tony Creek when the boundary conditions are increased to 830 and 850 m on the south and north side of the Wapiti Formation, respectively. The simulated water table remained very similar to that of the optimal scenario due to the localized nature of the window and the very small flux magnitudes that are generated.

Various anisotropy ratios were also used for the Scollard, Battle, and Wapiti formations for the scenarios showing the presence of upward flow. Results show that upward flow is again enhanced as the anisotropy value (*Kv*/*Kh*) increases (not shown).

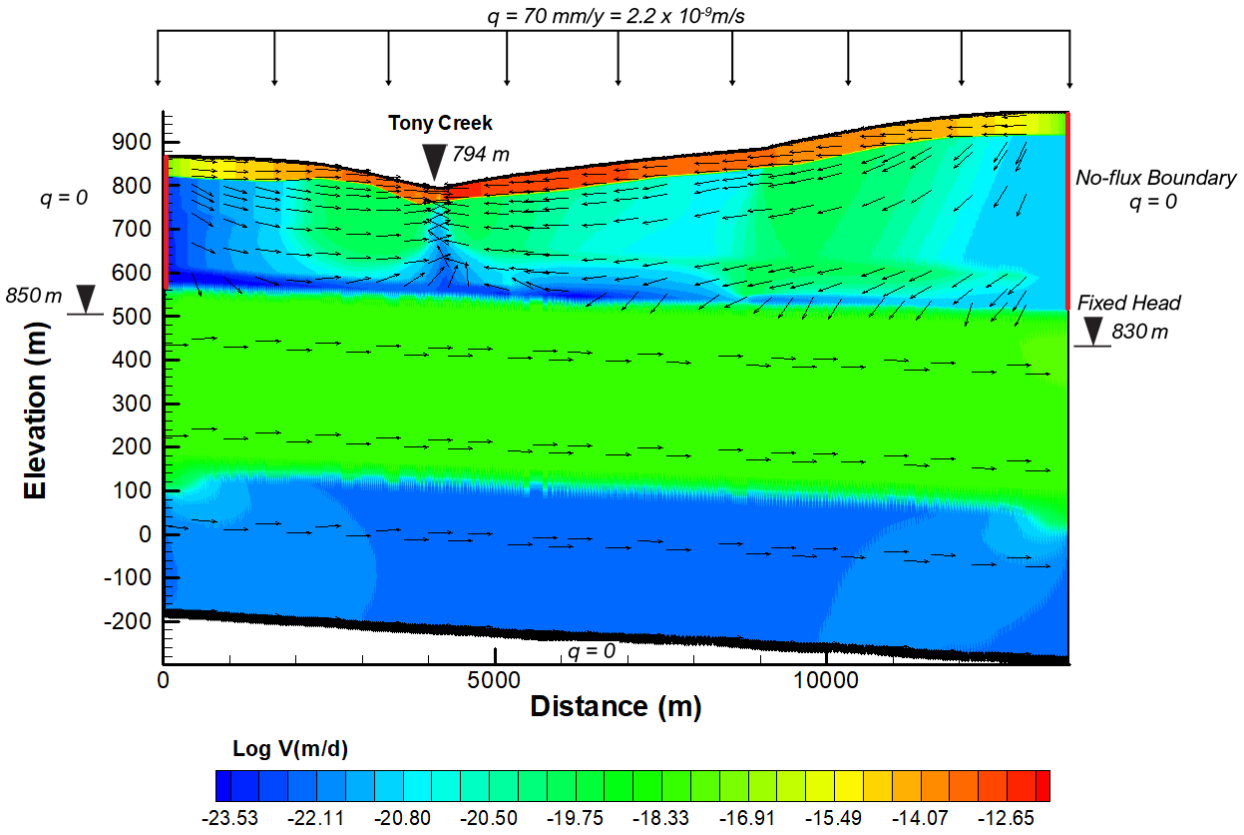

Figure 7.24. Velocity vectors for cross-section b (with a 3.6 km window) after increasing the boundary conditions of the Wapiti Formation from 726 to 830 m on the left/southern side and from 736.5 to 850 m on the right/northern side.

7.3 CATHY model

7.3.1 Model setup and scenarios without surficial sediments

The FLONET results provided an initial understanding of the flow system, including confirmation that flow is concentrated in the upper part of the Paskapoo Formation (96%) and that any hydraulic connection between the Wapiti Formation and the overlying formations is highly unlikely. Therefore, only the Paskapoo Formation was included for the 2D CATHY model simulations. Boundary conditions in the conceptual model, shown in Figure 7.1, were kept the same except for the bottom, where a Neumann boundary condition corresponding to the vertical hydraulic conductivity of the Scollard Formation was assigned. This boundary condition was assigned to represent the flow rate to the deeper formations found with the FLONET model.

The initial step with the CATHY model consisted in reproducing the FLONET configuration. Therefore, the surficial sediments were first neglected. Elevation data of the geological formations with a 500 m resolution (Corlett *et al.*, 2019) were interpolated to obtain surfaces compatible with the 20 m DEM (thus divided into 25 cells), from which the discretization mesh for the model was derived. Figure 7.25 shows the Paskapoo Formation surface elevation, with a maximum elevation of 960 m to the south and a minimum of 794 m at Tony Creek. At this resolution, the surface mesh contained 1366 cells.

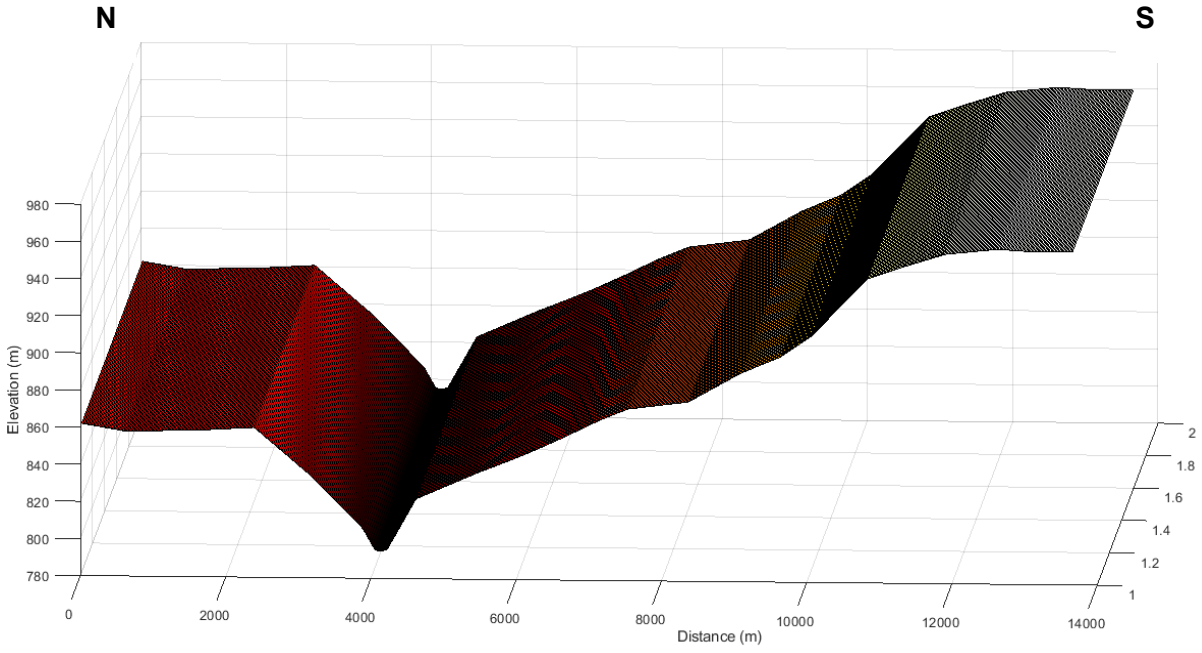

Figure 7.25. Surface elevation of the Paskapoo Formation at a 20 m resolution.

As with the FLONET model, the provincial geological model (Corlett *et al.*, 2019) was used to develop this model, although this time the top elevation of the Scollard Formation was used to represent the model base. The thickness of the domain (and thus of the Paskapoo Formation) ranges from 115.5 m (north) to 367.3 m (south). At the lowest point of the Paskapoo Formation, corresponding to Tony Creek, the thickness is 123.5 m.

CATHY requires a finer layer resolution close to the surface to accurately solve the highly nonlinear Richards' equation to simulate the infiltration and exfiltration fluxes. Therefore, the layers were progressively coarsened with depth, from a thickness of 0.06 m to 23.1 m at the center (Figure 7.26). A total of 15 layers was used for the vertical discretization, each layer parallel to the surface except for the bottom one. The first seven layers correspond to the uppermost part of the Paskapoo Formation (~100 m, i.e., the most fractured). Horizontally, the mesh size had a fixed width of 20 m corresponding to the DEM resolution.

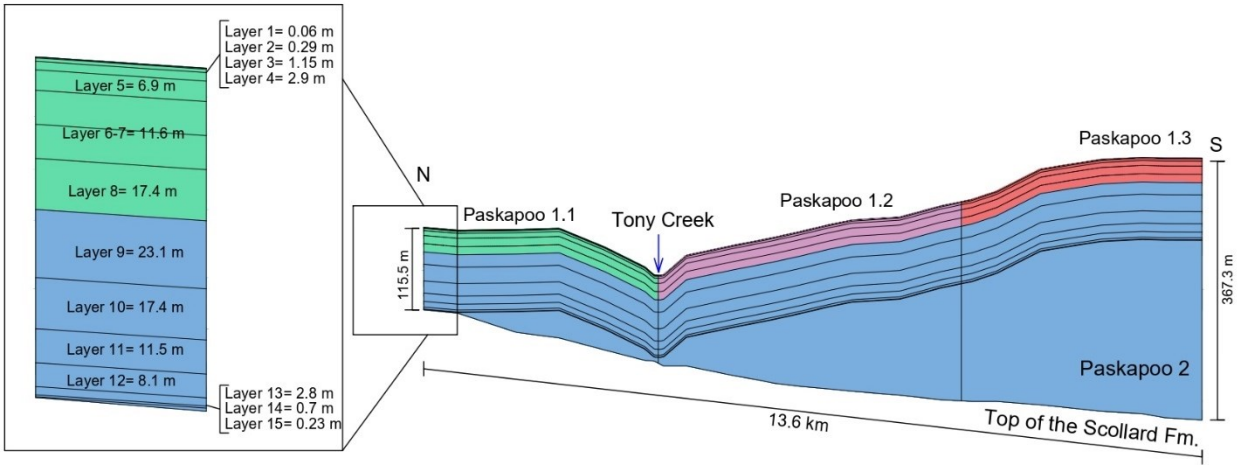

Figure 7.26. Characteristics of the 2D CATHY model mesh when the top of the Paskapoo Formation is assigned as the surface boundary.

In passing from the surface DEM-based discretization to the subsurface finite element discretization, each surface cell was divided into two triangles. Then, the triangular mesh was projected vertically for 15 layers into a tetrahedral grid, with 3 tetrahedra per triangle per layer. The resulting grid contains 32 832 nodes and 122 940 tetrahedral elements. This is much higher than the number of elements of the FLONET model (which had 23 001 elements).

CATHY allows the user to represent heterogeneity by layer (vertically) and by zone (laterally). Hydraulic conductivity values, obtained with the optimal scenario of FLONET, were assigned in the CATHY model. The 2D model in CATHY thus consists of three vertical zones corresponding to Paskapoo 1.1, 1.2, and 1.3 (see section 7.2) for the first 100 m.

A specific storage (S_s) value of 0.05 m^{-1} was used for the upper part of the Paskapoo Formation, while for the lower part of the Paskapoo Formation, a value of 0.005 m^{-1} was assigned. Since $S = S_s$ * b, where S is the storativity and b is the saturated (aquifer) thickness, these values might seem very high if the entire upper part of the Paskapoo Formation (100 m) is considered. However, Chen *et al.* (2007a) noted that the characteristic channel sandstone beds are typically 5 to 10 m thick (see section 2.3), which should likely better represent the aquifer thickness b, especially since all wells are cased and screened in this area. This would lead to S being in the order of 0.25 to 0.5 for the upper section, which is high, but reasonable. Nonetheless, a 50-year simulation with S_s values ten times smaller (Paskapoo1=0.005 m^{-1} and Paskapoo2=0.0005 m^{-1}) was performed, and it showed that these new values had little impact on the model results, especially on recharge, which remained the same. The overland and return flow showed a maximum reduction of 10%. For this simulation, the time step had to be significantly reduced, which translated into a high computational cost. The initial values were therefore retained. Initial conditions for the water table were set to 2 m below the surface.

Five-year simulations were performed using four soil types for which the van Genuchten coefficients, governing the unsaturated zone retention curves, are presented in Table 7.4. This relatively short time period was used initially for these simulations since the computational cost is high in CATHY and we wanted to investigate the effect of variations of the different parameters. The van Genuchten parameters for fine sand were then retained, as this soil produced a recharge that was within the plausible range of recharge (0-70 mm/y). This soil is probably representative of the sandy till (mixture of permeable and less permeable sediments) found in this area.

Table 7.4. Van Genuchten parameters used during calibration (taken from Carsel and Parrish (1988))

Van Genuchten Parameters			Soil type	Recharge (mm/y)
n	Ψs	θr		
1.7	-2.1	0.001	Loamy soil	146.4
2.8	-0.5	0.067	Silty Loam	123.0
1.9	-0.13	0.159	Sandy Loam	80.9
1.7	-0.05	0.065	Fine sand	71.0

Results for streamflow, overland flow, return flow (groundwater that returns to the surface), and annual recharge for a 5-year period are presented in Figure 7.27. A potential atmospheric flux (AtmPot), representing potential infiltration (rainfall, positive) or exfiltration (evaporation, negative) fluxes in the model, was assigned a constant value over time in these scenarios (rainfall of 70 mm/y). It is the actual atmospheric flux (AtmAct), representing the actual infiltration or exfiltration fluxes, that is resolved by the model via boundary condition switching. Since in these scenarios

there is no evaporation component in AtmPot (constant rainfall of 70 mm/y), any negative AtmAct fluxes generated by the model represent a return flow (RetFlow) contribution to overland flow (OvlFlow). An additional overland flow contribution that can arise is from rainfall falling upon a surface node that is fully saturated (this contribution plus RetFlow corresponds to the OvlFlow output). Initially, actual flow is equal to potential flow, as expected for a scenario of rainfall onto a surface boundary that is unsaturated (since the initial water table is below the surface). The strong topographic gradients in the transect generate an important lateral flow component, and water begins to exit the subsurface at lower surface elevation points, particularly around the topographic depressions.

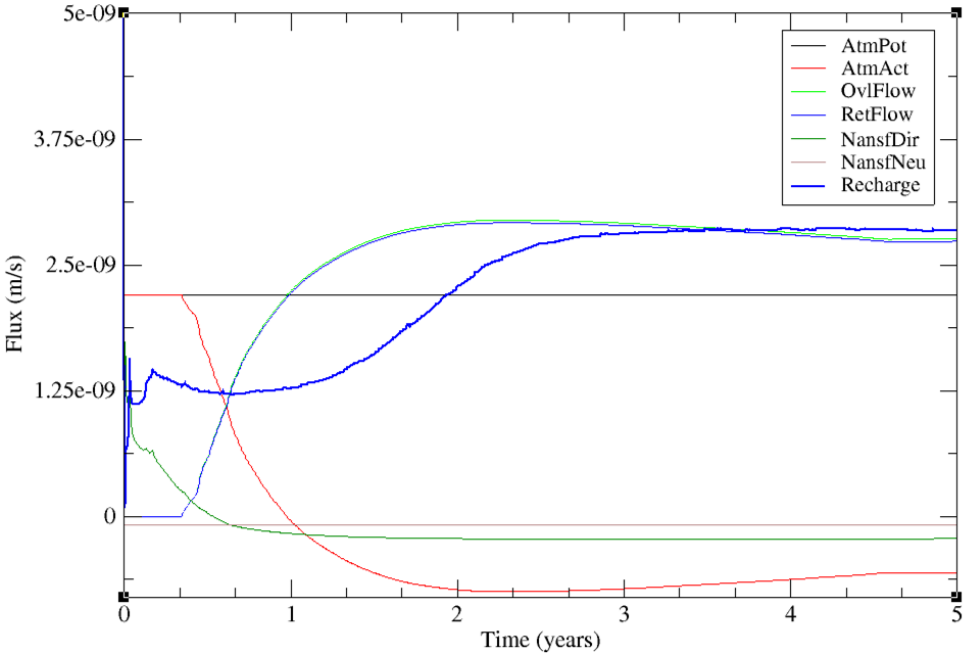

Figure 7.27. Fluxes acting over five years for the first configuration (no surficial sediments). Note: 70 mm/y corresponds to 2.22 x 10^{-9} m/s.

During the first year, the actual atmospheric flux becomes negative. Therefore, overland and return flow values are higher than the potential atmospheric flux since exfiltration occurs not only from incoming rainfall but also from pre-event water originally in the subsurface. This is caused by the topographic gradients and the shallow initial water table. At the beginning of the simulation, the groundwater recharge rate is highly variable, while the system balances the initial conditions, becoming relatively steady after three years. An annual average recharge rate of 56 mm/y was obtained from this model configuration (calculated using the cumulative recharge after 2 years).

The fluxes across the Dirichlet (NansfDir) and nonzero Neumann (NansfNeu) boundary conditions are also presented in Figure 7.27. The Dirichlet nodes, assigned at the surface nodes

corresponding to Tony Creek, represent a direct subsurface contribution to discharge, while the nonzero Neumann nodes are assigned at the bottom of the model domain and are set equal to the vertical hydraulic conductivity of the Scollard Formation, as described earlier. An output representing the total discharge (surface plus subsurface contributions) at Tony Creek is not possible in the model setup used here since there is no routing component for overland flow. In Figure 7.27, the subsurface contribution to discharge (RetFlow and OvlFlow) becomes steady after about one year of the simulation. The similarity between the RetFlow and OvlFlow curves reflects the influence of topography, with an overland (OvlFlow) flow mainly generated from groundwater that returns to the surface (RetFlow), quickly propagated over a surface with strong topographic gradients.

The previous simulation was extended to 100-year to evaluate the steady-state of the model (Figure 7.28). This figure shows that the achievement of a steady state depends on the variable being considered. It confirmed that a quasi steady state is reached after 3 years for groundwater recharge and after 1 year for NansfDir, the proxy used for streamflow (as these represent the fluxes across the Dirichlet BC stream nodes). These two variables remained relatively steady during the rest of the simulation. However, overland and return flow continue to change over time, slowly approaching the potential flux while the actual flux asymptotically approaches zero. Another perspective on the dynamics at the beginning of this long-term simulation is provided in Figure 7.28 (b), where the time axis is plotted logarithmically. It is important to note that the fluxes shown in figures such as 7.27 and 7.28 are the net fluxes over all nodes along the transect, and thus, for instance, an AtmAct flux that approaches zero represents an equilibrium state of sorts between areas of the transect that are infiltrating water and areas that are exfiltrating water (the classic paradigm of “mountain recharge / valley discharge”, for instance).

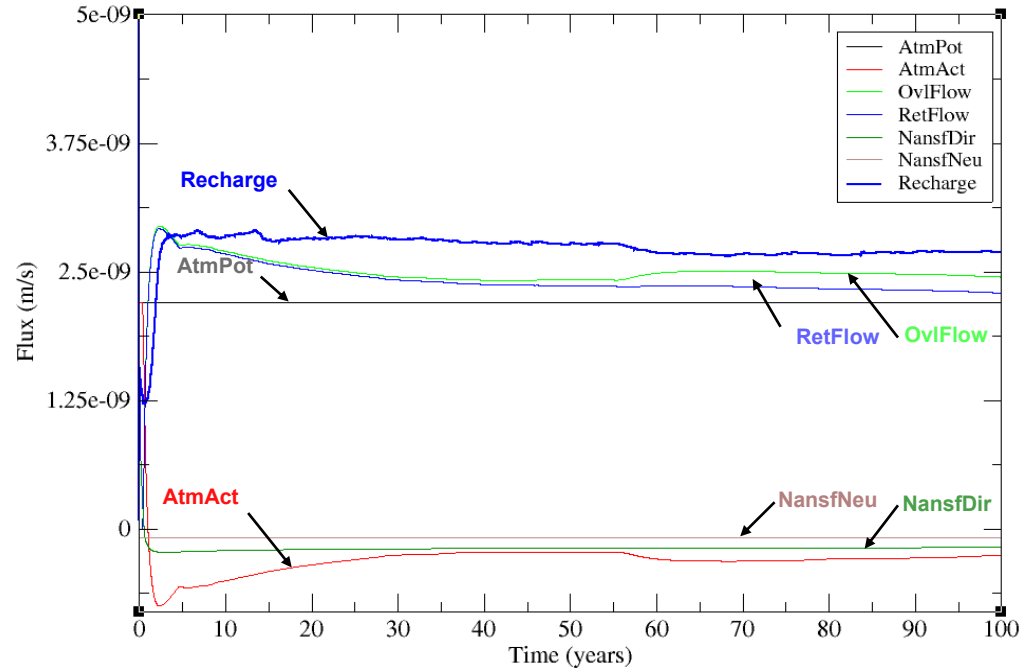

(a)

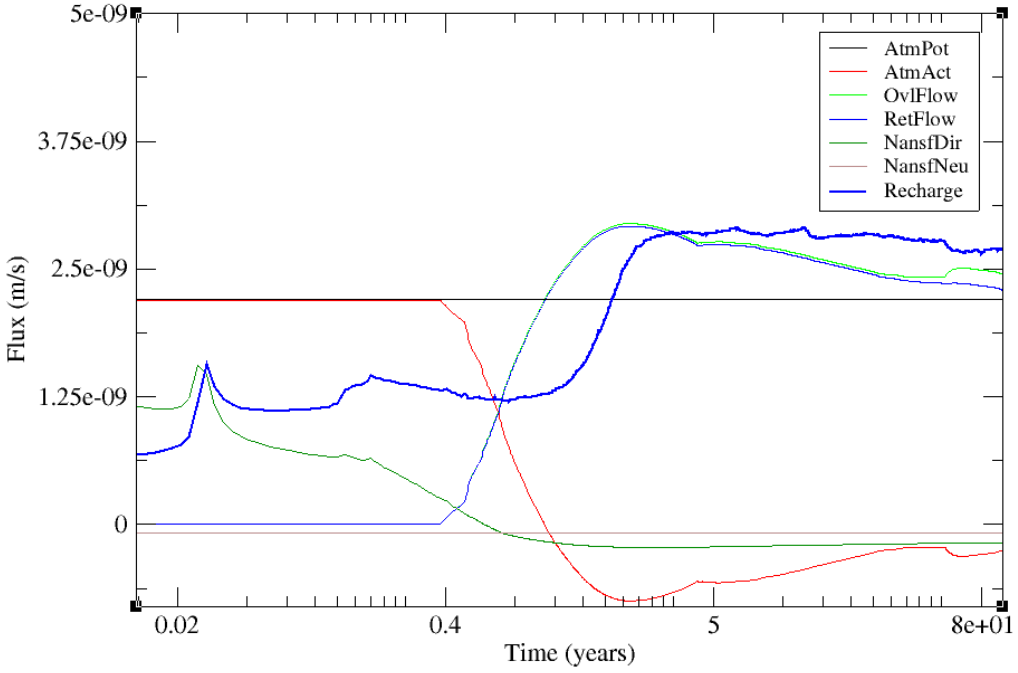

(b)

Figure 7.28. Various outputs (fluxes) from CATHY for a 100- year simulation for the first configuration (no surficial sediments). (a) Linear scale and (b) logarithmic scale.

The slightly higher overland flow after 55 years can be explained by the fact that at this time, the water table intersects the surface at certain locations, which correspond to fully saturated nodes (e.g., topographic depressions), creating a new discharge area where the rainfall will contribute directly to overland flow. In this later stage of the simulation, the actual flux (AtmAct) stays negative, which means that as a net flux over the entire transect, rainfall exits the transect. Therefore, runoff is mainly generated through return flow (i.e., subsurface runoff) and direct runoff on the variable source areas. An annual average recharge rate of 86 mm/y was obtained (calculated using the cumulative recharge over 100 years). This value is slightly higher than the recharge values previously found (section 6.5), but still in the same order of magnitude.

Figure 7.29 shows the spatial distribution of the modeled recharge rate over the transect at different times, from which the highly spatial and temporal variability of this flux is evident. As the simulation progresses, the recharge rate becomes less spatially variable, converging to the rainfall input value (2.22×10^{-9} m/s, corresponding to 70 mm/y). The highest temporal peaks occur during the first year of the simulation and hence, are not representative of the long-term dynamics. Spatially, the highest values are found on either side of Tony Creek, particularly on the right side, where a strong topographic gradient and higher *K* value (corresponding to Paskapoo 1.2) combine. The second highest peak corresponds to the location of the mound. This result confirms a soil/topography-driven system.

Groundwater recharge is zero where the water table intersects the land surface (discharge areas), which occurs at topographic depressions. After 100 years, the water table intersects the surface at four points (topographic depressions), including, as expected, Tony Creek since a zero pressure head Dirichlet boundary condition was imposed there.

It is important to remark, as mentioned in section 5.3.2, that groundwater recharge in CATHY is computed strictly as the amount of water that crosses the water table in a downward direction, whereas in other models and methods, recharge is generally conceptualized as that part of rainfall that reaches an aquifer. Thus, in CATHY, groundwater recharge is not as directly connected to rainfall and is instead a consequence of the interaction of many factors that include rainfall but also topography, heterogeneity, unsaturated zone storage, aquifer storage coefficient, and boundary conditions. For this last factor, the treatment of the bottom boundary is particularly important when the domain being modeled is relatively shallow. In this study, for instance, the thickness of the transect modeled in CATHY is on average ~300 m, while the transect in FLONET is on average ~1 km thick. As a result, in CATHY groundwater recharge fluxes can be very highly variable in space and time.

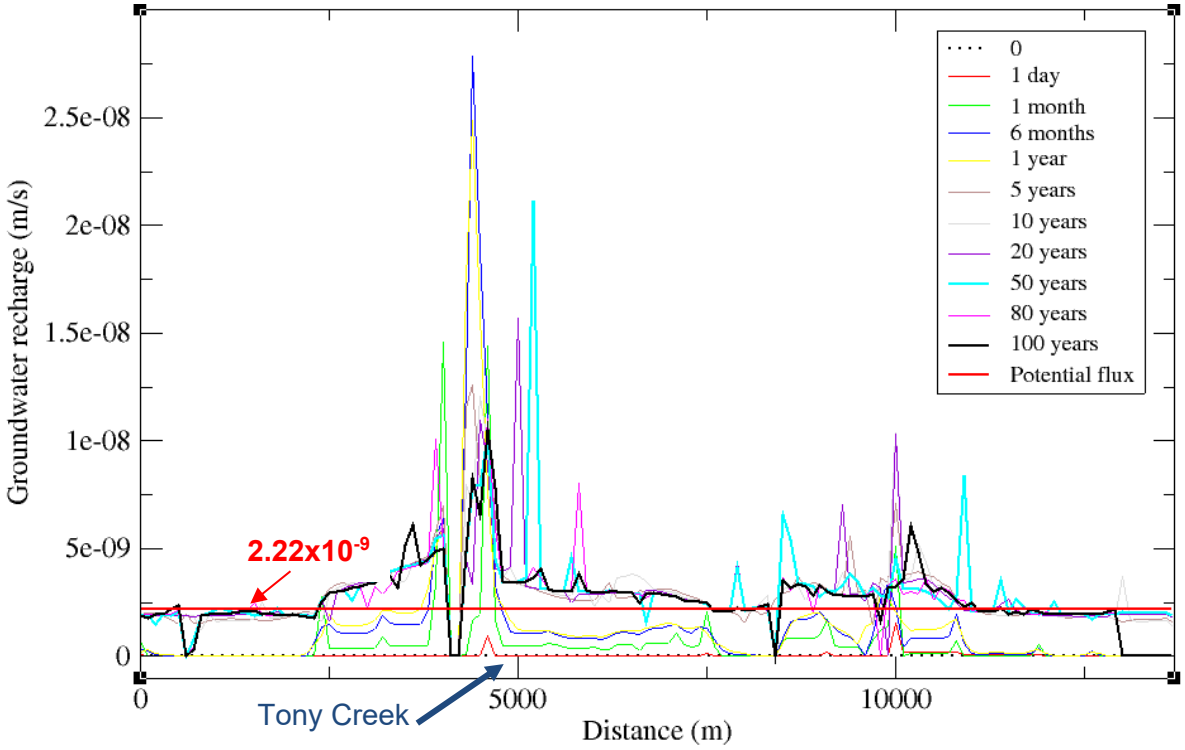

Figure 7.29. Spatially and temporally distributed groundwater recharge rates for the first configuration (no surficial sediments). The red line represents the base value of groundwater recharge. Note: 70 mm/y corresponds to 2.22 x 10^{-9} m/s.

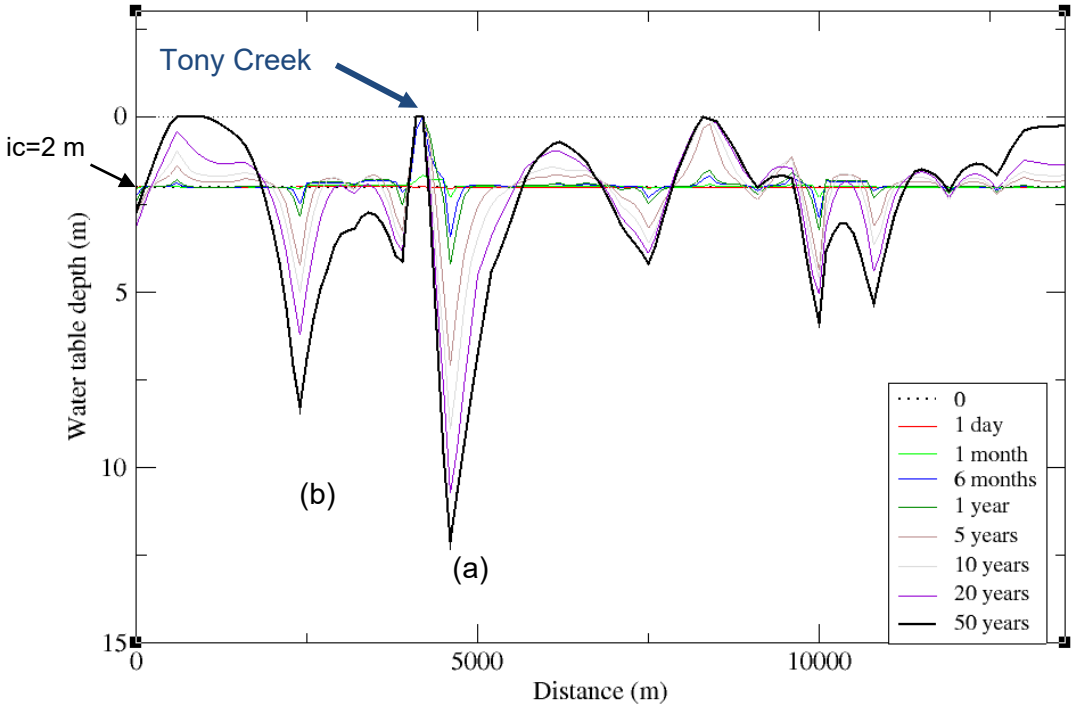

Figure 7.30. Spatially and temporally distributed water table depth for the first configuration (no surficial sediments). Zero depth corresponds to the top of the Paskapoo Formation. Note: ic = initial conditions for the water table.

The spatial distribution of the water table position is illustrated as depth below the surface in Figure 7.30 and m.a.s.l. elevation in Figure 7.31. The maximum water table depths are spatially consistent with the groundwater recharge maximum values presented in Figure 7.29. The deepest levels of the water table (marked as (a) and (b) in Figure 7.30) around Tony Creek correspond to the highest peaks of Figure 7.29 (note that the peaks appear abnormally sharp, due to the vertical scale used compared to Figure 7.30).

Figure 7.31 shows that the water table becomes smoother and generally lower over time. The water table position along the transect shows areas where water infiltrates and water exfiltrates (above the topography). The water table did not reach a steady state, continually decreasing or rising with respect to its initial position (2 m below the surface) along the transect, although variations over the last 50 years are minor.

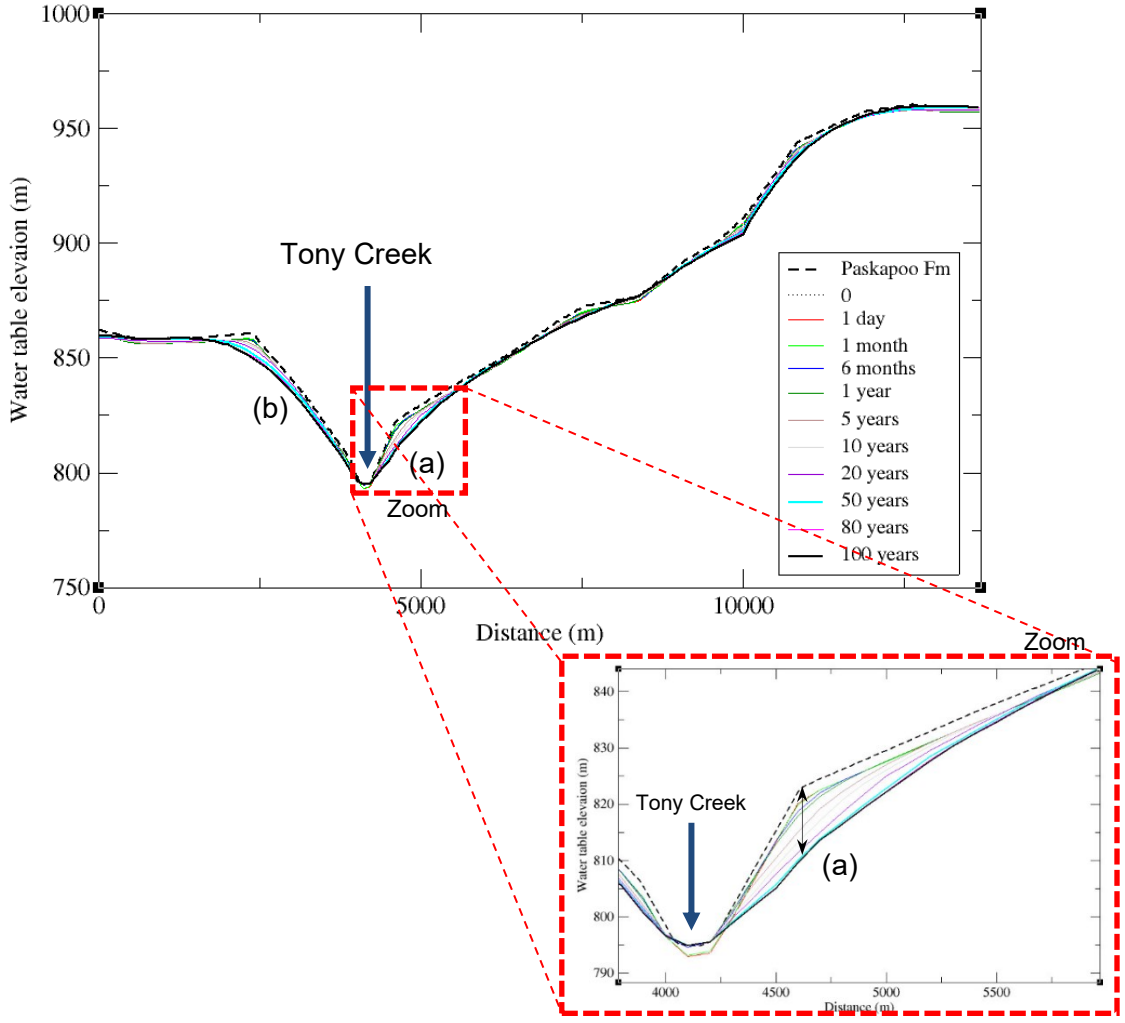

Figure 7.31. Water table elevation over time for the first configuration (no surficial sediments). The zoom in the red rectangle shows the area where the water table is the lowest (marked as (a) in Figure 7.30). It also shows that at Tony Creek, the water table intersects the top of Paskapoo Formation.

Figure 7.32 presents the evolution of the surface saturation fraction over the entire transect for the 100-year simulation. Initially, the surface was completely unsaturated, with a water table 2 m below the surface. Then, the model adapts gradually to the potential atmospheric flux and the fraction of the surface that is saturated increases. Rain that falls on these saturated portions generates direct runoff, which explains the increase of overland flow at 55 years (Figure 7.28 (a)). The mean degree of saturation over the entire surface after ~60 years is in the order of 8%. In other words, this percentage corresponds to the percentage of discharge areas (i.e., where the water table intersects the surface, so in this case, the top of the Paskapoo Formation).

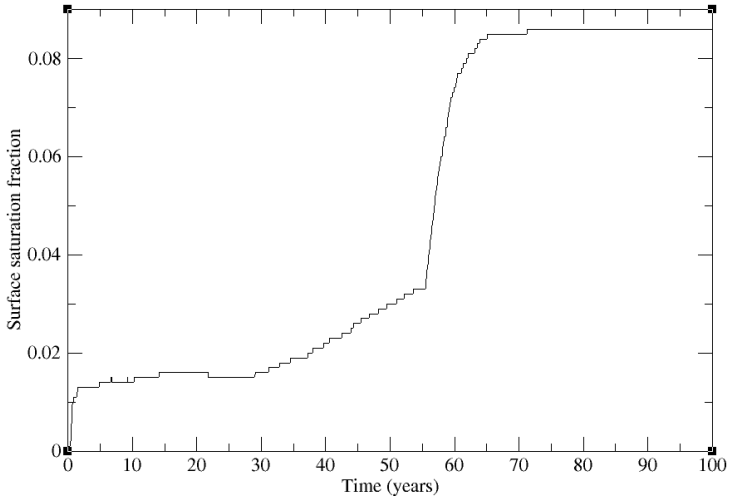

Figure 7.32. Surface saturation fraction for the first configuration (no surficial sediments).

For comparison, Figure 7.33 shows the simulated water table with FLONET and CATHY (after 100 years) and the interpolated water table. The CATHY water table shows a relatively good fit with that of FLONET and the interpolated water table, except at the boundaries of the cross-section. This is likely related to the fact that unsaturated conditions are considered in CATHY (unlike FLONET) and also because the interpolated water table is located in the surficial sediments, not included in this configuration. It has an RMSE of 12 m, which corresponds to 6.7% of the difference between the maximum and minimum hydraulic head elevations along this cross-section. Figure 7.34 presents the graphical comparison between the simulated and interpolated hydraulic head along cross-section B-B' for this scenario. Even more than with FLONET, the error (RMSE) is here strongly impacted by the values located below the topographic mound (circled in red). If these values are excluded, the RMSE decreases to 8.14 m, or 4.57% of the total hydraulic head elevation difference.

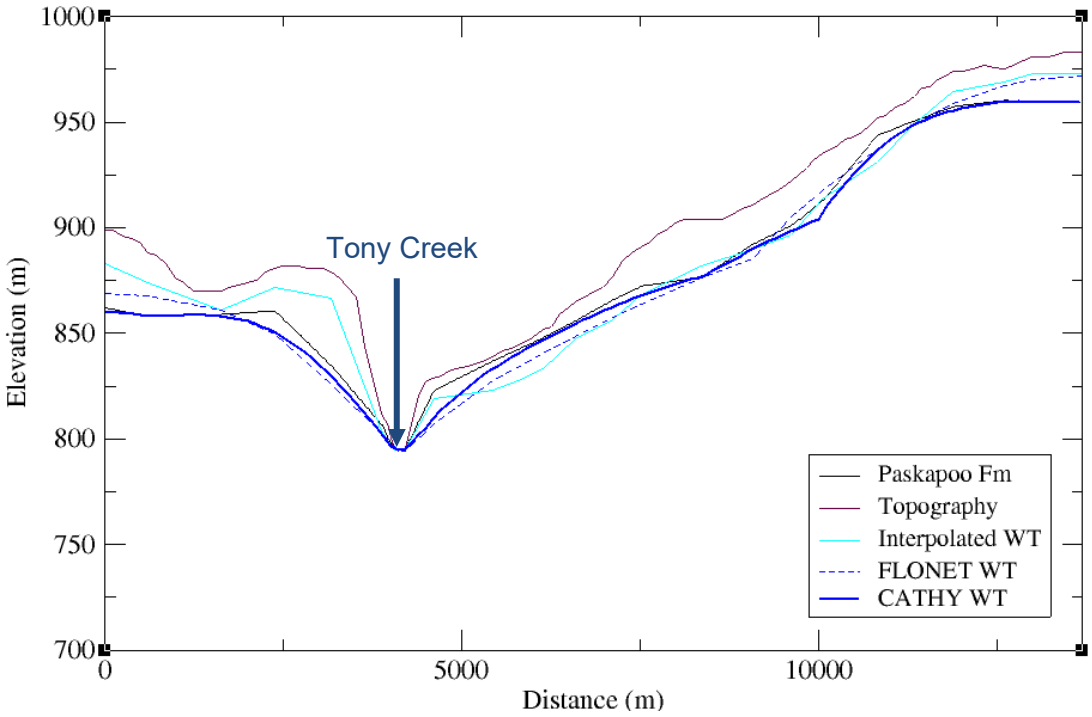

Figure 7.33. Comparison of the water table from the: 1) 100-year CATHY simulation for the first configuration (no surficial sediments), 2) saturated steady-state FLONET simulation (without surficial sediments) and 3) interpolated water table obtained from the piezometric map.

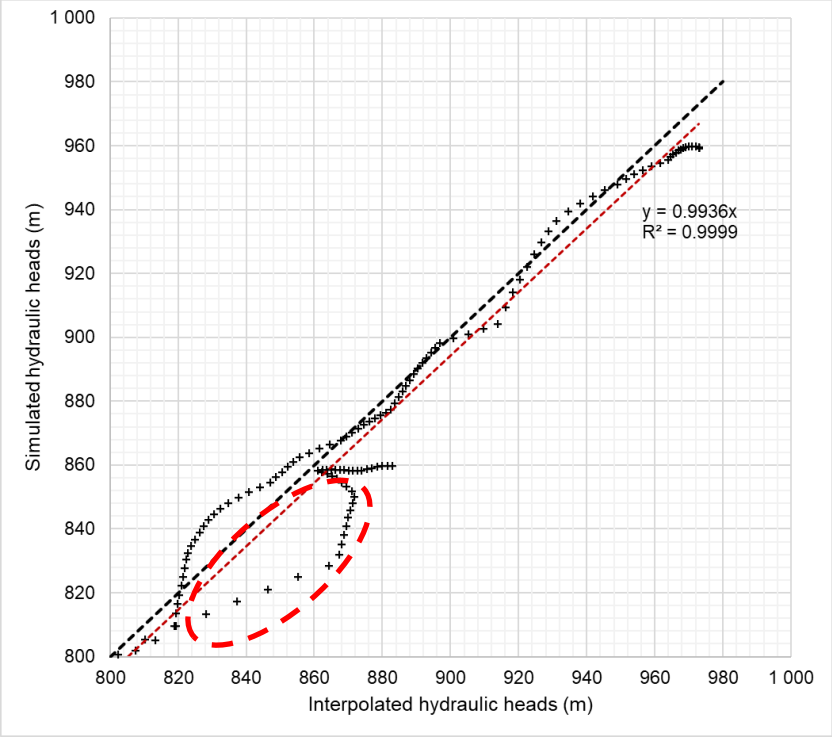

Figure 7.34. Comparison between the interpolated and CATHY simulated hydraulic heads. The black dotted line represents the 1:1 slope, while the red dotted line represents the linear regression line. The values located below the mound, north of Tony Creek, are circled in red.

Different boundary conditions were also tested in CATHY. Simulations without Dirichlet nodes imposed at Tony Creek were able to produce a water table that intersected the creek; thus the model was able to establish the main natural discharge area without imposing the creek as a boundary condition. Also, a no-flow condition at the bottom of the model was also tested. This simulation showed that the results were not significantly different from the results reported earlier, as could be expected since flow is concentrated primarily in the upper part of the Paskapoo Formation, driven by the topography and the rainfall input.

7.3.2 Scenarios including surficial sediments

For the inclusion of surficial sediments in the CATHY model simulations, the topography of the surficial unit tops with a resolution of 100 m (Atkinson & Hartman, 2017) was processed to obtain a 20 m resolution, from which the discretization mesh for the model was derived. Figure 7.35 shows the refined mesh, with a maximum elevation of 983 m to the south and a minimum of 794 m at Tony Creek. Compared to Figure 7.25 (i.e., elevations for the configuration without surficial sediment units), this configuration shows higher topographic gradients.

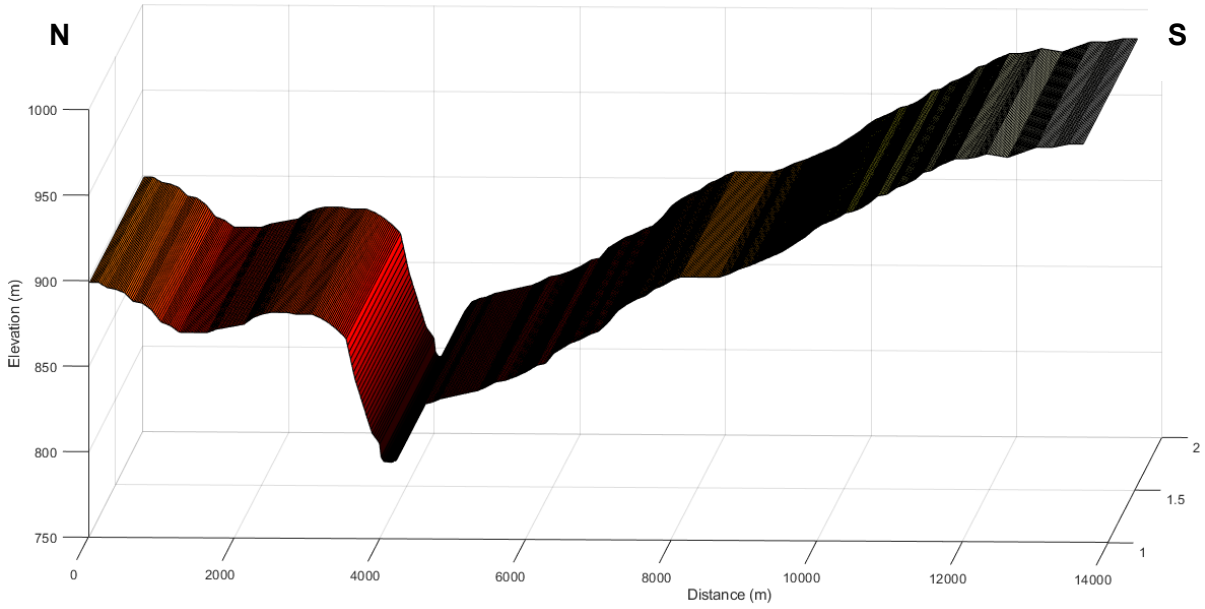

Figure 7.35. Topographic elevation representing the surficial sediments at a 20 m resolution.

For this mesh, the same number of elements as the previous configuration was retained. However, more zones had to be included to represent the bedrock formations (top of Paskapoo and Scollard), as layers have to parallel to the surficial sediments (Figure 7.36). The Paleogene–Quaternary sediments defined in the 3D geological model by Atkinson and Hartman (2017) are represented by two main units in cross-section B-B': SU4a and SU5 (see section 4.6). SU4a corresponds to a sandy silt diamict (till) described as "coarse-grained" although known to be variable in size, while SU5 corresponds to sand and gravel. The cross-section is dominated by 71% of SU4a.

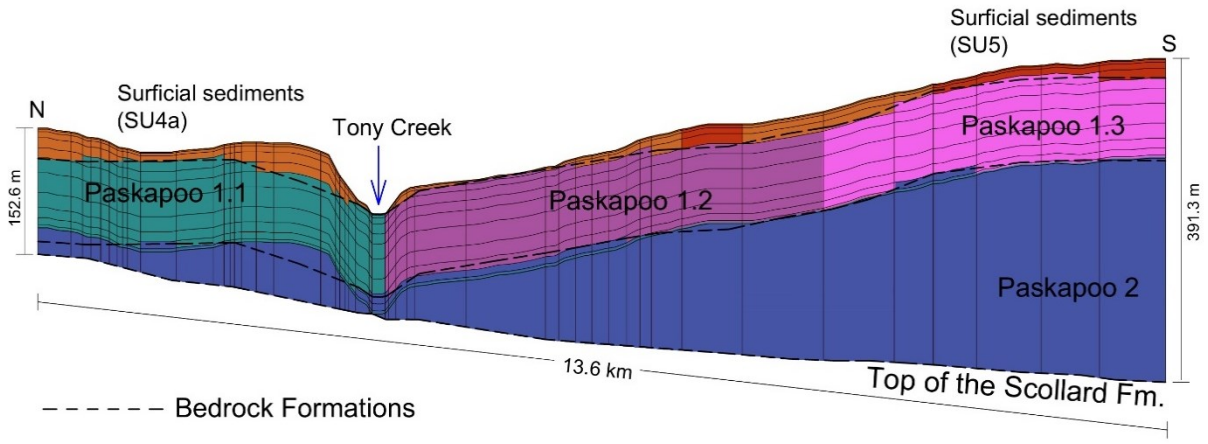

Figure 7.36. Characteristics of the 2D CATHY model mesh for the second configuration that includes the surficial sediments. The vertical grey lines represent the 46 horizontal zones. Unit SU5 is shown in red and SU4a in orange.

Based on the geological description, Smerdon *et al.* (2019) qualitatively correlated each stratigraphic unit to hydrogeological properties. As a result, a medium relative hydraulic conductivity was recommended for SU4a and a high value for SU5. Due to the uncertainty in these hydraulic conductivity values, several values within a plausible range (based on unit descriptions) were assigned to investigate the model response (Freeze & Cherry, 1979; Thompson *et al.*, 2015). These hydraulic conductivity values had a strong impact on the model outputs. The best results (in terms of RMSE) were obtained when a value of 9.5×10^{-6} m/s was assigned to SU4a and 1.1×10^{-5} m/s to SU5. These values are quite low for a sandy till and sand and gravel unit, but the surficial sediment cover in this area is known to contain, at least locally, some clay (section 2.3), which thus decreases the overal permeability of these units. These values are therefore in the same range as those selected for the three sections of the upper Paskapoo Formation (from 4.9×10^{-6} to 1.8×10^{-5} m/s).

The specific storage, van Genuchten coefficients, and atmospheric boundary conditions were kept the same as the previous configuration. Additionally, initial conditions were obtained from the median FLONET water table depth (13 m), calculated from the difference between the topography and the simulated water table.

Figure 7.37 presents streamflow, overland flow, return flow, and annual recharge. The actual atmospheric flux remains equal to the potential atmospheric flux for the first year, and later decreases as overland and return flow increase. Towards the end of the simulation period, overland and return flow approach the potential flux, while the actual flux approaches zero. Higher return and overland flows are obtained for this configuration since the topographic gradients are

more pronounced and a thicker unsaturated zone retains more water from rainfall that infiltrates the subsurface to exit further downslope. The recharge curve over time shows an initial peak during the model “spin up”, then a decrease, whose value appears to be constant for about 20 years, and finally a second, smoother increase, whose value remains relatively constant until the end of the simulation at a slightly higher value than the potential flux (AtmPot). An annual average recharge of 66 mm/y was obtained with this model configuration. The addition of the unconsolidated sediment units, affecting the topography, also strongly influences infiltration, generating higher values of overland and return flow. This scenario thus results in a reduction in recharge compared to the first configuration (i.e., without surficial sediments). Annual overland flow was estimated at 135 mm/y, which is slightly lower than the value (151 mm/y) estimated using the SCS method (in section 6.5.2).

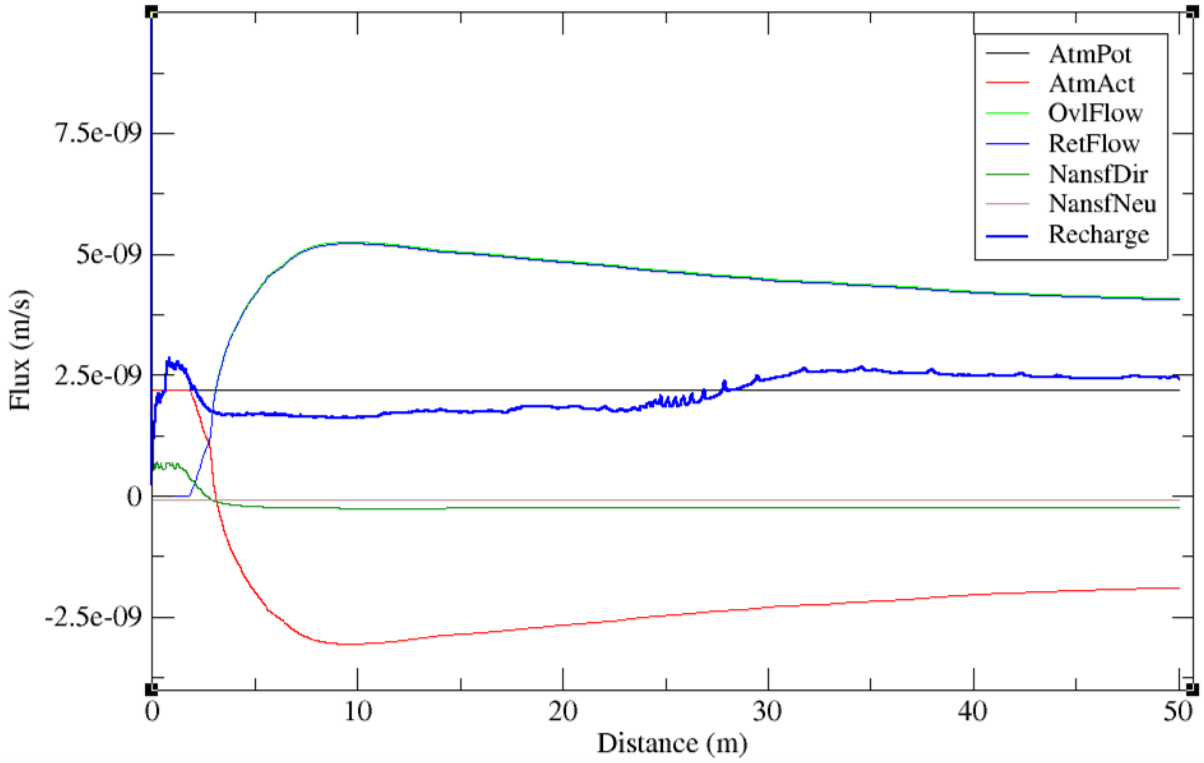

Figure 7.37. Various outputs from CATHY (fluxes) over 50 years for the second configuration that includes the surficial sediments.

Figure 7.38 shows a recharge rate much less spatially variable as the simulation progresses, especially near the southern boundary, converging towards 2.22 x 10^{-9} m/s (corresponding to the atmospheric input 70 mm/y). Spatially, the highest values are located north of Tony Creek, where the topographic mound is located. In this case, the *K* value of the unit at the surface is the same

on either side of Tony Creek (contrary to the first configuration where the Paskapoo Formation has different *K* values on both sides, see Figure 7.29).

In Figure 7.38, Tony Creek is represented by a larger zero recharge zone than in the first configuration. There are also two points with zero flux located around 6 and 7 km for the 50-year simulation (black line). However, Figure 7.39 shows that the water table does not intersect the surface at these points, so these values represent ephemeral zones of zero groundwater recharge.

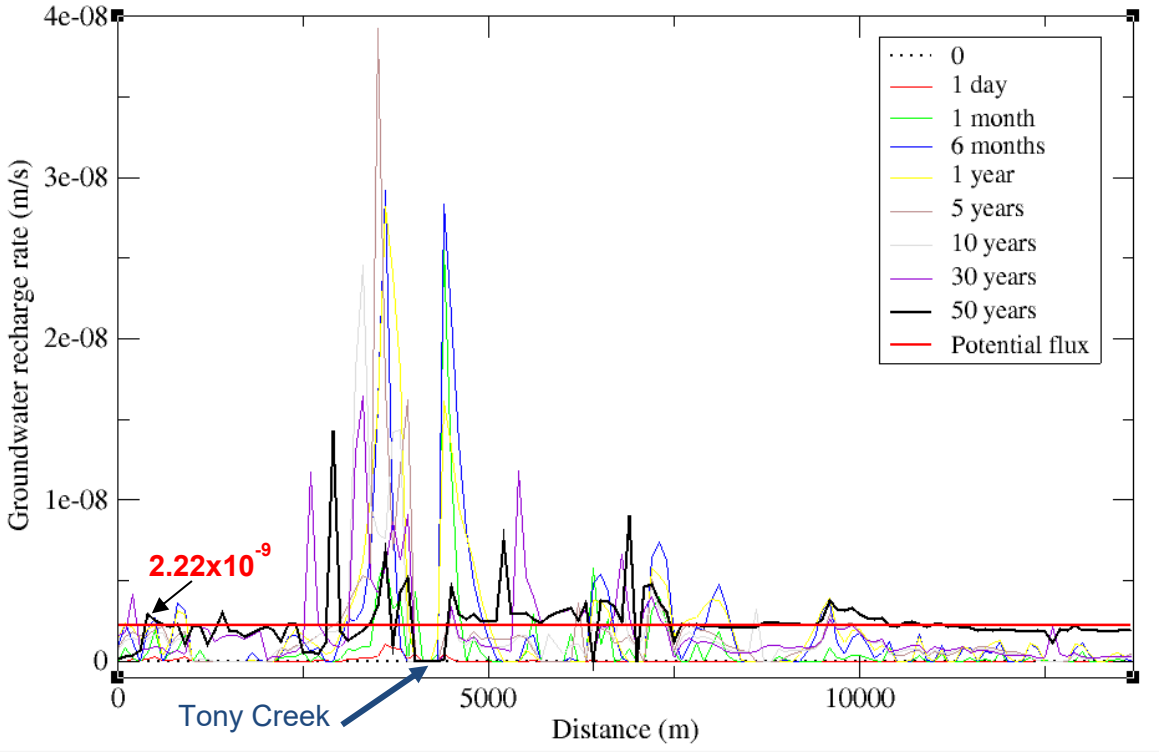

Figure 7.38. Spatially and temporally distributed groundwater recharge rates for the second configuration that includes the surficial sediments. The red line represents the base value of groundwater recharge.

Figure 7.39 and Figure 7.40 present the water table depth and the water table elevation, respectively. These figures show that the water table intersects the surface only at Tony Creek and that the deepest water table is located north of Tony Creek, below the ~2 km mound. It also corresponds to the area with the highest groundwater recharge. Figure 7.40 shows, as in the first configuration, that the water table becomes smoother as the simulation progresses.

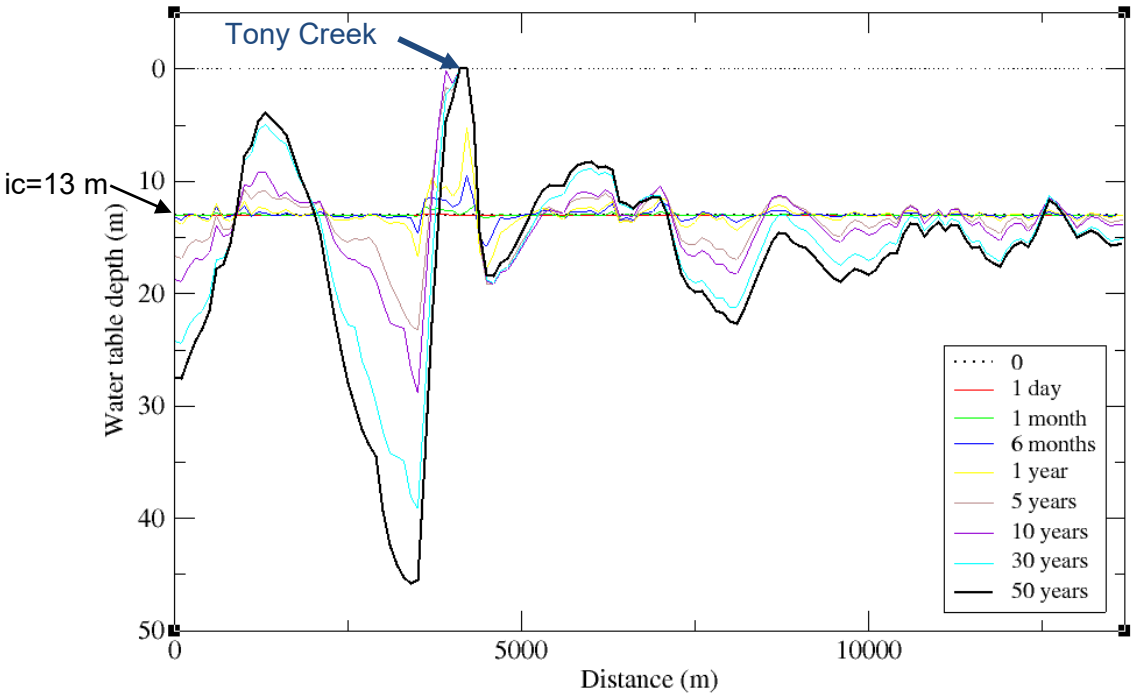

Figure 7.39. Spatially and temporally distributed water table depth for the second configuration that includes the surficial sediments. Note: ic = initial conditions for the water table.

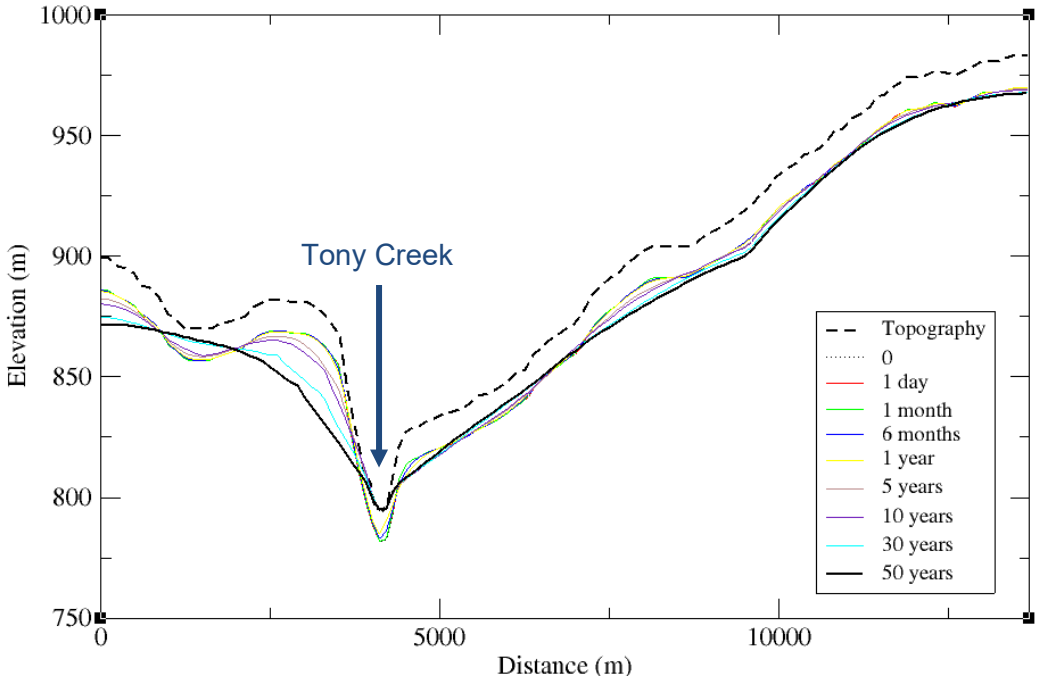

Figure 7.40. Water table elevation over time for the second configuration that includes the surficial sediments.

Figure 7.41 shows a transition from a transect that is entirely unsaturated at the surface (with a water table at 13 m below the surface) to a higher surface saturation fraction over time. The mean surface saturation fraction over the entire transect is smaller when including the surficial sediments since only one area, Tony Creek, intersects the surface with this configuration (a peak of about 1.5% is obtained with this configuration while over 8% was found with the configuration without surficial sediments).

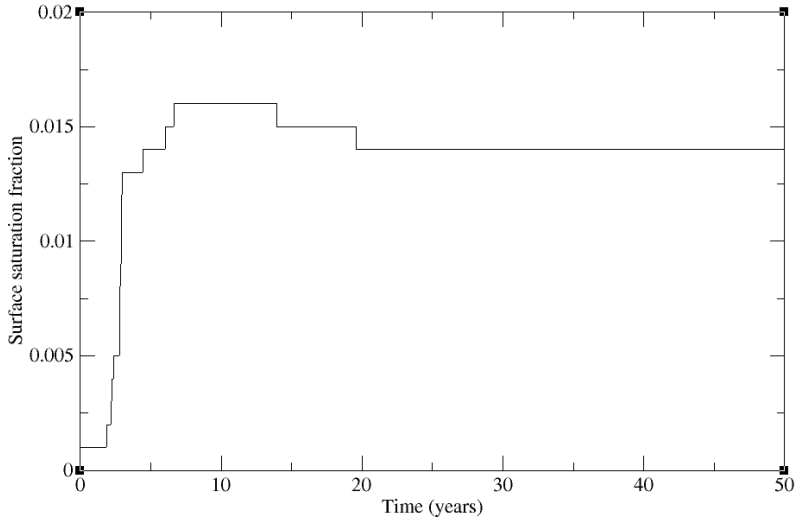

Figure 7.41. Surface saturation fraction for the second configuration that includes the surficial sediments.

Figure 7.42 presents the water table from the CATHY simulation including surficial sediments (after 50 years), the saturated steady state FLONET simulation, and the interpolated water table from the piezometric map for comparison. The CATHY water table shows a slightly better match to the interpolated water table than the FLONET simulation, with an RMSE of 8.9 m, corresponding to 5.01% of the difference between the maximum and minimum hydraulic head elevations. This result represents an improvement compared to the first configuration (RMSE = 12 m). In particular, a much better fit is obtained at both transect boundaries and, to a lesser degree, below the mound north of Tony Creek. This is likely mainly due to the slightly higher K values at these two ends of the transect, and the change in topography brought about by the addition of the surficial sediment units. However, the first configuration was not optimized as this configuration was only intended for comparison with the FLONET model. Figure 7.43 presents the graphical comparison between the simulated and interpolated hydraulic head along cross-section B-B'. Excluding the values located below the topographic mound north of Tony Creek, circled in red, the RMSE decreases to 4.7 m, or 2.6% of the total hydraulic head elevation difference. This error is well below the threshold of acceptability (5%) suggested by Anderson and Woessner (1992).

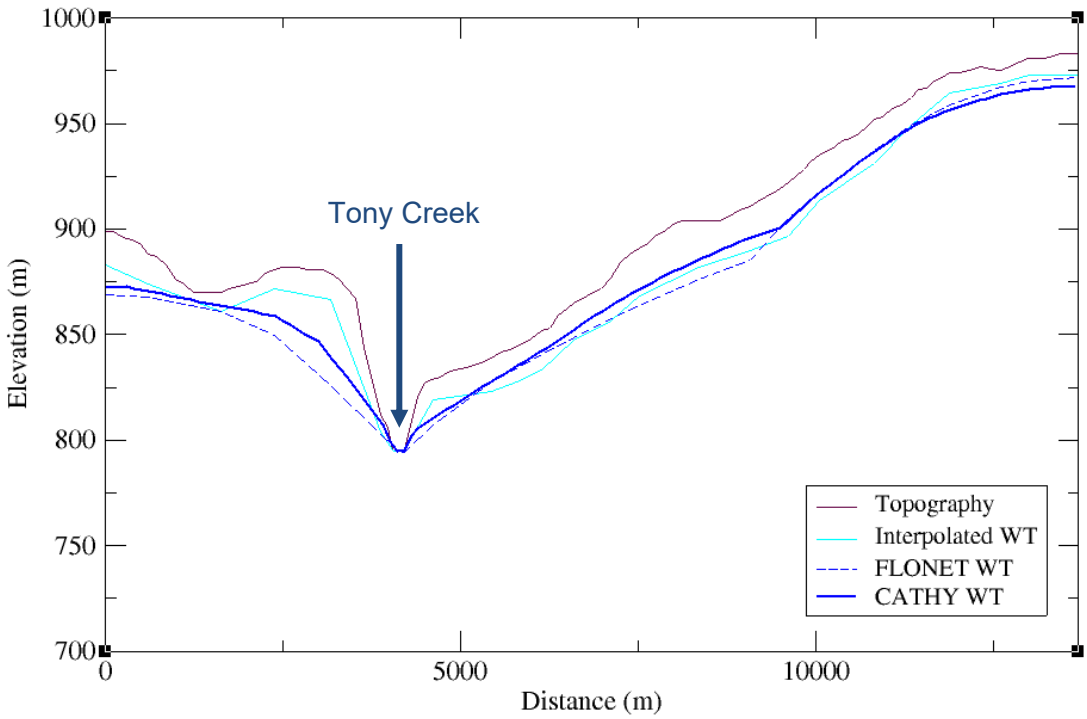

Figure 7.42. Comparison of the water table from the 1) 50-year CATHY simulation including the surficial sediments, 2) saturated steady state FLONET simulation (without surficial sediments) and 3) interpolated water table obtained from the piezometric map.

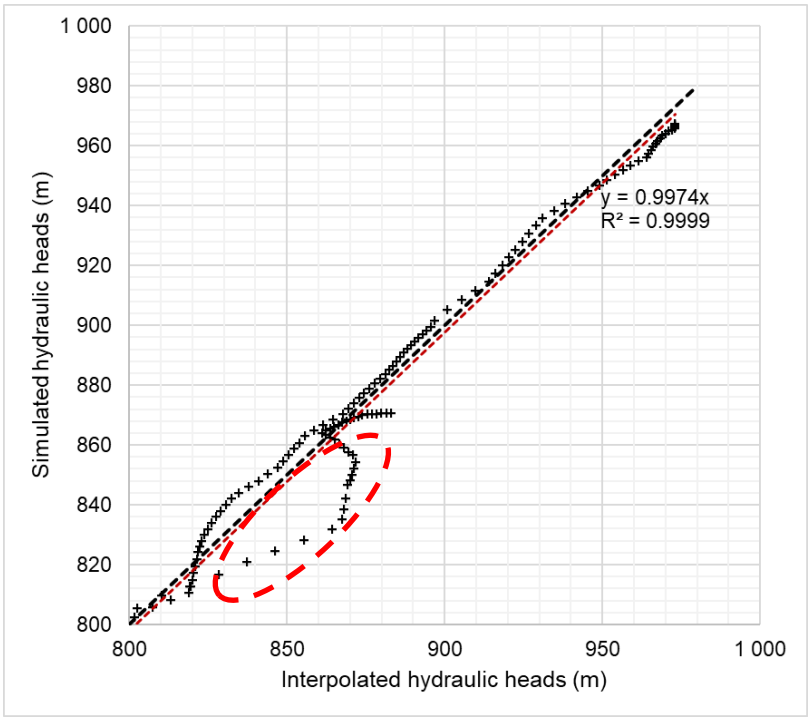

Figure 7.43. Comparison between interpolated and simulated hydraulic heads. The black dotted line represents the 1:1 slope, while the red dotted line represents the linear regression line. The values located below the mound, north of Tony Creek, are circled in red.

7.3.3 Scenarios with variable atmospheric boundary conditions and snowpack

Atmospheric boundary conditions, kept constant in the previous simulations, were included in this final scenario directly from observation records of daily precipitation and daily potential evapotranspiration. In addition, snow accumulation and snowmelt were also included using a degree-day method (USDA, 1985). The snow melting rate and the threshold snow melting temperature were selected based on the land cover in cross-section B-B'. The aim here was to investigate how seasonal variations in atmospheric forcing influence groundwater recharge. The 2007-2010 time period was selected because it has one of the most complete records, and the mean annual precipitation is around 70 mm/y.

Figure 7.44 presents the precipitation minus evapotranspiration record for 2007 to 2010 with and without snow accumulation and melt. An important precipitation event took place in May 2010, represented by a peak higher than 100 mm.

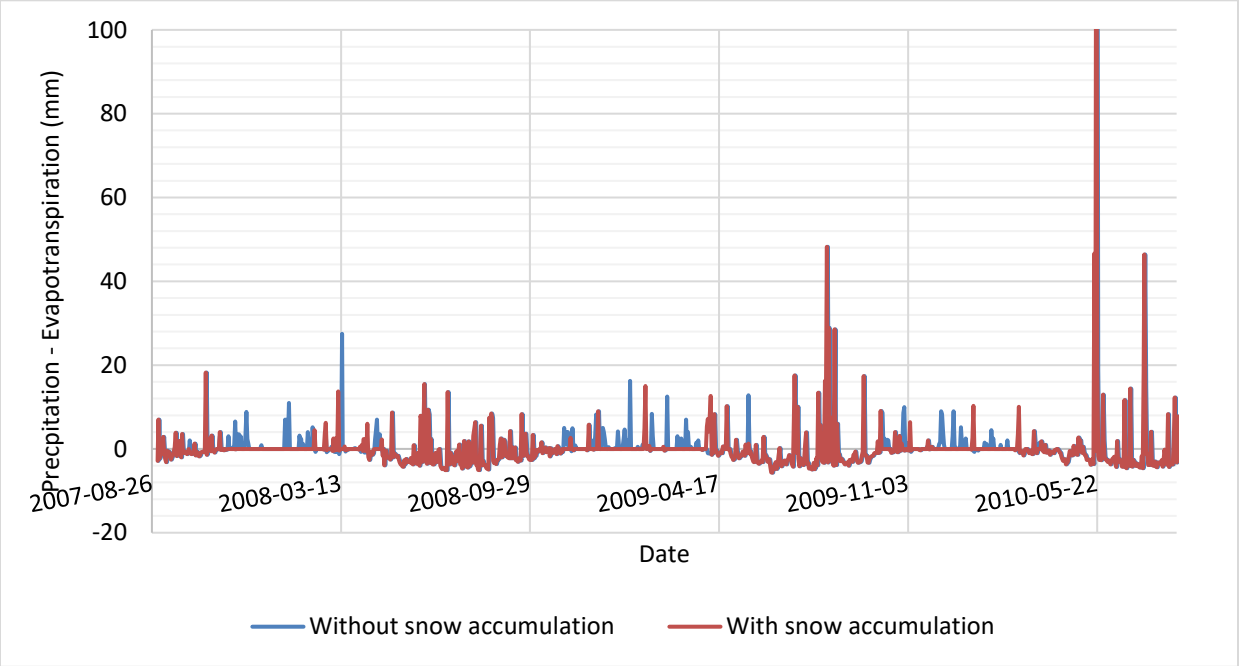

Figure 7.44. Input atmospheric forcing with and without snow accumulation minus evapotranspiration for the 2007-2010 period.

Figure 7.45 shows the simulation results over time for streamflow, overland flow, return flow, and annual recharge for this scenario obtained using the second configuration including surficial sediment units. The groundwater recharge flux reflects very well the seasonal patterns, for instance showing a high recharge event in the spring (May 2010, see blue circle in Figure 7.45) and a strong response to major precipitation events. The potential and actual atmospheric fluxes also show interesting results when a significantly long evaporation period occurs during the

summer months. The actual flux shows that the soil cannot evaporate at the assigned rate, so the actual flux is lower than the potential flux. This behavior is shown in detail in the zoom circled in black in Figure 7.45.

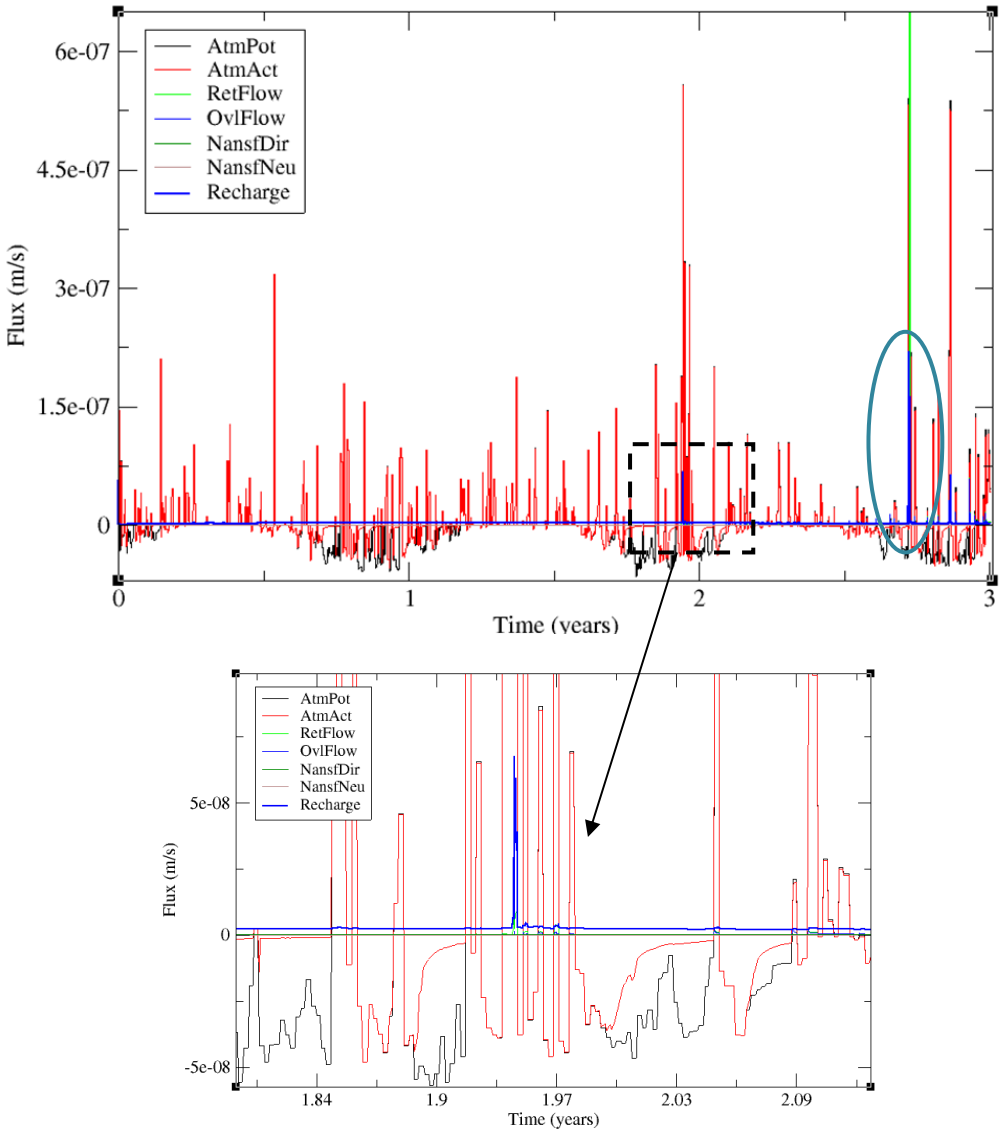

Figure 7.45. Simulated fluxes (m/s) when including variable atmospheric forcing for the 2007-2010 period.

The annual average recharge, including the effect of snow accumulation and melt, was found to be 75.4 mm/y, similar to the recharge simulated without snowmelt (76.36 mm/y) for the 2007-2010 period. These values are higher than when considering a constant recharge in time (66 mm/y) mainly due to the more important spring recharge caused by the snow accumulation. The effect of snow accumulation and melting can be seen in Figure 7.46, where the monthly recharge with and without snow accumulation is plotted. Recharge is slightly lower when including snow

accumulation during the winter months, higher in the spring when the snow melts, and identical during the summer months. Winter recharge is possible since positive temperatures during this season are not unusual in the study area.

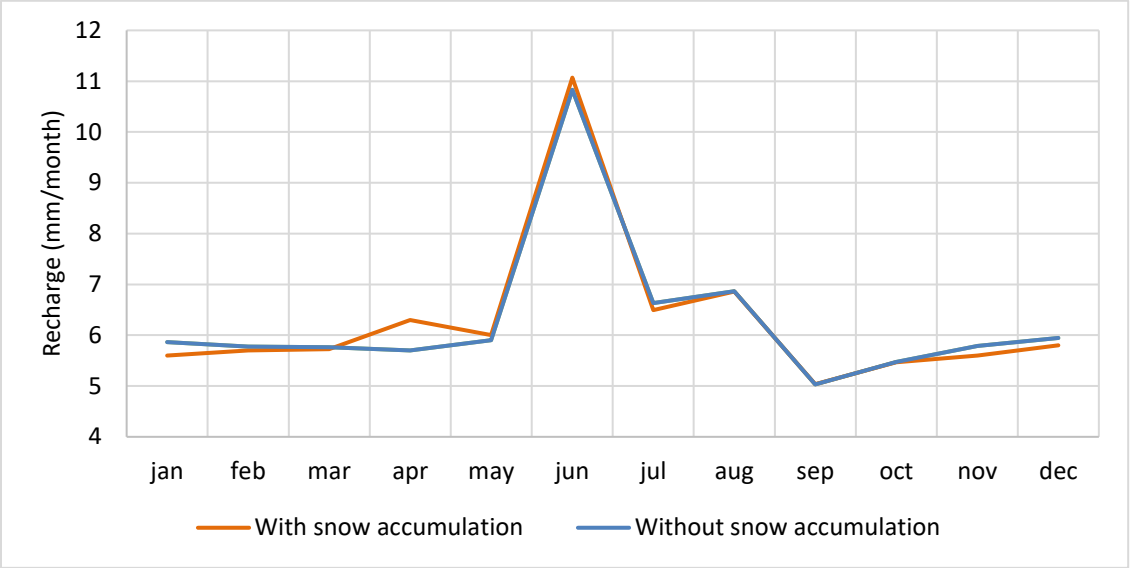

Figure 7.46. Monthly simulated recharge with and without snow accumulation for the 2007-2010 period.

7.3.4 Summary of recharge results

Table 7.5 summarizes the annual recharge rates found with CATHY for the various scenarios. Recharge estimates are slightly higher but close to the previous range found with the literature review (70 mm/y, in section 4.5) and the water budget (0-57 mm/y, in section 6.5.2). Future hydraulic conductivity values from *in situ* permeameter tests and inferred from grain-size analyses will help better estimate this important parameter.

Table 7.5. Summary of recharge results with CATHY

Surficial sediments	Atmospheric forces	Recharge (mm/y)
NO	Uniform Ptot – ET of 70 mm/y	86
YES	Uniform Ptot – ET of 70 mm/y	66
YES	Variable 2007-2010 Ptot – ET annual average value of 47 mm/y	76.36
YES	Variable 2007-2010 (including snowmelt) Ptot – ET annual average value of 36 mm/y	75.4

8 DISCUSSION AND CONCLUSION

A characterization and modeling study was conducted in the Fox Creek area, west-central Alberta, one of Canada's most active regions for hydrocarbon production over the last 50 years. This study is part of a larger project conducted by the Geological Survey of Canada that aims to assess the environmental cumulative effects related to the oil and gas industry.

The main objectives of this Master's thesis were to characterize the fractured bedrock aquifer of a 700 km^2 watershed, and more specifically of the 425 km^2 Tony Creek sub-watershed, to estimate a water budget including recharge rates, and to improve the understanding of potential hydraulic connections between deep geological units and shallow aquifers. To this end, the study focused on: 1) a characterization of the hydrogeological system including data collection from available databases, reports and papers, and the estimation of additional values inferred from specific capacities, 2) the assessment of recharge using the water budget equation through GIS tools and 2D numerical models, and 3) the development of scenarios including "windows" in the Battle Formation to investigate the possibility of upward fluid migration.

Data collection from previous studies confirmed the highly heterogeneous hydrogeological properties for the Paskapoo Formation, with hydraulic conductivity values ranging over several orders of magnitude. Specific capacity values, considered a good approximation for transmissivity, were also calculated from water wells in the provincial database where static and dynamic water levels were available, then converted to hydraulic conductivity (*K*) values. As a result, a median *K* value of 1.51 x 10^{-5} m/s was obtained. This value is an order of magnitude smaller than the median value found using pumping tests.

In the models, the uppermost 100 m of the Paskapoo Formation was considered to have higher *K* values than the lower part of this formation due to the presence of fractures. Therefore, values obtained from pumping tests, then from specific capacity were considered representative of the upper part, while values obtained from core samples were considered more representative of the lower part (Hughes *et al.*, 2017b). The modeling work indicated that values inferred from *Cs* values, found specifically with wells located within the 700 km^2 study area, are more representative than the larger value found from pumping tests for the northern part of the Paskapoo Formation.

A strong correlation between topography (ground elevation) and groundwater elevation was found for wells within (or close to) the study area, indicating that groundwater flow is strongly controlled

by topography. The topography was therefore used as secondary information for the piezometric map (created using kriging with an external drift), because no (or very few) water levels were available in different zones of the study area. As expected, this map shows that groundwater flows mainly from south to north towards the main streams, closely following the topography. Due to the interpolation method used, the estimated groundwater elevations are likely overestimated, especially in high topographic areas.

An annual recharge ranging from 0 to 70 mm/y was defined based on previous studies and a water budget. A marked difference between the western and eastern parts of the study area was found for the CN (curve number) values and, hence, for the runoff values. This difference is mostly due to the soil type distribution since the western part contains more permeable soils. Annual evapotranspiration was estimated to represent about 90% of precipitation (~550 mm/y), which is very high, but not unusual for the Prairies.

The hydrodynamics of a cross-section near the outlet of the Tony Creek sub-watershed was studied using two numerical models, FLONET and CATHY, developed based on the provincial geological models (Atkinson & Hartman, 2017; Corlett *et al.*, 2019). The FLONET model included the four upper formations of the sedimentary succession in this region (Paskapoo, Scollard, Battle, and Wapiti) and extended over more than 1 kilometer in depth. To properly represent the water table (corresponding to an interpolation made from the piezometric map) across the transect, the upper part of the Paskapoo Formation was divided into three sections and the different *K* values assigned were selected from the lower range (between the 20^{th} and 50^{th} percentiles) of the values estimated using the specific capacity of wells in the study area. These are, unsurprisingly, the parameters that have the most impact on the model response. A 70 mm/y recharge was used. A good root mean square error (RMSE) was obtained (9.67 m or 5.42%), especially when excluding values located below the mound north of Tony Creek (5.09 m or 2.86%), where the depth of the interpolated water table is very likely significantly underestimated. Nonetheless, these hydraulic conductivities were calibrated to the highest value of the recharge range (70 mm/y) based on the combination of hydraulic conductivity and recharge rate parameters. Therefore, a reduction in the input value of recharge would produce lower calibrated hydraulic conductivity values.

The occurrence of upward fluid migration from deeper formations was also investigated in line with the GSC project's objective of assessing the potential impacts on shallow aquifers of activities carried out at depth. Scenarios including gaps ("windows") in the Battle Formation show that upward flow is only present when hydraulic heads on both lateral boundaries of the Wapiti

Formation are increased by more than 100 m, which is not realistic in the context of the available data. Although the provincial piezometric map of the Wapiti Formation includes a zone northeast of the study area with such hydraulic head values, the possibility of upward fluid migration is considered very unlikely, but cannot be completely ruled out.

The CATHY model was implemented based on the results obtained with the FLONET model, where 96% of the flow is concentrated in the Paskapoo Formation. Therefore, this model included only the Paskapoo Formation, extending up to 367 m in depth. The first objective of the model was to reproduce the same conditions as in the FLONET model in order to compare the water table and recharge (obtained as an output in CATHY) with the values either assigned in FLONET (recharge) or obtained as output (water table). To do this, a long-term simulation was run to evaluate the quasi steady state conditions without including the surficial sediment units. A recharge value of 86 mm/y was obtained for this configuration over 100 years, which is slightly higher than the previous estimates. The water table showed a fairly good fit with the simulated water table, except at the lateral boundaries, where it was notably lower. The addition of slightly more permeable unconsolidated sediment units, which also increased topographic gradients, altered infiltration, generating higher values of overland and return flow. Therefore, recharge was reduced (66 mm/y) compared to the previous steady state configuration. This configuration provided a better fit with the interpolated water table, particularly on both lateral boundaries. An RMSE of 4.7 m (or 2.6%) was obtained when excluding the values below the mound.

Additional simulations incorporating time-varying precipitation and potential evaporation, as well as the effect of snow accumulation and melting were then performed. A recharge rate of 75 mm/y was found. This value is higher than the previous one since the spring recharge is more important than in the case of a constant recharge in time. The actual evaporation computed by the model's boundary condition switching feature confirmed a soil-controlled system that is able to significantly limit this component of the water balance compared to the quite high potential evapotranspiration that prevails in the Prairies.

Future work should include implementing the surface routing module to redirect the overland and return flow to the watershed outlet and the analysis and integration in the model of data collected in the field to obtain a fully coupled surface water/groundwater model. Field data will also be interpreted as they become available, including the assessment of recharge from hydrograph separation and river 7-day low flows using data from the gauging station and from well hydrographs using the GWHAT software (Gosselin *et al.*, 2017). Upcoming work also includes

the estimation of the bedrock aquifer vulnerability to surface contamination using the DRASTIC index.

9 BIBLIOGRAPHY

Abbott MB, Bathurst JC, Cunge JA, O'Connell PE & Rasmussen J (1986) An introduction to the European Hydrological System - Système Hydrologique Européen, SHE, 2: Structure of a physically-based, distributed modelling system. J. Hydrol., 87, 61-77.

Akinremi OO, McGinn SM & Barr AG (1996) Simulation of soil moisture and other components of the hydrological cycle using a water budget approach. *Canadian Journal of Soil Science* 76(2):133-142.

Alberta Climate Information Service (2013) Evaporation and Evapotranspiration in Alberta

Alberta Energy Regulator (2015) Play-based regulation: piloting a new approach to oil and gas development, 22 p.

Alberta Environment and Parks (2018) Alberta Water Well Information Database. Retrieved [june 2019], from http://groundwater.alberta.ca/WaterWells/d/.).

Anderson M & Woessner W (1992) *Applied groundwater modeling. Academic Press, San Diego, CA. 381 p.*

Atkinson LA & Hartman GMD (2017) 3D rendering of the regional stratigraphy of Paleogene−Quaternary sediments in west-central Alberta; Alberta Energy Regulator, AER/AGS Report 93, 44 p.

Baalousha HM (2016) Development of a groundwater flow model for the highly parameterized Qatar aquifers. *Modeling Earth Systems and Environment* 2(2).

Babakhani M, Mei S, Atkinson LA & Smerdon BD (2019) 3D property modelling of the bedrock hydrostratigraphy in the Fox Creek area, west-central Alberta; Alberta Energy Regulator / Alberta Geological Survey, AER/AGS Open File Report 2019-03, 19 p.

Barker AA, Riddell JTF, Slattery SR, Andriashek LD, Moktan H, Wallace S, Lyster S, Jean G, Huff GF, Stewart SA & Lemay TG (2011) Edmonton-Calgary Corridor groundwater atlas; Energy Resources Conservation Board, ERCB/AGS Information Series 140, 98 p.

Beckers J, Smerdon BD & Wilson M (2009) Review of Hydrologic Models for Forest Management and Climate Change Applications in British Columbia and Alberta. FORREX Forum for Research and Extension in Natural Resources, Kamloops, BC forrex Series 25. www.forrex.org/publications/forrexseries/fs25.pdf.

Bixio AC, Orlandini S, Paniconi C & Putti M (2000) Physically-based distributed model for coupled surface runoff and subsurface flow simulation at the catchment scale, in Computational Methods in Water Resources, Vol. 2, Surface Water Systems and Hydrology (L.R. Bentley, J.F. Sykes, C.A. Brebbia, W.G. Gray and G.F. Pinder, eds.), Balkema, Rotterdam, The Netherlands, 1115-1122.

Brooks RH & Corey AT (1964) Hydraulic properties of porous media. Hydrology Paper 3, Colorado State University, Fort Collins.

Camporese M, Daly E & Paniconi C (2015) Catchment-scale Richards equation-based modeling of evapotranspiration via boundary condition switching and root water uptake schemes. *Water Resources Research* 51(7):5756-5771.

Camporese M, Paniconi C, Putti M & Orlandini S (2010) Surface-subsurface flow modeling with path-based runoff routing, boundary condition-based coupling, and assimilation of multisource observation data. *Water Resources Research* 46(2).

Camporese M, Paniconi C, Putti M & Salandin P (2009) Ensemble Kalman filter data assimilation for a process-based catchment scale model of surface and subsurface flow. *Water Resources Research* 45(10).

Carsel RF & Parrish RS (1988) Developing joint probability distributions of soil water retention characteristics. Water Resources Research, 24(5), 755–769. doi:10.1029/wr024i005p00755

CDEM (2015) Canadian Digital Elevation Model (CDEM). Ottawa, ON: Natural Resources Canada. [consulted 07-2019] https://open.canada.ca/data/en/dataset/7f245e4d-76c2-4caa-951a-45d1d2051333.

Chemingui A, Sulis M & Paniconi C (2015) An assessment of recharge estimates from stream and well data and from a coupled surface-water/groundwater model for the des Anglais catchment, Quebec (Canada). *Hydrogeology Journal* 23(8):1731-1743.

Chen Z, Grasby SE, Hamblin T & Xiu S (2007a) Paskapoo Groundwater Study, Part II: Sandstone thickness and porosity estimations using well log data for the aquifer system in the Tertiary Paskapoo Formation, Alberta. :16.

Chen Z, Grasby SE & Wozniak PRJ (2007b) Paskapoo Groundwater Study Part VI: Aquifer transmissivity estimation and a preliminary data analysis of the Paskapoo Formation, Alberta. :31.

Chevron Canada Limited (2017) Fox Creek Area NE 24-061-22 W5M, SW 30-061-21 W5M, SE and SW 04-062-22 W5M, and SW 23-062-22 W5M. HCL Project No.: 17-0244.01. *Chevron Groundwater Term Licence Application,* 384 p.

Chunn D, Faramarzi M, Smerdon B & Alessi D (2019) Application of an Integrated SWAT–MODFLOW Model to Evaluate Potential Impacts of Climate Change and Water Withdrawals on Groundwater–Surface Water Interactions in West-Central Alberta. *Water* 11(1).

Corlett HJ, Playter TL, Babakhani M, Hathway B, Peterson JT & MacCormack KE (2019) Regional stratigraphic correlation and 3D geological modelling of west-central Alberta; Alberta Energy Regulator / Alberta Geological Survey, AER/AGS Open File Report 2019-04, 53 p.

Croteau A, Nastev M & Lefebvre R (2010) Groundwater Recharge Assessment in the Chateauguay River Watershed. *Canadian Water Resources Journal* 35(4):451-468.

Demchuk TD & Hills LV (1991) A re-examination of the Paskapoo Formation in the central Alberta Plains: the designation of three new members; Bulletin of Canadian Petroleum Geology. v. 39:270–282.

Desbarats AJ, Logan CE, Hinton MJ & Sharpe DR (2002) On the kriging of water table elevations using collateral information from a digital elevation model. *Journal of Hydrology* 255(1-4):25-38.

Devito KJ, Creed IF & Fraser CJD (2005) Controls on runoff from a partially harvested aspen-forested headwater catchment, Boreal Plain, Canada. *Hydrological Processes* 19(1):3-25.

Ferguson IM & Maxwell RM (2010) Role of groundwater in watershed response and land surface feedbacks under climate change. *Water Resources Research* 46(10).

Freeze RA & Cherry JA (1979) Groundwater. Prentice-Hall Inc., Englewood Cliffs, Vol. 7632, 604.

Gatel L, Lauvernet C, Carluer N, Weill S, Tournebize J & Paniconi C (2019) Global evaluation and sensitivity analysis of a physically based flow and reactive transport model on a laboratory experiment. *Environmental Modelling & Software* 113:73-83.

Gauthier MJ, Camporese M, Rivard C, Paniconi C & Larocque M (2009) A modeling study of heterogeneity and surface water-groundwater interactions in the Thomas Brook catchment, Annapolis Valley (Nova Scotia, Canada). *Hydrol. Earth Syst. Sci.* 13:1-14.

Goderniaux P, Brouyère S, Fowler HJ, Blenkinsop S, Therrien R, Orban P & Dassargues A (2009) Large scale surface–subsurface hydrological model to assess climate change impacts on groundwater reserves. *Journal of Hydrology* 373(1-2):122-138.

Gosselin J, Lefebvre R, Martel R & Rivard C (2017) GWHAT: Documentation - Release 0.2.0. (Institut National de la Recherche Scientifique, Centre Eau Terre Environnement, Québec, QC), p 33.

Government of Alberta (2019) *Groundwater – Overview. Information, resources and regulation and policy regarding groundwater.* Government of Alberta, https://www.alberta.ca/groundwater-overview.aspx

Government of Alberta (2020) Alberta Climate Information Service https://agriculture.alberta.ca/acis (01-2020). Alberta Agriculture and Forestry.

Government of Canada (2013) Water sources: groundwater. https://www.canada.ca/en/environment-climate-change/services/water-overview/sources/groundwater.html.

Government of Canada (2015) Canadian Land Cover, circa 2000 (Vector) – GeoBase Series – ARCHIVED. URL: https://open.canada.ca/data/en/dataset/97126362-5a85-4fe0-9dc2-915464cfdbb7.

Government of Canada (2020) Historical Climate Data, https://climate.weather.gc.ca/, Consulted 11-2020.).

Grasby S, Chen Z, Hamblin AP, Wozniak PRJ & Sweet AR (2008) Regional characterization of the Paskapoo bedrock aquifer system, southern AlbertaGeological Survey of Canada Contribution 2008-0479. *Canadian Journal of Earth Sciences* 45(12):1501-1516.

Grasby S, Tan W, Chen Z & Hamblin AP (2007) Paskapoo Groundwater Study. Part 1: Hydrogeological properties of the Paskapoo Formation determined from six continuous cores. Geological Survey of Canada, Open File 5392.

Guay C, Nastev M, Paniconi C & Sulis M (2013) Comparison of two modeling approaches for groundwater-surface water interactions. *Hydrological Processes* 27(16):2258-2270.

Hathway B (2011) Tops of the Horseshoe Canyon, Wapiti and Battle formations in the west-central Alberta Plains: subsurface stratigraphic picks and modelled surface; Energy Resources Conservation Board, ERCB/AGS Open File 2011-08, 24 p.

Healy RW (2010) Estimating groundwater recharge. Cambridge University Press, Cambridge, UK. 245 p.

Hill MC (2006) The practical use of simplicity in developing ground water models. *Ground water* 44(6):775-781.

Hufty A (2001) Introduction à la climatologie : le rayonnement et la température, l'atmosphère, l'eau, le climat et l'activité humaine. Presses Université Laval, Saint-Nicolas, QC. 545 p.

Hughes AT, Smerdon BD & Alessi DS (2017a) Hydraulic properties of the Paskapoo Formation in west-central Alberta. *Canadian Journal of Earth Sciences* 54(8):883-892.

Hughes AT, Smerdon BD & Alessi DS (2017b) Summary of hydraulic conductivity values for the Paskapoo Formation in west-central Alberta; Alberta Energy Regulator, AER/AGS Open File Report 2016-03, 25 p.

IHS Markit (2018) *AccuMap™; IHS Markit, mapping, data management and analysis software.*https://ihsmarkit.com/products/oil-gas-tools-accumap.html, (Consulté le April)

Khidir A & Catuneanu O (2010) Reservoir characterization of Scollard-age fluvial sandstones, Alberta foredeep. *Marine and Petroleum Geology* 27(9):2037-2050.

Kolditz O, Bauer S, Bilke L, Böttcher N, Delfs JO, Fischer T, Görke UJ, Kalbacher T, Kosakowski G, McDermott CI, Park CH, Radu F, Rink K, Shao H, Shao HB, Sun F, Sun YY, Singh AK, Taron J, Walther M, Wang W, Watanabe N, Wu Y, Xie M, Xu W & Zehner B (2012) OpenGeoSys: an open-source initiative for numerical simulation of thermo-hydro-mechanical/chemical (THM/C) processes in porous media. *Environmental Earth Sciences* 67(2):589-599.

Kollet S, Sulis M, Maxwell RM, Paniconi C, Putti M, Bertoldi G, Coon ET, Cordano E, Endrizzi S, Kikinzon E, Mouche E, Mügler C, Park Y-J, Refsgaard JC, Stisen S & Sudicky E (2017) The integrated hydrologic model intercomparison project, IH-MIP2: A second set of benchmark results to diagnose integrated hydrology and feedbacks. *Water Resources Research* 53(1):867-890.

Kollet SJ & Maxwell RM (2006) Integrated surface–groundwater flow modeling: A free-surface overland flow boundary condition in a parallel groundwater flow model. *Advances in Water Resources* 29(7):945-958.

Loague K, Heppner CS, Abrams RH, Carr AE, VanderKwaak JE & Ebel BA (2005) Further testing of the Integrated Hydrology Model (InHM): event-based simulations for a small rangeland catchment located near Chickasha, Oklahoma. *Hydrological Processes* 19(7):1373-1398.

Lyster S & Andriashek LD (2012) Geostatistical rendering of the architecture of hydrostratigraphic units within the Paskapoo Formation, central Alberta. *Energy Resources Conservation Board, ERCB/AGS Bulletin 66* :106.

Maxwell RM, Putti M, Meyerhoff S, Delfs J-O, Ferguson IM, Ivanov V, Kim J, Kolditz O, Kollet SJ, Kumar M, Lopez S, Niu J, Paniconi C, Park Y-J, Phanikumar MS, Shen C, Sudicky EA & Sulis M

(2014) Surface-subsurface model intercomparison: A first set of benchmark results to diagnose integrated hydrology and feedbacks. *Water Resources Research* 50(2):1531-1549.

Molson JW & Frind EO (2017) FLONET/TR2 User Guide, A two-dimensional simulator for groundwater flownets, contaminant transport and residence time, Version 5. *Université Laval and University of Waterloo, 57 p.* .

Monfet J (1979) Évaluation du coefficient de ruissellement à l'aide de la méthode SCS modifiée. Gouvernement du Québec, Ministère des Richesses naturelles, Service de l'hydromètrie, Québec, QC. 35 p.

Panday S & Huyakorn PS (2004) A fully coupled physically-based spatially-distributed model for evaluating surface/subsurface flow. *Advances in Water Resources* 27(4):361-382.

Paniconi C & Putti M (2015) Physically based modeling in catchment hydrology at 50: Survey and outlook. *Water Resources Research* 51(9):7090-7129.

Riddell JTF, Andriashek LD, Jean G & Slattery SR (2009) Preliminary results of sediment coring in the Edmonton–Calgary Corridor, central Alberta; Energy Resources Conservation Board, ERCB/AGS Open File Report 2009-17, 81 p.

Rivard C, Lefebvre R & Paradis D (2014) Regional recharge estimation using multiple methods: an application in the Annapolis Valley, Nova Scotia (Canada). *Environmental Earth Sciences* 71(3):1389-1408.

Scanlon BR, Healy RW & Cook PG (2002) Choosing appropriate techniques for quantifying groundwater recharge. *Hydrogeology Journal* 10(1):18-39.

Singh A & Nakevska N (2019) Distribution of hydraulic head in the Wapiti / Belly River hydrostratigraphic unit. Alberta Energy Regulator / Alberta Geological Survey, AER/AGS Map 543

Smerdon BD, Atkinson LA, Hartman GMD, Playter TL & Andriashek LD (2016) Field evidence of nested groundwater flow along the Little Smoky River, west-central Alberta; Alberta Energy Regulator, AER/AGS Open File Report 2016-02, 34 p.).

Smerdon BD, Hughes AT & Jean G (2017) Permeability measurements of Upper Cretaceous and Paleogene bedrock cores made from 2004-2015 (tabular data, tab-delimited format, to accompany Open File Report 2016-03); Alberta Energy Regulator, AER/AGS Digital Data 2016-0042. .

Smerdon BD, Klassen J & Gardner WP (2019) Hydrogeological Characterization of the Upper Cretaceous–Quaternary units in the Fox Creek area, west-central Alberta; Alberta Energy Regulator / Alberta Geological Survey, AER/AGS Report 98, 35 p.

Smerdon BD, Mendoza CA & Devito KJ (2007) Simulations of fully coupled lake-groundwater exchange in a subhumid climate with an integrated hydrologic model. *Water Resources Research* 43(1).

Smerdon BD, Mendoza CA & Devito KJ (2008) Influence of subhumid climate and water table depth on groundwater recharge in shallow outwash aquifers. *Water Resources Research* 44(8).

Soil Landscapes of Canada Working Group (2010) Soil Landscapes of Canada version 3.2. Agriculture and Agri-Food Canada.

Stisen S, Sonnenborg TO, Højberg AL, Troldborg L & Refsgaard JC (2011) Evaluation of Climate Input Biases and Water Balance Issues Using a Coupled Surface-Subsurface Model. *Vadose Zone Journal* 10(1):37-53.

Sulis M, Meyerhoff SB, Paniconi C, Maxwell RM, Putti M & Kollet SJ (2010) A comparison of two physics-based numerical models for simulating surface water–groundwater interactions. *Advances in Water Resources* 33(4):456-467.

Sulis M, Paniconi C, Rivard C, Harvey R & Chaumont D (2011) Assessment of climate change impacts at the catchment scale with a detailed hydrological model of surface-subsurface interactions and comparison with a land surface model. *Water Resources Research* 47(1).

Therrien RE, Sudicky EA & Park Y-J (2012) *HydroGeoSPhere: A Three-dimensional Numerical Model Describing Fully-integrated Subsurface and Surface Flow and Transport, User Guide. Aquanty Inc, Waterloo, Ontario, Canada.*

Thompson C, Mendoza CA, Devito KJ & Petrone RM (2015) Climatic controls on groundwater–surface water interactions within the Boreal Plains of Alberta: Field observations and numerical simulations. *Journal of Hydrology* 527:734-746.

Thornthwaite CW (1948) An Approach toward a Rational Classification of Climate. *Geographical Review* 38(1).

USDA (1985) National Engineering Handbook: Section 4—Hydrology. US Department of Agriculture, Natural Resources Conservation Service, available from United States Government Printing Office, Washington, DC, http://www.hydrocad.net/neh-4.htm.).

Van Genuchten MT (1980) A Closed-form Equation for Predicting the Hydraulic Conductivity of Unsaturated Soils. *Soil Science Society of America Journal* 44(5):892-898.

VanderKwaak JE & Loague K (2001) Hydrologic-Response simulations for the R-5 catchment with a comprehensive physics-based model. *Water Resources Research* 37(4):999-1013.

Wels C, Mackie D & Scibek J (2012) Guidelines for Groundwater Modelling to Assess Impacts of Proposed Natural Resource Development Activities. Report No. 194001. British Columbia Ministry of Environment

Zerihun D, Furman A, Warrick AW & Sanchez CA (2005) Coupled Surface-Subsurface Flow Model for Improved Basin Irrigation Management. *Journal of Irrigation and Drainage Engineering* 131(2):111-128.